Paleogene evolution of the Burmese forearc basin and implications for the history of India-Asia convergence

Alexis Licht, Guillaume Dupont-Nivet, Zaw Win, Hnin Hnin Swe, Pierrick Roperch, Et Al.

Article published in the *Geological Society of America Bulletin*, Geological Society of America

Alexis Licht, Guillaume Dupont-Nivet, Zaw Win, Hnin Hnin Swe, Pierrick Roperch, et al.. Paleogene evolution of the Burmese forearc basin and implications for the history of India-Asia convergence. *Geological Society of America Bulletin*, Geological Society of America, 2019, 131 (5-6), pp.730-748. ⟨10.1130/B35002.1⟩. ⟨insu-01901808⟩

Paleogene evolution of the Burmese forearc basin and implications for the history of India-Asia convergence

Alexis Licht[1,†], Guillaume Dupont-Nivet[2,3,4], Zaw Win[5], Hnin Hnin Swe[6], Myat Kaythi[6], Pierrick Roperch[2], Tamas Ugrai[1], Virginia Littell[1], Diana Park[1], Jan Westerweel[2], Dominic Jones[1], Fernando Poblete[2,7],Day Wa Aung[6], Huasheng Huang[8], Carina Hoorn[8], and Kyaing Sein[9]

[1]*Department of Earth and Space Sciences, University of Washington, Seattle, Washington 98195, USA*

[2]*Géosciences Rennes, UMR CNRS 6118, Université de Rennes, 35042 Rennes Cedex, France*

[3]*Potsdam University, Institute of Earth and Environmental Science, 14476 Potsdam, Germany*

[4]*Key Laboratory of Orogenic Belts and Crustal Evolution, Ministry of Education, Beijing, China*

[5]*Geology Department, Shwe Bo University, Sagaing Region, Myanmar*

[6]*Geology Department, University of Yangon, Pyay Road, Yangon, Myanmar*

[7]*Instituto de Ciencias de la Ingeniería, Universidad de O'Higgins, Rancagua, Chile*

[8]*Institute for Biodiversity and Ecosystem Dynamics, University of Amsterdam, 1098 XH Amsterdam, The Netherlands*

[9]*Myanmar Geosciences Society, Yangon, Myanmar*

Abstract

The geological history of the Burmese subduction margin, where India obliquely subducts below Indochina, remains poorly documented although it is key to deciphering geodynamic models for the evolution of the broader Tibetan-Himalayan orogen. Various scenarios for the evolution of the orogen have been proposed, including a collision of India with Myanmar in the Paleogene, a significant extrusion of Myanmar and Indochina from the India-Asia collision zone, or very little change in paleogeography and subduction regime since the India-Asia collision. This article examines the history of the Burmese forearc basin, with a particular focus on Eocene–Oligocene times to

reconstruct the evolution of the Burmese margin during the early stages of the India-Asia collision. We report on sedimentological, geochemical, petrographical, and geochronological data from the Chindwin Basin—the northern part of the Burmese forearc—and integrate these results with previous data from other basins in central Myanmar.

Our results show that the Burmese margin acted as a regular Andean-type subduction margin until the late middle Eocene, with a forearc basin that was open to the trench and fed by the denudation of the Andean volcanic arc to the east. We show that the modern tectonic configuration of central Myanmar formed 39–37 million years ago, when the Burmese margin shifted from an Andean-type margin to a hyper-oblique margin. The forearc basin was quickly partitioned into individual pull-apart basins, bounded to the west by a quickly emerged accretionary prism, and to the east by synchronously exhumed basement rocks, including coeval high-grade metamorphics. We interpret this shift as resulting from the onset of strike-slip deformation on the subduction margin leading to the formation of a paleo-sliver plate, with a paleo fault system in the accretionary prism, pull-apart basins in the forearc, and another paleo fault system in the backarc. This evolution implies that hyper-oblique convergence below the Burmese margin is at least twice older than previously thought. Our results reject any India-Asia convergence scenario involving an early Paleogene collision of India with Myanmar. In contrast, our results validate conservative geodynamic models arguing for a close-to-modern pre-collisional paleogeometry for the Indochina Peninsula, and indicate that any post-collisional rotation of Indochina, if it occurred at all, must have been achieved by the late middle Eocene.

1. INTRODUCTION

The Himalayan-Tibetan orogen, a result of the India-Asia collision, is commonly considered as the type orogen for continent-continent collisional systems and a natural laboratory to study the dynamics of continental convergence (Yin and Harrison, 2000). Our seemingly vast knowledge of the Himalayan-Tibetan system comes from decades of work along ~2600 km of the approximately west-east–trending arcuate strike of the orogen in NW India, Nepal, Bhutan, and Tibet (e.g., Allègre et al., 1984; Chen et al., 1993; Yin et al., 1994; Searle et al., 1997; Harrison et al., 1998; DeCelles et al., 2002, 2014; Najman et al., 2010, 2017; McQuarrie et al., 2014; Ma et al., 2016). Yet, the pre-collisional

paleogeography of the Asian active margin, the chronology of the collision, and the deformation mechanisms accommodating the post-collisional convergence remain debated (e.g., Shen et al., 2001; Royden et al., 2008; van Hinsbergen et al., 2011a; Replumaz et al., 2010, 2013). Noticeably, an enormous spatial gap is left in our understanding of the convergence. With some notable exceptions (Pivnik et al., 1998; Socquet et al., 2002; Rangin et al., 2013), ~1500 km of the orogen trending north-south in Myanmar is underrepresented in our efforts to understand this complex system. The histories of the Burma Terrane, a small individual continental block located at the edge of the eastern Himalayan syntaxis, and of the active margin on the Burma Terrane, where the Indian plate subducts below the western edge of peninsular Indochina (Fig. 1A), remain virtually undocumented and are the focus of intense speculation. Reconstructing the history of the Burmese margin is, however, a prerequisite for any paleotectonic and geodynamic understanding of the broader Tibetan-Himalayan orogen.

Two end-member geodynamic models are proposed to explain how Asian lithospheric deformation has accommodated the convergence of India and Asia since the collision began: (1) lateral extrusion of Asian lithospheric blocks away from the collision zone with partial underthrusting of Asian blocks along strike-slip faults (e.g., Tapponnier et al., 1982; Replumaz and Tapponnier, 2003; Royden et al., 2008; Replumaz et al., 2010, 2013; Cogné et al., 2013), and (2) homogeneous thickening and continuous deformation of weaker Asian lithosphere (e.g., England and Houseman; 1986, Molnar et al., 1993; Hallet and Molnar, 2001; Shen et al., 2001; van Hinsbergen et al., 2011a). In most plate kinematic models dominated by extrusion, India collides with the Burmese subduction margin in the early time of the collision ca. 55 Ma (Fig. 1B; Tapponnier et al., 1982; Replumaz and Tapponnier, 2003; Replumaz et al., 2010; Cogné et al., 2013; Gibbons et al., 2015). The Burma Terrane and Indochina are later extruded from the collision zone to end up in their modern position, south of the Eastern Himalayan syntaxis. In other kinematic models dominated by extrusion, India does not collide with the Burma Terrane but with the Lhasa Terrane in Tibet (Fig. 1B); the Burma Terrane is located to the southeast of the Lhasa Terrane and is dragged northward by the Indian Plate while Indochina is extruded eastward (Royden et al., 2008). By contrast, models dominated by homogeneous thickening and continuous deformation of Asian lithosphere propose a more conservative paleogeography for the Burmese margin (Fig. 1C): pre-collisional Myanmar and peninsular Indochina already form a narrow peninsula at the

southeastward extremity of East Asia very close to their modern position (Molnar et al., 1993; Hallet and Molnar, 2001; Shen et al., 2001; van Hinsbergen et al., 2011a). Most of the continuous deformation models suggest that the Burmese subduction margin lies to the east of the collision zone and is thus not particularly impacted by post-collisional deformation (van Hinsbergen et al., 2011a, 2012; Hall, 2012), but others propose that India collided first with the Burmese margin before continuing northward to its modern position (Aitchison et al., 2007; Vérard et al., 2017).

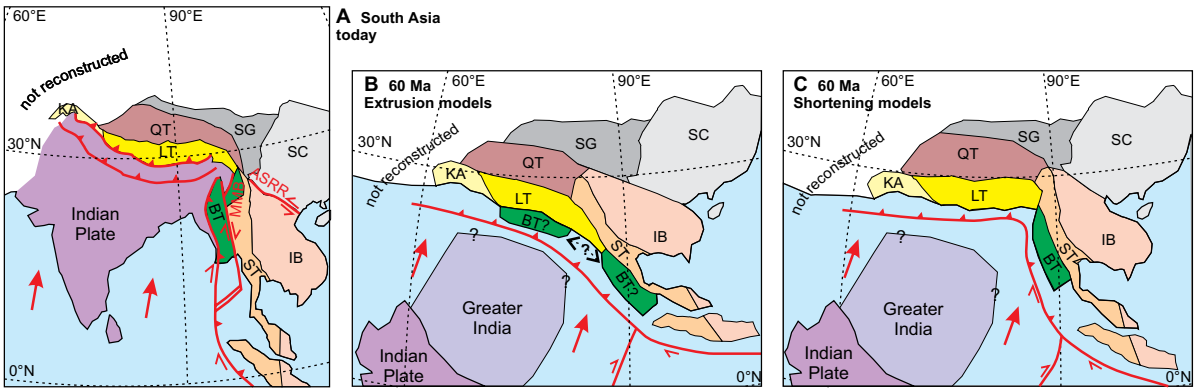

Figure 1. *Structural map of South Asia today (A) and hypothetical maps 60 million years ago following deformation models dominated by extrusion (B) or shortening processes (C). Modified after Replumaz and Tapponnier (2003), Pubellier (2008), van Hinsbergen et al. (2011a), Hall (2012), and Royden et al. (2008). KA—Kohistan Arc; LT—Lhasa Terrane; QT—Qiangtang Terrane; SG—Songpan Ganzi complex; SC—South China Craton; BT—Burma terrane; ST—Sibumasu Terrane; IB—Indochina Terrane; MMB—Mogok Metamorphic Belt; ASRR—Ailao Shan–Red River shear zone. The red arrows indicate the direction of convergence (after Lee and Lawver, 1995; van Hinsbergen et al., 2011b). Note that before the India-Asia collision, extrusion models propose that the Burma Terrane was located either along the collision front (e.g., Replumaz and Tapponnier, 2003) or farther east, away from the collision zone (e.g., Royden et al., 2008).*

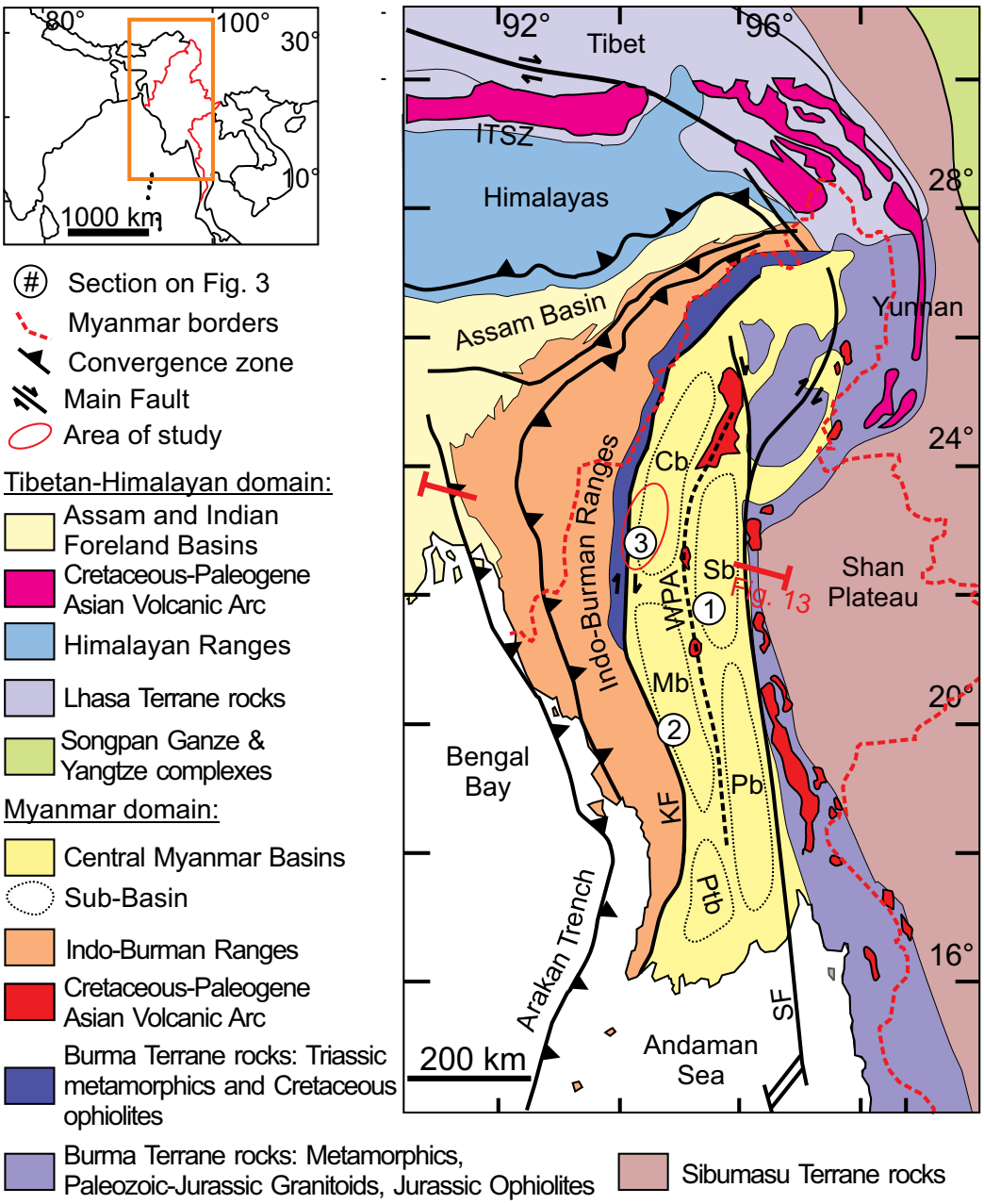

Figure 2*. Schematic map of the eastern Himalayan syntaxis and central Myanmar, with the main geological units, after Licht et al. (2013); boundaries between Tibetan and SE Asian terranes are not precisely drawn because they are poorly known. The approximate axis of the Wuntho-Popa Andean arc (WPA) is shown by a thick, dashed black line. The sub-basins of central Myanmar are indicated with thin, dashed black lines: the Chindwin, Minbu, and Pathein basins (Cb, Mb, and Ptb) in the forearc, the Shwebo and Pegu basins (Sb and Pb) in the backarc. ITSZ—Indus-Tsangpo Suture Zone; SF—Sagaing Fault; KF—Kabaw Fault. Numbers in circles indicate the location of the synthetic logs in Figure 3, and the red line indicates the location of the cross section in Figure 13. Area of study* is shown by a red circle. Symbol (3) sits at the location of our composite section.

The sedimentary deposits of the forearc basin of central Myanmar provide a unique opportunity to document the paleogeography and deformation history of the Burmese subduction margin and decipher these different models. This article examines the history of the Burmese forearc basin, with a particular focus on Eocene–Oligocene times to reconstruct the evolution of the Burmese margin during the early stages of the India-Asia collision. Here, we report on sedimentological, geochemical, modal petrographical, and U-Pb detrital zircon geochronological data from the Chindwin Basin (northern part of the Burmese forearc basin), and integrate these results with previous data from other basins of central Myanmar to reconstruct the evolution of the Burmese margin through the Paleogene.

2. GEOLOGICAL CONTEXT

2.1. The Burma Terrane and the Burmese Subduction Margin

Myanmar can be divided into two roughly north-south–trending belts that lie on two basement blocks: central Myanmar on the Burma Terrane, and the Shan Plateau on the Sibumasu Terrane (Fig. 2). At the transition between both terranes, the deep basement of the Burma Terrane, consisting of Middle Jurassic ophiolites of the Burma-Sibumasu suture and metamorphics from the basement of the Sibumasu Terrane, is partially exposed and forms a succession of metamorphic belts (Jade Mine Belt, Slate Belt, Mogok Metamorphic Belt; Bertrand and Rangin 2003; Mitchell et al. 2007, 2012; Searle et al., 2012, 2017; Liu et al., 2016). It is not clear when the Burma Terrane collided with the Sibumasu Terrane; various unconstrained age estimates are proposed ranging from the Middle Jurassic to the latest Cretaceous, and the existence of a suture between both terranes is even challenged (Mitchell, 1993; Metcalfe, 2013; Sevastjanova et al., 2016; Liu et al., 2016; Searle et al., 2017); U-Pb zircon ages from intrusions and gneisses in the Mogok Metamorphic belt suggest a latest Jurassic–early Cretaceous age for the collision event (Mitchell et al., 2012).

The mid Cretaceous–early Paleogene tectonic evolution of Myanmar is marked by the subduction of the Neotethyan Ocean below western Myanmar along the Arakan Trench (Bender, 1983). The modern Burmese subduction margin formed as an Andean-type accretionary setting after rapid, forearc supra-subduction ophiolite spreading at ca. 125 Ma and the set-up of the Central Myanmar Basins developed in a forearc/backarc setting on the Burma Terrane (Bender, 1983; Pivnik et al., 1998; Liu et al., 2016; Zhang et al.,

2017a). The timing of this onset mirrors the evolution of the Xigaze forearc Basin in Tibet (Maffione et al., 2015; Liu et al., 2016; Wang et al., 2017). This period is marked by intense magmatic activity in the Andean-type Wuntho-Popa Arc, today represented by several large batholiths and related volcanic rocks that straddle the middle of the Central Myanmar Basins (Fig. 2; Zaw, 1990; Maury et al., 2004; Gardiner et al., 2015, 2017; Lee et al., 2016). The Wuntho-Popa Arc is commonly considered the eastern continuation of the Gangdese Arc of Tibet (Ma et al., 2013; Wang et al., 2014) and consists of widespread I-type batholiths and andesitic bodies punctuated with isolated S-type intrusions (Zhang et al., 2017b). Recently published U-Pb ages suggest a period of activity spanning from 110 to 30 Ma (Mitchell et al. 2012; Wang et al., 2014; Gardiner et al., 2015, 2017; Zhang et al., 2017b), with a main magmatic stage between 110 and 80 Ma and a subordinate magmatic stage at ca. 70–40 Ma. Cretaceous-Paleogene plutons are also present farther east along the Shan Scarp (Granitic Tin Belt of Gardiner et al., 2017) and may reflect temporary periods of eastward migration of the Andean-type arc (Gardiner et al., 2015), but their chronology and relationship with the Wuntho-Popa Arc remain poorly understood. The Burmese margin was then deformed by dextral strike-slip shear and other faulting, resulting in partitioning by pull-apart subsidence of the Central Myanmar Basins (Pivnik et al., 1998; Rangin et al., 1999) and in high-grade metamorphism in the Mogok Metamorphic Belt (Bertrand et al., 2001; Bertrand and Rangin, 2003; Barley et al., 2003; Searle et al., 2007). This strike-slip deformation regime is commonly explained as resulting from the hyper-oblique convergence of the Indian plate below the Burmese margin. As a result of this oblique convergence and subsequent deformation, central and western Myanmar were dragged northward (Socquet et al., 2006; Morley, 2009). The timing for the onset of strike-slip deformation and hyper-oblique regime is not clear, but oldest U-Pb zircon ages and 40K-40Ar cooling ages of gneisses in the Mogok Metamorphic Belt indicate that high-grade metamorphism had started by the late Eocene (ca. 37–36 Ma) along a paleo “Shan Scarp Fault” following the eastern margin of the Burma Terrane (Bertrand et al., 2001; Searle et al., 2007; Morley, 2009; 2017). Two U-Pb ages in metamorphic overgrowths of zircons suggest that it might have started even earlier, by the middle Eocene (47 and 43 Ma; Barley et al., 2003). Since the middle Miocene, following the opening of the Andaman Sea between Myanmar and Sumatra, the strike-slip motion has been partitioned and accommodated by the Sagaing Fault along the Mogok Metamorphic Belt, the Kabaw Fault in the Indo-

Burman Ranges, and the Arakan Trench (Khan and Chakraborty 2005; Socquet et al., 2006). Since then, central Myanmar has formed an individual and complex sliver plate between these two faults, the total dextral displacement of which is variously estimated at 400–500 km to more than 1000 km (Maung 1987; Mitchell, 1993; Socquet et al., 2006; Morley, 2009, 2017).

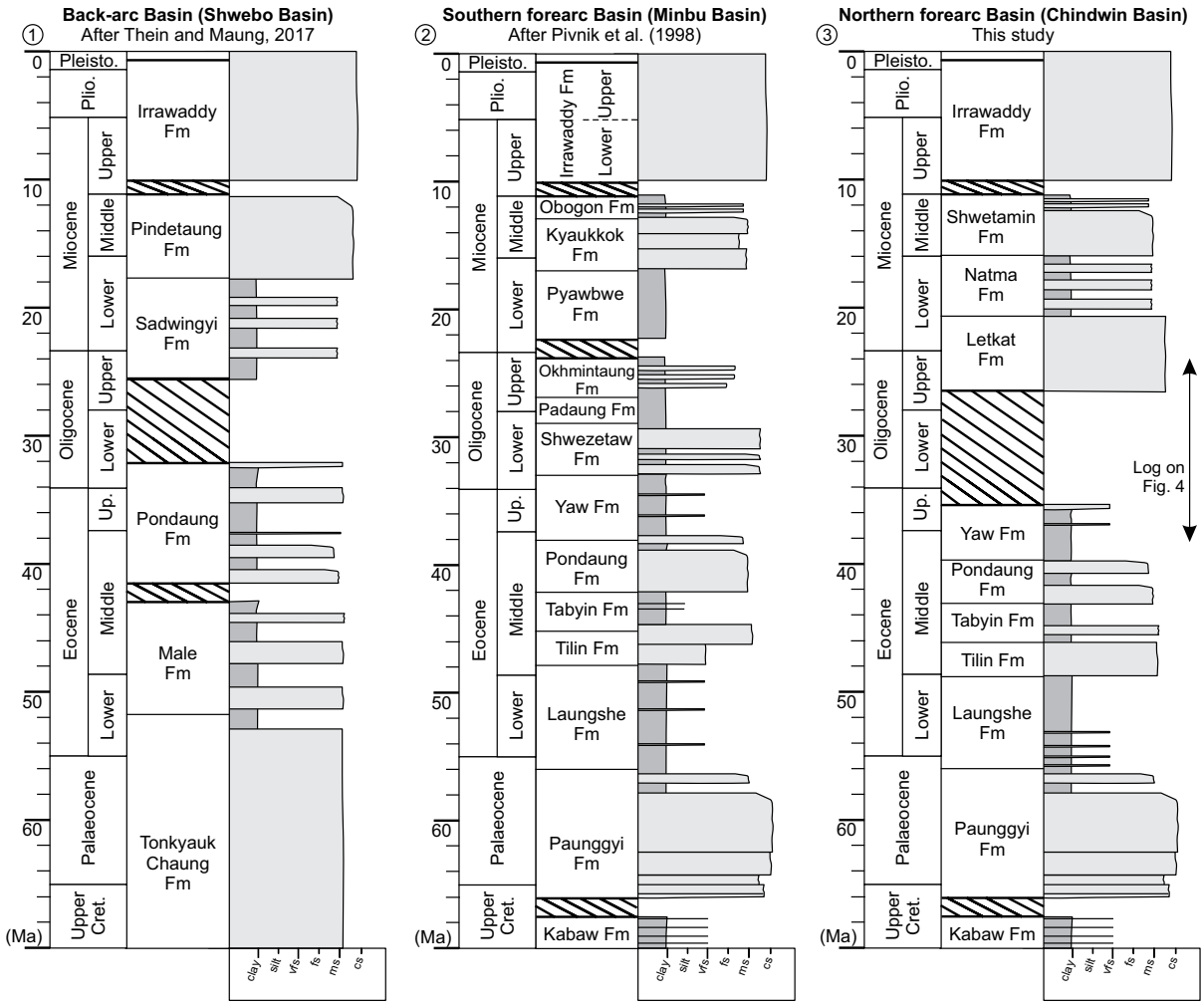

Figure 3. *Synthetic logs for the three main basins of central Myanmar: (1) the Shwebo Basin in the backarc (after Thein and Maung, 2017), (2) the Minbu Basin, (southern forearc; after Pivnik et al., 1998), and (3) the Chindwin Basin (northern forearc; Bender, 1983; this study). Location of the three logs is shown on Figure 2. vfs—very fine sand; fs—fine sand; ms—medium sand; cs—coarse sand.*

2.2. The Indo-Burman Ranges

On its western margin, the Burma Terrane is separated from the Indian Foreland Basin and the Bengal Bay by the Indo-Burman Ranges, which constitute the accretionary complex produced by the Indian subduction under the Burmese active margin (Brunnschweiler, 1966; Maurin and Rangin, 2009; Bannert et al., 2011; Zhang et al.,

2017a). The Indo-Burman Ranges are divided into an outer wedge made of Neogene Himalayan-sourced clastic sequences affected by folds and thrusts, and an inner wedge mainly constituted of early Cretaceous ophiolites and Triassic schists covered by Upper Cretaceous–Eocene marine turbidites (see also Figure 13C; Maurin and Rangin, 2009; Bannert et al., 2011). The origin of the Triassic schists is still unclear, but they may belong to a micro-continent accreted and thrusted on the Burmese margin between 125 and 110 Ma (Morley, 2012), or be part of the pre-Jurassic Burma Terrane basement that was dismantled after supra-subduction spreading of the forearc (Sevastjanova et al., 2016). The oldest Cretaceous marine turbidites overlying the Triassic schists in the Indo-Burman Ranges are dated to the Campanian, but some deposits contain allochthonous blocks of Albian limestones (Bender, 1983). The outer wedge experienced uplift starting in the late Miocene as a consequence of either increased and potentially faster subduction of sediment from the Bengal Basin and Syllet Trough on the Indian Plate (Maurin and Rangin, 2009) or westward crustal flow from southeastern Tibet resulting in E-W shortening on the Burma Terrane (Rangin et al., 2013). The structure, timing of uplift, and emergence of the inner wedge remain poorly understood.

The most common view is that the inner wedge was exhumed during an early episode of accretionary building along the Burmese active margin, either during the early Cretaceous (Liu et al., 2016; Zhang et al., 2017a) or Late Cretaceous–Paleogene (Bender, 1983; Socquet et al., 2002). Acharyya (2007, 2015) and Metcalfe (2013) proposed that the early uplift of the inner wedge was caused by the accretion of individual island arc fragments that accreted along the Burmese margin during the Paleogene, but evidence for these island arc fragments in the inner wedge is lacking. Nielsen et al. (2004) and Maurin and Rangin (2009) argue that the inner wedge is more complex than a simple accretionary wedge; the core of the inner wedge follows a N-S strike-slip fault system and displays a positive flower structure, similar to retro-wedges formed along hyper-oblique convergence zones (Burbidge and Braun, 1998; McClay et al., 2004; Leever et al., 2011). Today, the inner wedge fault system is traversed by the Kabaw strike-slip fault system and accommodates a significant component (1/4–1/3) of the N-S strike slip deformation of the Burma Terrane (Nielsen et al., 2004; Socquet et al., 2006).

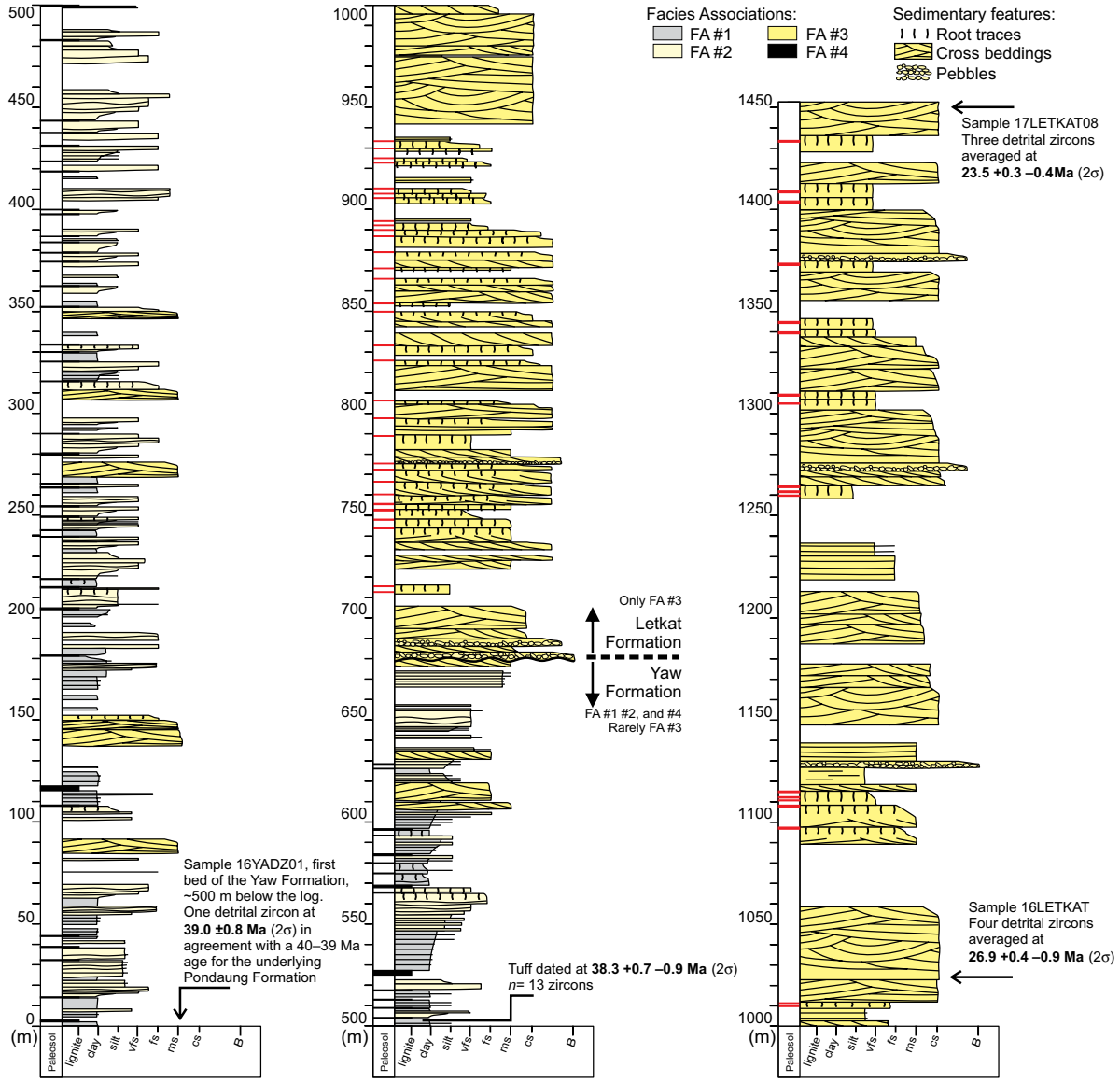

Figure 4. *Composite log of the upper part of the Yaw Formation and lower part of the Letkat Formation, Chindwin Basin, with their facies associations (description in Table 1). Maximum depositional ages for our sandstone samples and age of the Tuff layer dated in this study are also shown. In the Paleosol column, black lines indicate histosols whereas red lines indicate ultisols. vfs—very fine sand; fs—fine sand; ms—medium sand; cs—coarse sand; B—Boulder.*

A combined petrographic and isotopic study of Paleogene marine turbidites from the inner wedge of the Arakan Yoma (southern edge of the Indo-Burman Ranges) identified a persistent youngest zircon-fission track population of 37 Ma in the sandstones (Allen et al. 2008). It is not clear if this fission-track age reflects a volcanic age—thus giving a maximum age for the deposition of the last flysch in the accretionary prism, suggesting that the inner wedge was emerged quickly thereafter—or if this age has been reset and

reflects an episode of exhumation, indicating that the inner wedge was getting uplifted at that time. Both interpretations suggest a first, late Eocene uplift for the Indo-Burman Ranges. In addition, sedimentary provenance databased on Nd and Sr isotopes of late Paleogene units in the Central Myanmar Basin suggests that the Indo-Burman Ranges emerged in the early Oligocene (Licht et al., 2013, 2016). However, the precise timing of uplift and its mechanisms remain unknown.

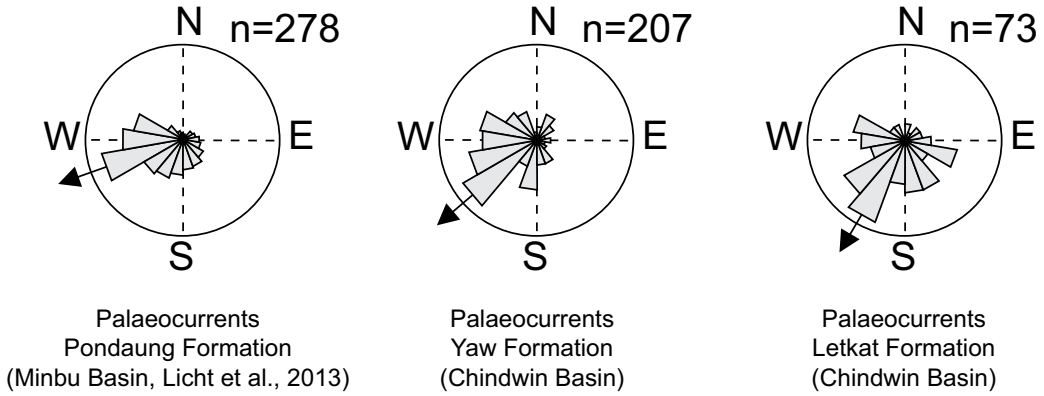

Figure 5. *Paleocurrents for the Pondaung Formation in the Minbu Basin (after Licht et al., 2013), the Yaw Formation in the Chindwin Basin (including new measurements and data from Licht et al., 2013), and the Letkat Formation in the Chindwin Basin (this study). Palaeocurrent directions were measured on 3-D exposures of trough cross-beddings (facies St, Table 1).*

2.3. The Burmese Forearc and Backarc Basins

The Central Myanmar Basins comprise two N-S–trending lateral troughs of Late Cretaceous–Cenozoic sub-basins, located both east (in a backarc position) and west (in a forearc position) of the Wuntho-Popa Arc.

The backarc basin of central Myanmar itself comprises two sub-basins, the Shwebo Basin to the north and the Pegu Basin to the south (Bender, 1983). Deposits overlie basement rocks constituted of Mesozoic marine turbidites and metamorphics and Middle Jurassic ophiolitic material (Morley, 2017; Searle et al., 2017). The sedimentary sequence starts with Upper Cretaceous–middle Eocene conglomerates, volcaniclastics, and sandstones of the Tonkyauk Chaung and Male Formations, followed by the upper Eocene–lowermost Oligocene Pondaung Formation (Fig. 3A; Thein and Maung, 2017; Zhang et al., 2017b). The Paleogene deposits of the Shwebo Basin are exclusively continental (Thein and Maung, 2017); it is not known whether the deposits in the Pegu

Basin are marine or freshwater. and constitutes a local (and recent) topographic high (Bender, 1983).

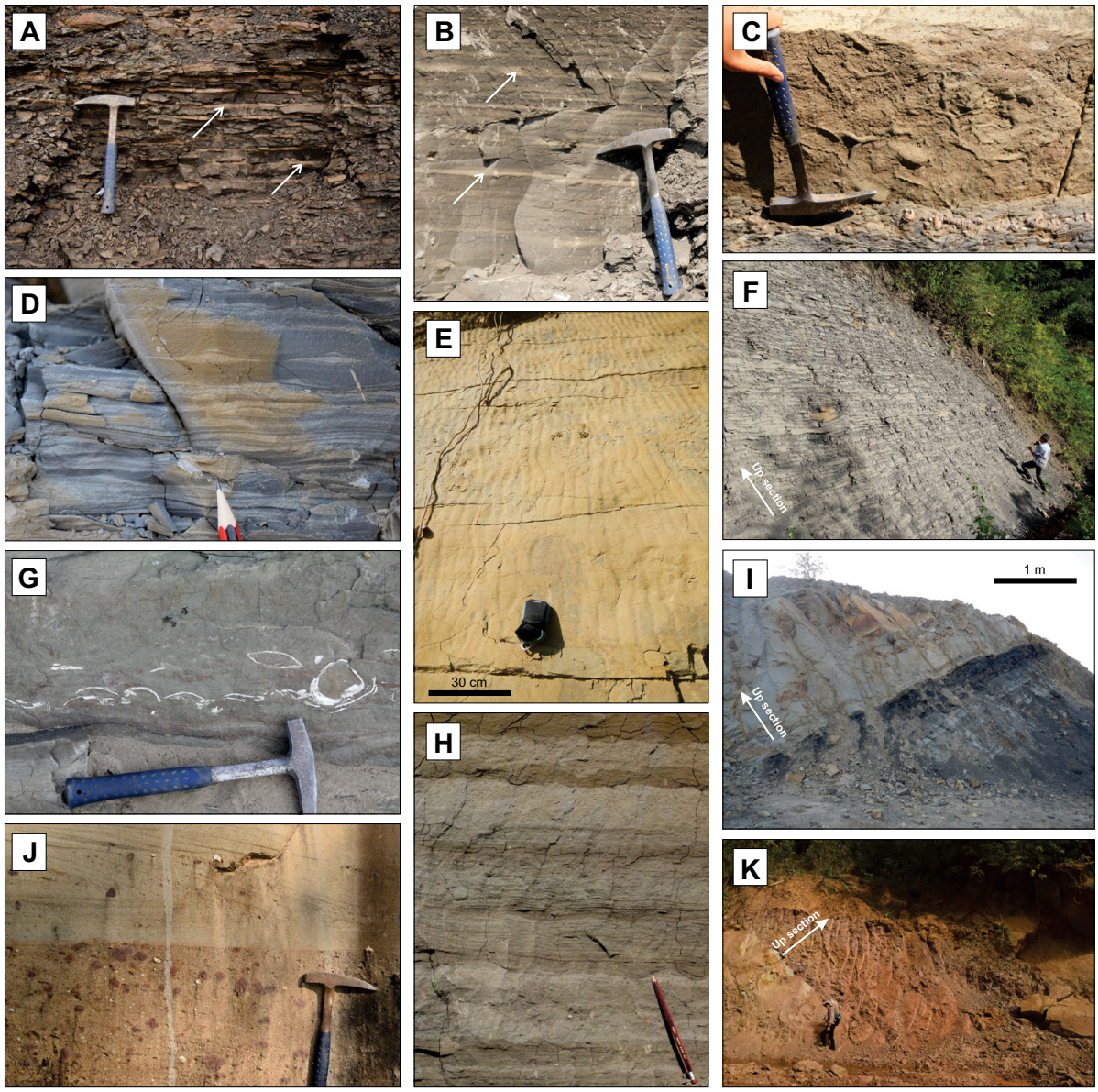

Figure 6. *(A) and (B): black mudstones with cm thick siderite beds, shown by white arrows (facies Ls/Fm). (C) Trace fossil Thalassinoides in siltstone beds (facies Sw). (D) Wavy bedding with symmetrical cross-laminations (facies Sw). (E) Bed of symmetrical ripples in facies Sw (typical of wave-formed ripples) viewed from above. (F) Thick accumulation of wavy and flaser bedding (facies Sw). (G) Unionid fossils in massive very fine sandstone (facies Ssm). (H) Wavy and flaser bedding with planar laminations and asymmetrical cross-laminations (facies Sw). (I) Meter-thick lignite (facies Cv) overlain by a sandstone body of facies St. (J) Trough cross-bedding (facies St) rich in reworked, oxidized sedimentary clasts in the Letkat Formation. (K) Pedogenised sandstones and mudstones (facies Sm) in the Letkat Formation. When the scale is not displayed, rock hammers, pencils, and humans can be used for scale.*

The Paleogene sequence ends with a major Oligocene (?) unconformity observable in seismic lines (Zhang et al., 2017b). Neogene deposits consist of southward prograding tidal-influenced estuarine sequences: the Sadwingyi and Pindetaung Formations in the Shwebo Basin, and the Taungtalon, Moza, and Khabo Formations in the Pegu Basin (Khin and Myitta, 1999). These formations are unconformably overlain by the late middle Miocene–Quaternary fluviatile Irrawaddy Formation (Pivnik et al., 1998; Chavasseau et al., 2006). The Pegu Basin has been inverted and uplifted since the late Miocene

The forearc basin of central Myanmar comprises two major sub-basins, the Chindwin Basin to the north and the Minbu (also called Salin) Basin to the south. These basins are separated today by the Pondaung Ranges, a small topographic high at ~22°N latitude where Paleogene units crop out (Bender, 1983; Pivnik et al., 1998; MGS, 2014). These two sub-basins have also been subdivided into smaller basins by previous authors (including the Pathein Sub-basin to the south; e.g., Bender, 1983) but we will keep things simple and refer only to the two main basins. On the western margin of both basins, supra-subduction ophiolites of the forearc basement crop out along a narrow window stretching along the east side of the Indo-Burman Ranges, and are presumably directly overlain by sedimentary deposits (Liu et al., 2016). On the basins' eastern edges, sediments onlap granitic rocks of the Wuntho-Popa Arc (Zhang et al., 2017b). The Cretaceous–early Cenozoic depositional history is largely similar in both sub-basins. The sequence starts with the poorly exposed Kabaw Formation, constituted of marine limestones and mudstones spanning from the Albian to the Maastrichtian (Figs. 3B and 3C; Bender, 1983). The early Cenozoic sequence includes the Paunggyi, Laungshe, Tilin, and Tabyin Formations spanning from the latest Maastrichtian (?) to the middle Eocene (Nagappa, 1959), all of which consist of shallow-marine siliciclastics with rare continental episodes (Bender, 1983). These units are only differentiated by their dominant grain-size (sandstone or mudstone); their lithostratigraphic boundaries remain vague. The late middle Eocene Pondaung Formation, present in both basins (and here older than in the backarc basin), is the only unit that has received considerable attention, because of its prolific mammalian faunal and paleobotanical remains (e.g., Jaeger et al., 1999; Chaimanee et al., 2012; Licht et al., 2014a, 2015). The Pondaung Formation reflects westward directed fluvio-deltaic systems, the upper member of which is continental with carbonate-bearing paleosols, stacked channels, fossil vertebrates, and freshwater gastropods (Licht et al., 2013, 2014b, 2014c). In the Minbu

Basin, the fossiliferous upper member is precisely dated at ca. 40–39 Ma via a combination of magnetostratigraphy, biostratigraphy, and geochronology (see review of dating results in Licht et al., 2015).

The late middle Eocene–upper Eocene Yaw Formation of central Myanmar represents a period of significant changes in Burmese stratigraphy, with the first pieces of evidence for differentiation between the Minbu and Chindwin Basins. In the Minbu Basin, the Yaw Formation only comprises shallow-marine, fine-grained nummulite-bearing deposits (Nagappa, 1959; Adnet et al., 2008); in the Chindwin Basin, the lithofacies of the Yaw Formation are more varied, with evidence for marine intervals, freshwater gastropods, and lignites yielding continental vertebrates (Licht et al., 2013, 2014c).

Subsequent younger geological units are significantly different in both basins (Figs. 3B and 3C). In the Minbu Basin, the Yaw Formation is followed by the Shwezetaw, Padaung, and Okhmintaung Formations, which all yield shallow-marine Oligocene gastropods, bivalves, and foraminifera (Bender, 1983). Gough and Hall (2017) recently interpreted these units as representing southwards-trending deltaic systems; once again, the boundaries of these units are lithologically based and often vague. They are followed by the lower to middle Miocene fluvio-deltaic Pyawbwe, Kyaukkok, and Obogon Formations (Bender, 1983) that are overlain by the fluviatile late middle Miocene–Pliocene Irrawaddy Formation (Bender, 1983; Chavasseau et al., 2006, 2010). In the Chindwin Basin, the Yaw Formation is overlain by the Letkat Formation, an ~1.5-km-thick sequence of afossiliferous fluviatile sandstones (United Nations, 1978). Some authors have proposed that the contact between the Letkat and the Yaw Formation is unconformable and that the Oligocene is missing in the Chindwin Basin (United Nations, 1978; Wang et al., 2014), whereas Bender (1983) proposes a conformable contact and indicates the presence of undescribed Oligocene sporomorphs in the Letkat Formation. The Letkat Formation is overlain by the afossiliferous fluviatile Natma and Shwetamin Formations of hypothetical Miocene age (United Nations, 1978; Bender, 1983) that are eventually unconformably overlain by the same fluviatile Irrawaddy Formation found in the Minbu Basin.

3. METHODS

3.1. Sedimentology and Stratigraphy

To determine the Paleogene evolution of the Burmese forearc basin, we explored and described deposits along a ~100 km north-south–trending portion of the Chindwin

Basin in the rainshadow of the Indo-Burman Ranges. We started south of the city of Kalewa and continued up to the north of the city of Mawlaik, with a particular focus on the middle Eocene–Oligocene Pondaung, Yaw, and Letkat Formations (Fig. 2). Additionally, we measured a composite section spanning the Yaw and Letkat Formations, composed of five stratigraphic sections correlated in the field (distance between sections is ~200–2000 m). The location of the composite section is indicated on Figure 2. Detailed logs are available in Figure DR11, and are combined into a composite log in Figure 4. We described the sedimentary facies of these two formations, classified them into ten lithofacies adapted from the classification of Miall (2013), and grouped them into four facies associations (Table 1). Finally, we measured paleoflow directions on 3-D outcrops of sandstone trough cross-bedding (facies "St" of Table 1) according to standard field methods (Collinson et al., 2006); results are displayed on Figure 5.

3.2. Sulfur Isotope Analysis

Employing a common way to distinguish brackish from freshwater swamp deposits (Casagrande, 1987), lignite samples from the Yaw Formation were crushed and weighted for sulfur content and isotopic composition (measured as δ34S in ‰ relative to the VCDT [Vienna Canyon Diablo Troilite] standard). Weighted samples were flash combusted at 1000 °C with excess oxygen in a Eurovector Elemental Analyzer (EA) equipped with a Costech zero-blank autosampler, and connected to a ThermoFinnigan MAT253 isotope ratio mass spectrometer for measurement of δ34S. Internal laboratory reference materials were interspersed with samples for a two-point calibration, allowing for conversion to the δ34S VCDT scale and estimations of total sulfur content (see also Fry et al., 2002).

3.3. Sandstone Petrography and U-Pb Dating

Medium-grained sandstone samples were collected along our composite section for petrological and geochronological analyses. Thin sections of 13 sandstone samples were prepared and counted according to the Gazzi-Dickinson method to determine their quartz, feldspar and lithic grains content (Dickinson, 1985); 300–350 grains were counted per section. Detailed results and stratigraphic location of the samples are available in Table DR2 (see footnote 1).

Paleogene sedimentary rocks below and along our composite section were sampled for U-Pb dating of zircons, including one sample from the Paleocene Paunggyi Formation,

two sandstones and one tuff from the Yaw Formation and four sandstones from the Letkat Formation. Detailed analytical protocols and information about the data reduction schemes are provided in the supplementary methods. Briefly, zircon crystals were extracted by traditional methods of heavy mineral separation, including concentration with a Holman-Wilfley gravity shaking table, density separation with methylene iodide and magnetic separation with a Frantz Magnetic separator. U-Pb ages were generated using laser-ablation–inductively coupled plasma–mass spectrometry (LA-ICP-MS), using an iCAP RQ Quadrupole ICP-MS coupled to an Analyte G2 excimer laser at the University of Washington, using a spot diameter of 25 microns. Data reduction was conducted with Iolite, using their Geochron Data Reduction Scheme to calculate U-Pb ages uncorrected for common lead (Paton et al., 2010), and with the Andersen Routine of the Vizualage Data Reduction Scheme (Chew et al., 2014) for U-Pb ages corrected for common lead. Both approaches yielded quasi-identical zircon ages in our data set, and ages used in this manuscript are uncorrected for common lead. Detailed location, stratigraphic level, and U-Pb data are available in Table DR3 (see footnote 1). Stratigraphic locations for the Yaw and Letkat Formation samples are also indicated on Figure 4. Maximum depositional age for detrital samples and crystallization age for volcanic samples with multiple zircon ages were calculated using Tuffzirc (Ludwig, 2003) and are also displayed on Figure 4. The final age error calculated for each sample is the quadratic sum of the uncertainty of Tuffzirc age calculation and of the systematic uncertainty during each session (~1.3%).

4. RESULTS

4.1. Sedimentology of the Eocene and Oligocene Deposits in the Chindwin Basin

Deposits and associated lithofacies of the Pondaung Formation are identical to those in the Minbu Basin farther south and have already been extensively described in Licht et al. (2014b); in the southernmost part of the Chindwin Basin, they have also been described by Oo et al. (2015). Briefly, the formation mainly consists of large, coarse-grained, sandstone bodies, 2–18 m thick, >100 m wide and are dominated by large sets (up to 1 m thick) of trough cross-bedding. The sandstone bodies are interfingered with fine-grained sequences, with pedogenised heterolithic deposits and extensive paleosol-bearing mudstone successions. Paleosols display vertic features and pedogenic nodules, as well as different stages of hydromorphic development, and were identified as

hydromorphic vertisols. In the Minbu Basin, these deposits have yielded a mix of freshwater riparian and brackish water mangrove trees (Licht et al., 2014a, 2015), continental vertebrates (Jaeger et a., 1999; Chaimanee et al., 2012), freshwater gastropods (Licht et al., 2014c), and occasional seawater fishes (Adnet et al., 2008). Paleocurrent measurements indicate an unequivocal westward flow (Fig. 5).

Our 1450 m composite sedimentary log of the Yaw and Letkat Formations is displayed in Figure 4. The sedimentary log starts ~500 m above the transition from the Pondaung Formation to the Yaw Formation, which is marked by the first occurrence of lignites and black mudstones. The log ends ~700 m below the transition from the Letkat to the Natma Formation, which is marked by a significant increase in fine-grained deposits (United Nations, 1978). In total, the thickness of the Yaw Formation is estimated to be around ~1000 m, and the Letkat Formation to be around ~1500 m.

Deposits of the Yaw Formation display ten lithofacies that can be divided into four facies associations (Table 1). Facies association FA1 is mainly made of massive black mudstones (Fm) interfingered either with siderite beds (Ls/Fm; Figs. 6A and 6B) or thinly planar laminated siltstones (Fs/Fm). Facies association FA2 is more diverse and is mainly composed of beds of siltstone to very fine sandstone showing planar laminations, small planar cross-laminations, and symmetrical cross-laminations with bundled and chevron upbuilding typical of wave-formed cross-laminations (Nichols, 2009). These fine-grained beds are sometimes interfingered with gray mudstones, forming flaser, lenticular, and wavy beddings (facies Sw); these interfingered beddings can contain trace fossils of Thalassinoides and Skolithos (Figs. 6C to 6H). More commonly, these beds show evidence for partial mixing and rootlets, and yield amber, fish bones, freshwater gastropods (thiarids; Licht et al., 2013) and unionid bivalves (facies Ssm; Fig. 6G). Sapropelic lignites rich in plant debris (facies Cs) also occur in sequences of facies Sw and Ssm, together with sequences of coarser, cross-laminated sandstones that are also rich in plant debris and occur in thick (commonly >1m) tabular sets (facies Sp).

TABLE 1.
LITHOFACIES AND FACIES ASSOCIATIONS IDENTIFIED IN THE YAW AND LETKAT FORMATIONS, CHINDWIN BASIN

Facies	Description	Interpretation
Facies association FA1		
Fm	Massive black mudstones; sets of 10 cm to 2 m; rare preserved planar laminations with millimeter spacing.	Settling in subaqueous anoxing conditions, below depth of wave action
Fs/Fm	Grey siltstones, either showing planar laminations or small planar cross-lamination (<1 cm); occurring in small sets (<5 cm); interfingered with thicker sets of massive black mudstones.	Settling in subaqueous anoxing conditions, close to the depth of wave action
Ls/Fm	Siderite beds; nodular or continuous; 5–20 cm thick. Always interfingered with thicker sets of black mudstones, creating apparent cycling mudstone/siderite alternations.	Post-depositional mineralization in subaqueous anoxic conditions
Facies association FA2		
Sw	Heterolithic facies dominantly made of siltstones to very fine sandstones forming either climbing ripple cross-laminations, symmetrical cross-laminations with bundled and chevron upbuilding, or wavy laminations. Set thickness varies from 5 to 40 cm, with undulating bounding surfaces, and interfingered with grey mudstone beds forming flaser, lenticular, or wavy beddings. In rare places, display trace fossils *Thalassinoides* and *Skolithos*.	Tidal flats
Ssm	Dark-grey siltstones to very fine sandstones, occurring in sets of 20 cm to 4 m. commonly structureless and mixed with mud, but can sometime show either planar lanimations, small (<3 cm) trough cross-laminations, symmetrical cross-laminations with bundled and chevron upbuilding. Yield amber; fish bones; freshwater gastropods and bivalves; rich in plant debris. Show sometimes rootlets.	Coastal marsh
Cs	Sapropelic lignite, 5–50 cm thick, made of thinly laminated organic debris, interfingered with millimeter-thick layers of silt to very fine sand.	Delta front deposits of a bay-head delta
Sp	Very fine to fine sandstones occurring in 20 cm to 4 m thick beds of small (3-15 cm) sets made of horizontal laminations, planar or trough cross-laminations. Rich in plant debris; can be rich in gastropods.	Distributary mouth, bay-head delta
Facies association FA3		
St	Fine to gravelly sandstones in 50 cm to 2 m sets of trough cross-laminations. Occurs in cosets of 2 to 5 sets, arranged in wing-shaped bodies that can be 10 to 100s of meters wide. Erosive lower bounding surface, sometimes accompanied with a 5–30 cm lag of mud clast breccias, conglomerates, rounded fossil bones, and fossil wood. Commonly rich in plant debris. Uppermost sets commonly show evidence of pedogenic development.	River channel
Sm	Very fine to coarse structureless, massive sandstones, in 50 cm to 4 m thick beds commonly overlying cosets of facies St. Mud matrix, dominantly red to brown, with green to blue mottles and rare pedogenic nodules.	Pedogenised overbank
Facies association FA4		
Cv	Massive lignite, laterally extensive, 20 cm to 2 m, commonly capping cosets of facies Sw, Ssm, or St. In some locations yields lignified fossil trunks, turtle plates, and continental vertebrates.	Swamp

Facies association FA3 is dominated by facies St, which consists of fine to coarse sandstones organized in meter-thick sets of trough cross-stratifications. These sets commonly occur in cosets of 3–5 sets, have an erosional base, and occasionally have a

basal lag full of mud-clast breccias and plant debris. These cosets occur in wide (sometimes >200 m) bodies that decrease in grain-size near their wings. In the area of Mawlaik, ~100 km north of Kalewa, sandstones are occasionally capped by structureless, pedogenised sandy beds mixed with a mudstone matrix, displaying a dominant brownish color, green mottles, sparse slickensides, and pedogenic nodules (facies Sm). This facies has, as of yet, only been observed in the uppermost layers of the Yaw Formation preceding the transition to the Letkat Formation. Finally, facies association FA4 is made of a single facies Cv, constituted of thick (up to 2 m), massive lignites that yield lignified fossil trunks and occasional vertebrate remains (Fig. 6I).

The four facies associations alternate following regular coarsening-upward cyclothems (FA1 to FA3) capped by lignites (FA4). FA3 is relatively rare and FA4 lignites can cap a smaller, FA1-FA2 sequence. The last 100 m of the Yaw Formation follows an overall coarsening upward sequence and FA3 sandstones become more common. The same facies associations can be found over the 100 km N-S area we investigated; lignite beds can be tracked over distances greater than 10 km and are currently mined for coal production. Palaeocurrents measured in FA3 trough crossbeds (facies St) cover a broad range of directions from S to WNW, with an average direction toward the southwest (Fig. 5).

There is no obvious angular unconformity at the contact between the Yaw Formation and Letkat Formation, but this contact is sharp, marked by the occurrence of several sandstones bodies with thick (>2 m) basal lags made of blocks of reworked sediment, altered siderite, and lignified fossil trunks (Fig. 6J). The Letkat Formation is only constituted of FA3. Facies St is commonly coarser than the sandstone beds observed in the Yaw Formation, and can be associated with gravels, silicified fossil trunks, and rounded vertebrate bones. We did not observe any inclined heterolithic stratification in the sandstone bodies; cosets of facies St are commonly occurring in wide (tens of meters) tabular or wing-shaped bodies. Facies Sm is also more present, usually capping 10–15 m cosets of facies St. Pedogenic features are different from what is found in the Pondaung and Yaw Formations; pedogenic nodules are rare, mottles are dominantly reddish or yellow, sometime root-shaped, and form well developed, 1–3-m-thick paleosol profiles, with increasing mottling and mixing upward resembling modern Ultisols (Fig. 6K). The first 200 m of the Formation are particularly coarse, with gravel beds made of rounded quartz being common. Gravels disappear after ~250 m, and most

of the remaining deposit is made of coarse St sandstones with occasional pedogenised Sm beds. Palaeocurrents measured in FA3 trough crossbeds (facies St) cover a broad range of directions from W to E, with an average direction toward the south-southwest.

4.2. Sulfur Content and Isotopic Composition

Lignites sampled for sulfur analysis can be grouped into two families (Fig. 7). A first family, with a low amount of sulfur (~<0.8%) and a narrow range of δ34S values, between –2 and +12‰ VCDT, corresponds to the values found in modern freshwater peats, where sulfur is particularly limited and mostly comes from plant sulfates (Casagrande, 1987). The second family display a much broader range of sulfur amount (up to 5%) and varying sulfur isotopic composition, from –10 to +20‰ VCDT, similar to those of peats formed under brackish water influence where regular inputs of seawater sulfate increases the availability of sulfur for bacterial reduction (Casagrande, 1987).

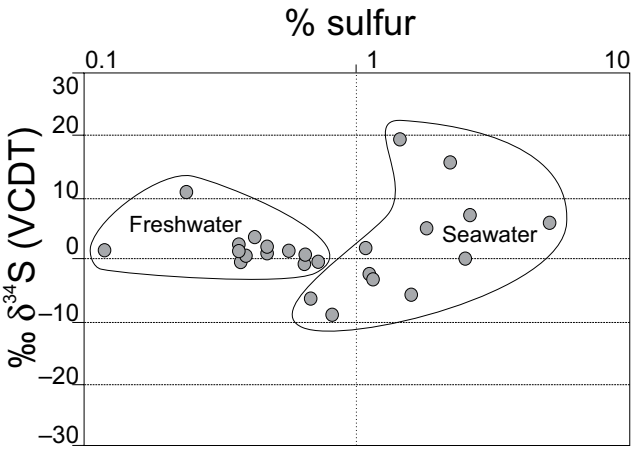

Figure 7*. Percentage of sulfur and sulfur isotopic composition (expressed in ‰ of deviation from the VCDT [Vienna Canyon Diablo Troilite] international standard) in lignites of the Yaw Formation. Values form two distinct families: one with low amount of sulfur (<1%) and a homogeneous sulfur isotopic composition, around 2‰ VCDT, and one with a wide array of sulfur content (up to 5%) and isotopic compositions (–6 to +6‰ VCDT).*

4.3. Sedimentary Provenance of the Paleogene Units

Sandstone grain-counting results are plotted on Q-F-L and Lm-Lv-Ls diagrams (Fig. 8) and compiled with previous data from Paleocene to middle Eocene units in the same section (Paunggyi, Tilin, and Pondaung Formations; Wang et al., 2014). Paleocene to middle Eocene sandstones are volcanic-rich, litharenitic and display similar grain-

counting results to those of the Paleogene turbidite sample from the Indo-Burman Ranges of Allen et al. (2008). By contrast, the Letkat Formation is dominated by volcanic-depleted quartzarenites. Sandstones from the Yaw Formation display intermediate features between both end-members. This evolution follows the same long-term pattern as sandstones in the nearby Minbu Basin (Licht et al., 2016). Eocene sandstones in the Minbu Basin are much poorer in volcanic lithics compared to the Chindwin Basin; only Miocene sandstones are purely quartzarenitic, plotting in the same area as Letkat sandstones on the QFL ternary diagram (Fig. 8). Carbonate lithic fragments were detected in insignificant proportions in all samples, as is also observed in the Minbu Basin (<1%).

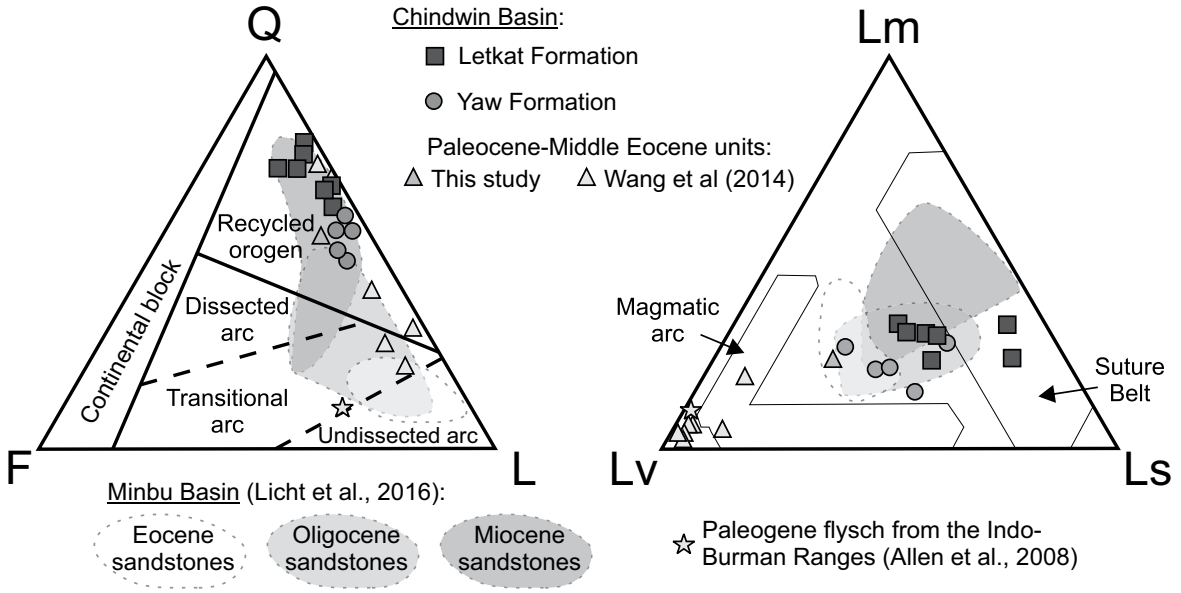

Figure 8*. QFL and LvLsLm plots of the Letkat Formation, Yaw Formation, and Paleocene-middle Eocene units from the Chindwin Basin (data from Wang et al., 2014, and this study), compared with Eocene to Miocene sandstones from the Minbu Basin (Licht et al., 2016) and a Paleogene turbidite from the Indo-Burman Ranges (Allen et al., 2008). Main provenance provinces following Dickinson (1985). Q—quartz; F—feldspar; L—lithic fragments; Lm—metamorphic; Ls—sedimentary; Lv—volcanic.*

Kernel density estimates (KDE) and age histograms of U-Pb age distributions of individual samples are shown in Figure DR2 (see footnote 1); individual samples are also compared with other samples from the forearc and backarc basin of central Myanmar on a multidimensional scaling map (MDS; Fig. 9). An MDS is a visual way to assess the misfit between age distributions using the Kolmogorov-Smirnov (KS) statistic

as the dissimilarity measure (Vermeesch, 2013). Ages from individual samples are grouped with previous samples of the Chindwin Basin from Wang et al. (2014) into three groups on Figure 10: Paleocene to middle Eocene units (n = 601 from six samples, including five samples from the Paunggyi, Tilin, and Pondaung Formations by Wang et al., 2014), the Yaw Formation (n = 202, from two samples), and the Letkat Formation (n = 470 from five samples, including one sample from Wang et al., 2014).

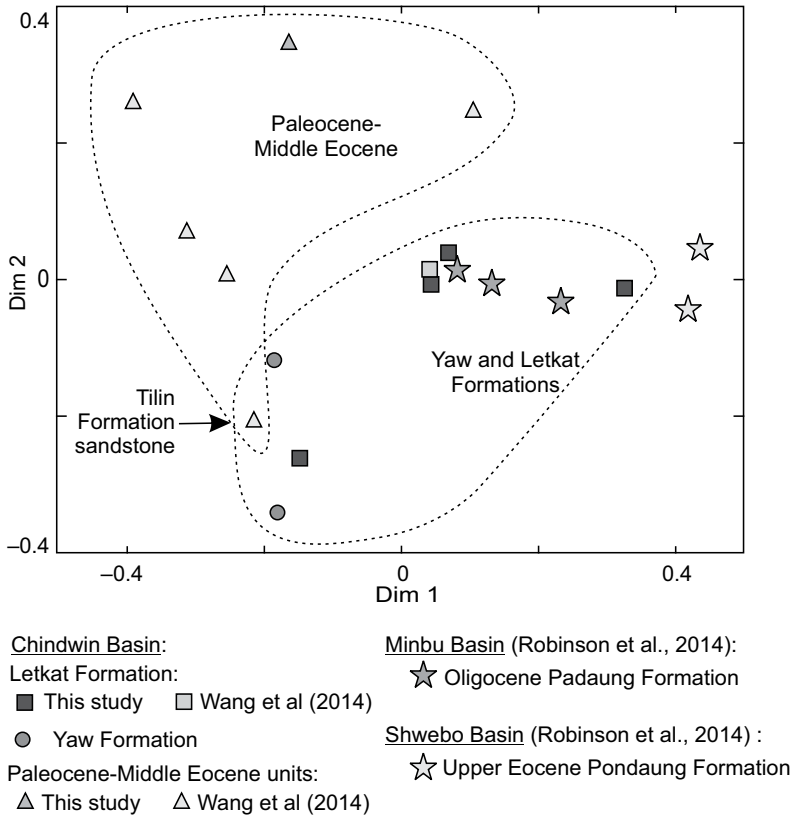

Figure 9*. Multidimensional scaling map showing the dissimilarities between individual samples of this study and previously published samples (Wang et al., 2014; Robinson et al., 2014). Axes are in dimensionless "KeS units" (–1 < KS < 1) of dissimilarity between samples. Final "stress" value is 0.06, indicating a fit between "good" and "fair" (Vermeesch, 2013). Ranges of variation for individual samples of Paleocene–middle Eocene and younger deposits from the forearc basin are highlighted by dashed lines.*

Paleocene to middle Eocene sandstones from the Chindwin Basin are dominated by Late Cretaceous (ca. 90–120 Ma) zircons, with a secondary population of Paleogene (40–60 Ma) zircons. Except for a single sample (sandstone from the Tilin Formation; Wang et al., 2014), Paleocene to middle Eocene sandstones lack grains older than Late Cretaceous and are statistically distinct from younger sandstones on the MDS plot (Fig. 9). U-Pb zircon ages from a sandstone of the Pondaung Formation at the southernmost edge of

the Chindwin Basin (Oo et al., 2015) corroborate the lack of older zircons in Paleocene-middle Eocene sandstones but should be interpreted with caution because of the low amount of zircon ages (n = 54). Upper Eocene to lower Oligocene sandstones from the backarc basin (Robinson et al., 2014) are similarly exempt of older zircons, but are dominated by Paleogene grains.

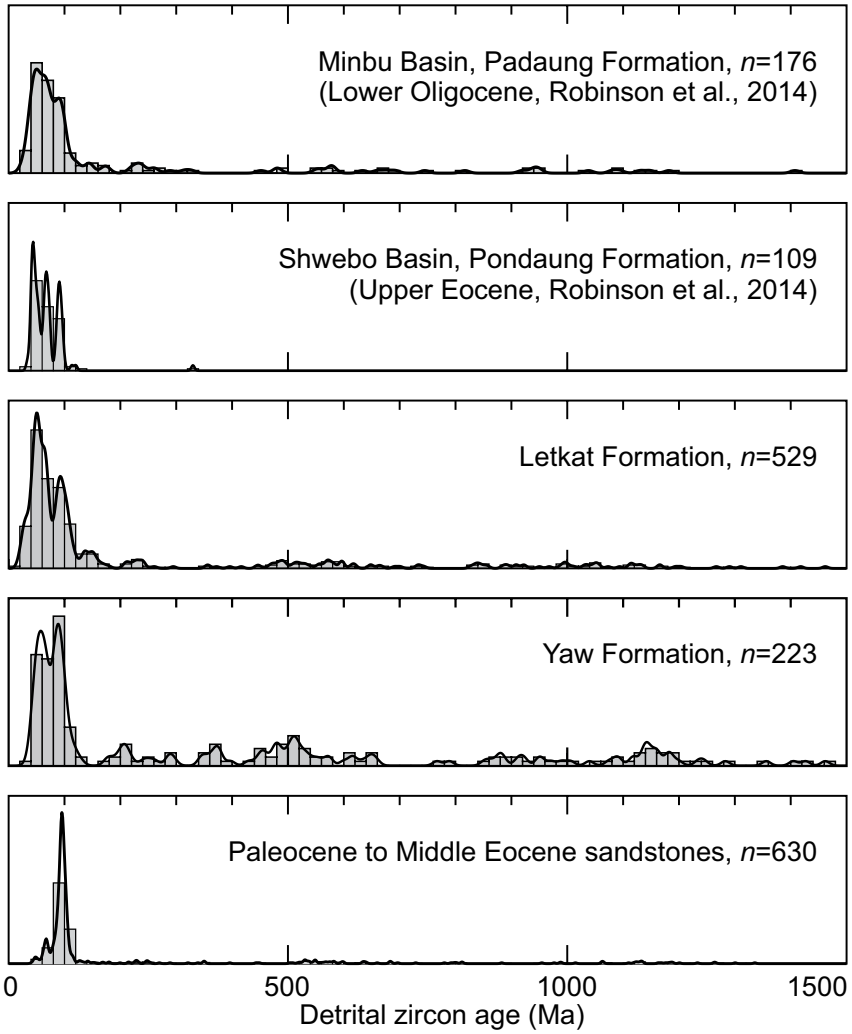

***Figure 10**. Kernel density estimators (KDE) and histograms (20 m.y. bins) for Paleocene to middle Eocene sandstones from the Chindwin Basin (n = 601, combining two samples from the Paunggyi Formation, one sample from the Tilin Formation, and two samples from the Pondaung Formation, all from Wang et al., 2014, and one sample from the Paunggyi Formation from this study), from the Yaw Formation (n = 202, two samples from this study), and from the Letkat Formation (n = 470, combining four samples from this study and one from Wang et al., 2014), compared to upper Eocene sandstones from the Shwebo (backarc) Basin (n = 109, two samples from Robinson et al., 2014) and lower Oligocene sandstones from the Minbu Basin (n = 176, three samples from Robinson et al., 2014). The kernel density bandwidth of each plot was determined with the plug-in bandwidth selection method of Botev et al. (2010).*

Samples from the Yaw Formation yield a significant proportion of older zircons, with two notable peaks at 500 and 1200 Ma, as well as a prominent population of Paleogene zircons. This trend continues in the sandstones of the Letkat Formation, which display a dominant Paleogene peak and numerous Proterozoic zircons. Yaw and Letkat samples occupy the same space on the MDS plot. Samples from the lower Oligocene Padaung Formation (Robinson et al., 2014) in the nearby Minbu Basin display the same features. These features are also shared by Neogene samples from central Myanmar (Wang et al., 2014), as well as in most modern river samples draining the central Myanmar Basins (Garzanti et al., 2016).

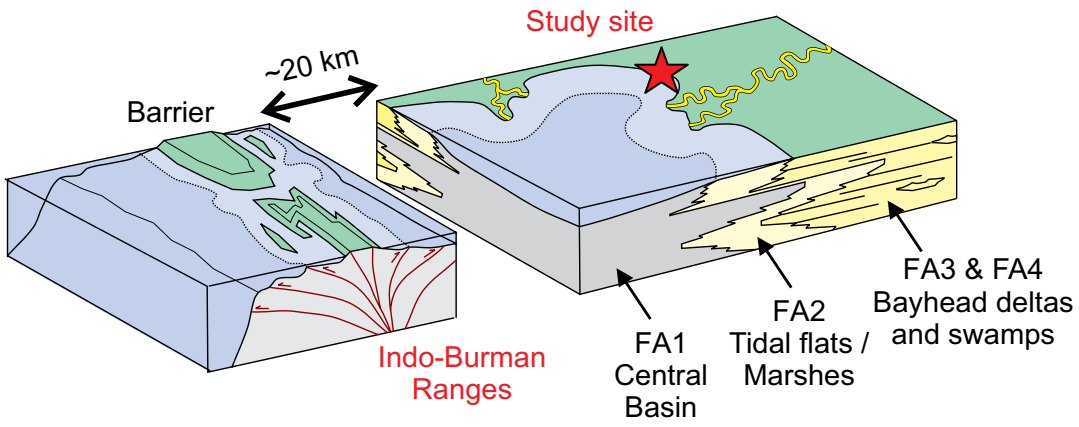

Figure 11. *Depositional model for the Yaw Formation, inspired from the depositional model of tropical estuary of the Ouémé River in Benin (Anthony et al., 2002). Facies Association FA1 represents the central basin of a quasi-closed estuary; FA2 reflects the coastal/intertidal component; FA3 represents distributary channels of the bayhead delta; and FA4 deltaic swamps. We propose that the nascent Indo-Burman Ranges provided the necessary barrier to close the estuary.*

4.4. Age Model for the Yaw and Letkat Formations

Youngest U-Pb ages of detrital zircons from three samples and U-Pb ages of a sampled tuff are displayed on Figure 4. The maximum age of the Yaw Formation is constrained by a maximum depositional age of 39.0 ± 0.8 Ma (2σ; n = 1 zircon) at the very most base of the formation ~500 m below the composite log. Although ages based on a single zircon must be interpreted with caution, this age is in agreement with the age estimate for the unit just below, the Pondaung Formation, the upper member of which is dated at 40–39 Ma in the Minbu Basin via a combination of biostratigraphy, geochronology, and

magnetostratigraphy (see review in Licht et al., 2015). The tuff is located at level ~1000 m in the formation, ~180 m below the transition to the Letkat Formation, and yields a 38.3 +0.7/–0.9 Ma (2σ; n = 13 zircons) volcanic age. This indicates an upper Bartonian age for the Yaw Formation and extremely fast sedimentation rates (>1 m/k.y.). Assuming a similar accumulation rate, the last beds of the Yaw Formation occurred close to the Bartonian–Priabonian Boundary at 37.8 Ma (Gradstein et al., 2012).

Sandstones from the base of the Letkat Formation did not yield younger zircons, but a sample ~350 m above the base of the formation yielded a maximum depositional age of 26.9 +0.4/–0.9 Ma (2σ; n = 4 zircons). A second sample at the top of our section, ~780 m below the top of the Letkat Formation yielded a single zircon at 20.2 ± 0.5 Ma (2σ); however, a more robust maximum depositional age of 23.5 +0.3/–0.4 Ma (2σ; n = 3 zircons) was calculated using more zircons. This suggests that the upper part of the Letkat Formation is upper Oligocene or possibly lower Miocene in age. Assuming that these maximum depositional ages are close to actual depositional ages due to the proximity of an active volcanic arc, the sedimentation rate of the Letkat Formation was much lower than for the Yaw Formation (~15 cm/k.y.). This slow accumulation rate suggests that the base of the Letkat Formation would start, or be younger than, ca. 29 Ma and that most of the lower Oligocene is missing in our section.

5. DISCUSSION

5.1. Depositional Environments of the Paleogene Forearc

The depositional environments of the Pondaung Formation in the Minbu Basin have previously been interpreted as reflecting a deltaic floodplain environment created by westward-prograding fluvial systems, where avulsive channels, crevasse belts with heterolithic deposits, and pedogenic floodplain fines laterally grade into each other (Licht et al., 2014b). Our observations in the Chindwin Basin are in line with this interpretation.

The combination and alternation of facies association FA1 to FA4 in the Yaw Formation is in many ways diagnostic of barrier-bound estuaries (Dalrymple et al., 1992). FA4 and FA3 are attributed to coastal swamps (paleo-histosols) and bayhead deltaic river distributaries, respectively. Sulfur content and isotopic composition indicate that whereas some of the swamps developed in a brackish setting, most were freshwater (Casagrande, 1987). FA2 reflects near-shore environments with several variations. Facies Sp and Cs can be interpreted as representing deltaic lobes and the delta front of

bayhead deltas in the estuary bay (Anthony et al., 2002; Leeder, 2009). Facies Sw, with its evidence for wave-action, heterolithic stratifications with flaser, lenticular, and wavy bedding, indicates a tidal flat environment, which are commonly found along the shores of estuaries (Tessier et al., 1995).

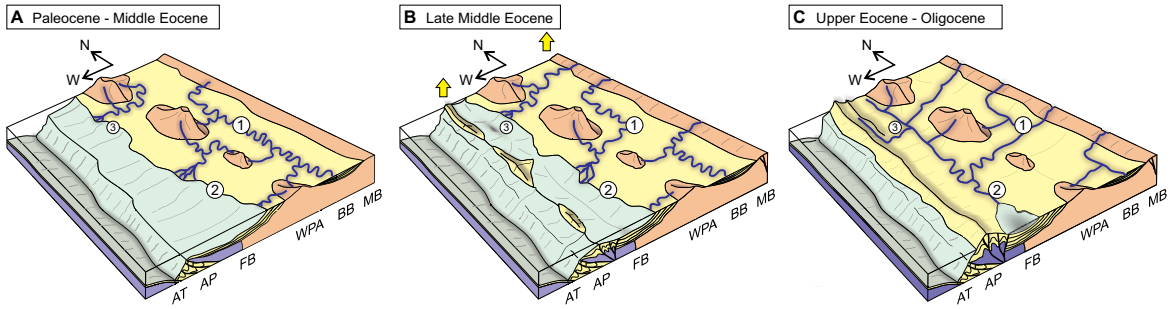

Figure 12*. Evolution of the Burmese subduction margin and forearc basin from the Paleocene–middle Eocene (A), the late middle Eocene (B), and the upper Eocene–Oligocene (C). 1, 2, and 3 indicate the location of the Shwebo, Minbu, and Chindwin basins respectively (same as on Fig. 2). AT—Arakan Trench; AP—accretionary prism; FB—forearc basin; WPA—Wuntho-Popa Arc; BB—backarc basin; MB—metamorphic belts.*

This interpretation is corroborated by the presence of trace fossils Thalassinoides and Skolithos commonly found on firm grounds of tidal flats (Gingras et al., 2001). The prominent facies of this facies association, Ssm, contains evidence of wave-action and pedogenesis, but lacks well-marked tidal influence, and is interpreted here as reflecting either an intertidal marsh or a more vegetated shoreline (Allen, 2000). Finally, facies association FA1 reflects the sub-tidal central basin depositional environment of a barrier-bound estuary, where massive organic-rich mud is prominent (Anthony et al., 1996). The presence of marked anoxic conditions in the central basin, shown by the common occurrence of siderite beds (Mozley and Wersin, 1992), suggests poor mixing of deep water and a quasi-closed character for the estuary. Taken together, these facies associations closely resemble those of the tropical estuary of the Ouémé River in Benin, which is bounded by a large sand barrier created by longshore drift (Anthony et al., 2002). Interestingly, the relative rarity of facies Sw, the notable absence of any marine fossils, the relative abundance of freshwater gastropods and unionids, and the overall low sulfur content in most of the coal suggests periods of intermittent estuary closure and shift to lacustrine setting, as is sometimes observed in barrier-bound estuaries (Roy et al., 1994).

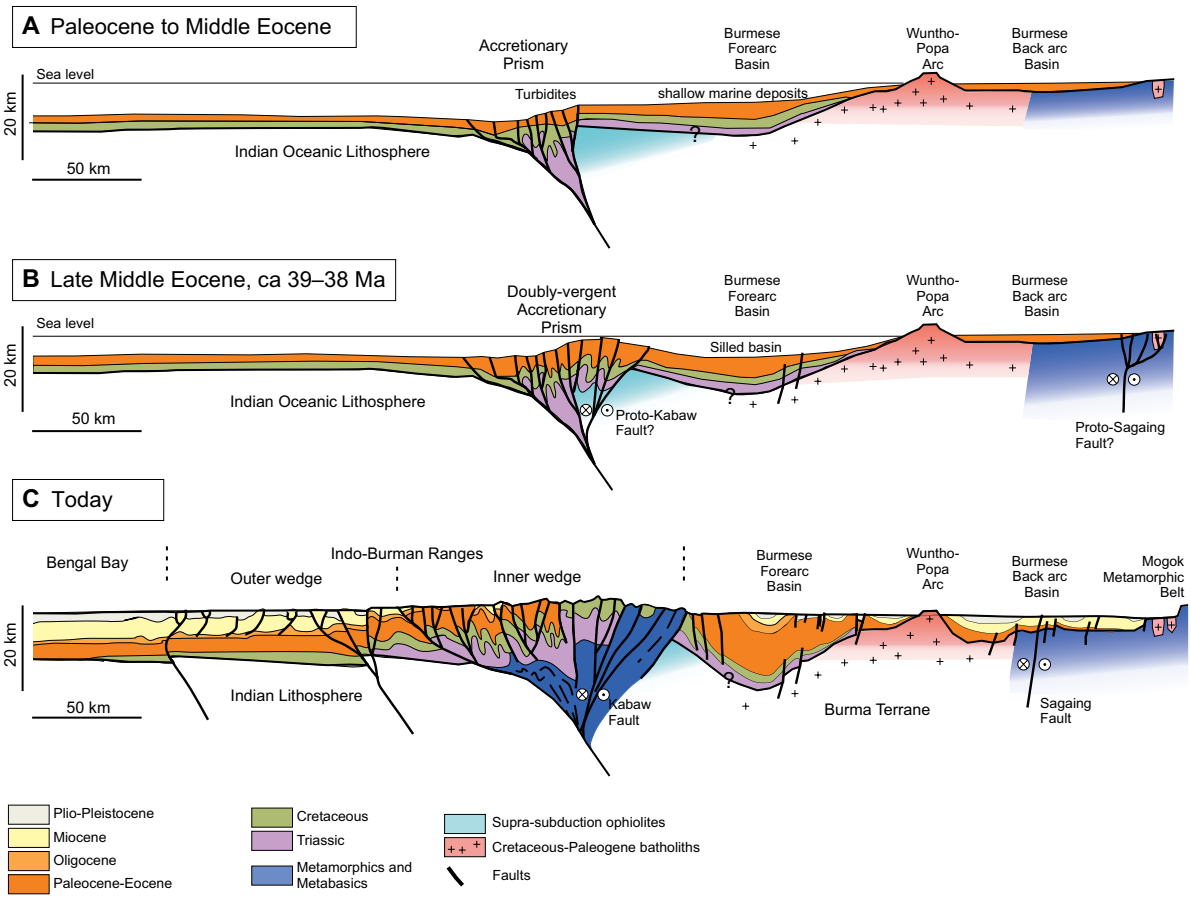

Figure 13. *Schematic cross section across a W–E transect in western and central Myanmar (location on Fig. 2) during the Paleocene–middle Eocene (A), late middle Eocene (B), and today (C; after Maurin and Rangin, 2009). The question mark indicates that the presence of Triassic rocks thrusted on the ophiolitic basement of the forearc is still unclear.*

Thick, wide bodies made of cosets of facies St that lack any clear inclined heterolithic stratification and are capped by pedogenised, finer grained sets of facies Sm suggest fluvial channel bodies typical of braided river systems and associated overbank deposits (Leeder, 2009). The shift to pure fluviatile deposition and the presence of a depositional hiatus at the contact between the Yaw and Letkat Formations indicate that by the end of the Yaw Formation and for most of the Oligocene, the Chindwin Basin was overfilled. Moreover, paleocurrent flow measurements from the Letkat Formation indicate a shift in drainage orientation from westward-oriented in the Eocene to southwestward-oriented in the Oligocene.

5.2. Tectonic Implications for the Evolution of the Accretionary Prism

Extremely high accumulation rates (>1 km/m.y.) imply similar rates of basin subsidence to keep the bathymetry close to the tidal/shallow lacustrine domain, and indicate an

active tectonic regime during the deposition of the Yaw Formation. To maintain the quasi-closed estuarine conditions over hundreds of meters of section, a permanent barrier is needed offshore to the west of our site in the area that is today occupied by the Indo-Burman Ranges. Wave-formed sandspits could have partly acted as a barrier, but the scale of the estuary (>100 km wide along the Burmese coast) is 5–10 times larger than modern wave-formed estuaries (Dalrymple et al., 1992).

Southward-directed flow measurements in the Letkat Formation indicate that by the late Oligocene, the Indo-Burman Ranges must have emerged on the western side of the Chindwin Basin in order to stop the westward progradation of fluvio-deltaic systems and instead drain fluvial systems southward. This corroborates preliminary work in the Minbu Basin farther south, where southward-prograding deltaic systems are observed starting in the early Oligocene (Gough and Hall, 2017). Incipient uplift of the accretionary prism must thus have started during or before the Oligocene. We propose that the quasi-closed estuarine conditions of the Yaw Formation in the Chindwin Basin reflect the initial emergence of the Indo-Burman Ranges offshore, which provided the necessary near-sea level topographic barrier (Fig. 11). This interpretation implies that by 39–38 Ma, the Indo-Burman Ranges were already being uplifted and were partly emerged. This timing is in agreement with geochronological data from Paleogene turbidites in the accretionary wedge farther south in the Indo-Burman Ranges, which yielded a persistent youngest zircon-fission track population at 37 Ma (Allen et al. 2008), roughly coeval to the unconformity at the top of the Yaw Formation and the complete in-filling of the estuary. A major shift from westward-oriented drainage into the proto–Bengal Bay to southward-oriented drainage systems parallel to the subduction margin would have occurred after the complete emergence of the accretionary prism and the in-filling of the Chindwin basin estuary around ca. 37 Ma.

5.3. Comparison with the Minbu Basin and Implications for the Onset of Pull-Apart Subsidence

There is a lack of sedimentological data regarding the Yaw Formation in the Minbu Basin, but the little we know contrasts with our observations in the Chindwin Basin. In the Minbu Basin, the Yaw Formation consists of gray shales with occasional limestone beds rich in shallow-marine trace fossils and fossil mollusks (Bender, 1983; Licht et al., 2013). Lignites and organic-rich black mudstones are absent. Additionally, the Minbu Basin lacks a depositional hiatus in the upper Eocene, and instead records continuous

sedimentation into the lower Oligocene Padaung Formation (Nagappa, 1959). The Minbu Basin Yaw Formation is also much thinner (only ~700 m thick at the western edge of the basin; United Nations, 1978). This indicates much lower accumulation rates (<200 m/m.y.) in the late Eocene and similarly slow rates of basin subsidence to keep the bathymetry close to shallow-marine conditions. Similar shallow-marine environments, accumulation rates and associated subsidence continued through the late Oligocene, with the deposition of the Shwezetaw, Padaung, and Okhmintaung Formations (United Nations, 1978).

During the late Paleogene, the Chindwin and Minbu Basins thus appear to have followed a significantly different subsidence history. Whereas subsidence was continuous in the Minbu Basin and bathymetry kept pace with moderate accumulation rates, subsidence was extremely high around 39–38 Ma in the Chindwin Basin and significantly slowed down at 37 Ma, leading to a stop of accumulation for most of the late Eocene and early Oligocene—resulting in the observed unconformity between the Yaw and Letkat Formations. These results indicate that by 39 Ma, the forearc was already partitioned into individual sub-basins with different histories. The high subsidence rates in the Chindwin Basin are in agreement with strike-slip deformation and pull-apart subsidence as the main mechanisms for forearc basin partitioning, as proposed by Rangin et al. (1999). The ~22°N latitude topographic high, that today geomorphologically separates the two basins might have already been partly emerged or at least might have subsided more slowly, partly closing the Chindwin estuary to the south. Precise age constraints for the other Cenozoic units of the forearc basin—for a detailed backstripping analysis—and basin-wide seismic lines are as of yet still lacking, preventing us from unequivocally confirming pull-apart subsidence as the main mechanism here; however, our interpretations suggest that the onset of basin pull-apart formation and strike-slip deformation of the basin margin dates back to at least 39 Ma, if not older.

5.4. Provenance of the Paleogene Forearc Sediment and Implications for the Exhumation of the Metamorphic Belts

Our grain-counts and U-Pb ages distributions from Paleocene to middle Eocene sandstones indicate a provenance from Late Cretaceous–Paleogene rocks, likely the Wuntho-Popa magmatic arc located ~100 km to the east, which was active during the same period and displays the same age peaks (Mitchell et al. 2012; Wang et al., 2014; Gardiner et al., 2015, 2017; Zhang et al., 2017b). Robinson et al. (2014) proposed a

provenance from the Gangdese Arc in Tibet via a paleo-connection between Tibet and the Central Myanmar Basins using εHf fingerprinting of detrital zircons, but Zhang et al. (2017b) showed that zircons from the Wuntho-Popa Arc hold the exact εHf fingerprint as Gangdese batholiths. Additionally, a proximal source is corroborated in the Minbu Basin by Nd and Sr isotopic values, grain-counts, and paleocurrents that all indicate a nearby volcanic source located east of the forearc (Licht et al., 2013). Interestingly, the relatively high amount of quartz in samples from both Chindwin and Minbu basins suggests that part of the arc plutonic root might have already been exhumed in the late middle Eocene, corroborating a possible early uplift of the volcanic arc (Zhang et al., 2017b). Paleocene to middle Eocene samples from the Chindwin Basin contain slightly more volcanic lithic grains compared to coeval samples from the Minbu Basin (Fig. 8), indicating small lateral changes in the lithology of the exposed rocks along the Burmese subduction margin. The higher amount of sedimentary lithics in the Minbu Basin could reflect the recycling of older sedimentary rocks upstream, or ephemeral connections to the backarc basin and areas farther east, as one sample from the Tilin Formation seems to suggest (Fig. 9).

Sandstones from the Yaw Formation are marked by an increase of petrographic maturity and a significant amount of older (>150 Ma) zircons, which are almost absent in older sandstones. This trend is even more pronounced in sandstones of the Letkat Formation and indicates an increased contribution from older, quartz-rich basement rocks. In central Myanmar, basement rocks crop out in only a few areas: (1) to the east of the backarc basins along the Mogok, Slate, and Gaolingong metamorphic belts, where Paleozoic plutons and older metamorphics are prevalent; (2) occasionally farther east on the Shan Plateau, where Paleozoic and upper Mesozoic clastics crop out; and (3) to the west of the forearc in the metamorphosed core of the inner wedge of the accretionary prism, where small pockets of Triassic metamorphics crop out (Fig. 2; Licht et al., 2016). Our paleocurrent measurements in the Yaw Formation rule out the accretionary prism as a potential source; rather, our results indicate an increased contribution from the metamorphic belts and the Shan Plateau to the east. The absence of carbonate clasts—the dominant lithology on the Shan Plateau—suggests that the metamorphic belts are the primary contributor.

Similar age distributions are found in lower Oligocene samples from the Minbu Basin (Fig. 10; Robinson et al., 2014), suggesting a similar provenance. Following the onset of

southward drainage systems ca. 37 Ma, a portion of the lower Oligocene material reaching the Minbu Basin might have transited via the Chindwin Basin. We unfortunately do not have any U-Pb data from the Yaw Formation in the Minbu Basin to test if the shift to a more mature source is older or coeval to the provenance change at ca. 39–38 Ma observed in the Chindwin Basin. However, Nd isotopes, Sr isotopes, and grain-counts on sandstones in the Minbu Basin corroborate an increased contribution of the metamorphic belts in the sedimentary supply starting in the late Eocene (Licht et al., 2016).

There are unfortunately few geochronological and petrographic data from the backarc basin to compare our results with. Two upper Eocene samples from the backarc basin contain only Cretaceous-Eocene zircons (Robinson et al., 2014), unlike what we see in Yaw and Letkat Formation sandstones. Although any interpretation based on only two, low n (<60) samples is premature, we suspect that these samples might reflect local tributaries flowing down the Wuntho-Popa volcanic arc that do not reflect any contribution from the metamorphic belts that would have supplied older (>150 Ma) grains.

Our results thus show that by 39–38 Ma the Chindwin Basin had started receiving a regular supply of sediment from the metamorphic belts to the east. Interestingly, this age is roughly coeval with the 37.4 ± 1.3 Ma (2σ) onset of gneiss formation and proposed onset for high-grade metamorphism (Searle et al., 2007), as well as the 36.2 ± 1.6 Ma (2σ) age for the oldest 40K-40Ar exhumation age along the metamorphic belts (Bertrand et al., 2001), showing the existence of a paleo–"Shan Scarp fault" system in the backarc areas predating the modern Sagaing Fault system. Our results thus confirm that the onset of high-grade metamorphism during the late middle Eocene is associated with an early exhumation episode of the metamorphic belts, which started providing sediment to the forearc basin. Ephemeral exhumation events might have started earlier in the middle Eocene, as suggested by one sample from the middle Eocene Tilin Formation (Fig. 9) and two middle Eocene overgrowth ages in zircons of the Mogok Metamorphic Belt (Barley et al., 2003).

5.5. Evolution of the Burmese Subduction Margin during the Paleogene and Mechanisms of Uplift for the Indo-Burman Ranges

We propose a three-step scenario for the evolution of the Burmese margin during the Paleogene (Figs. 12 and 13).

(1) From the Paleocene to the middle Eocene, the Burmese subduction margin displays the regular morphology of Andean-type margins, with a nascent, underwater accretionary prism, and a forearc basin open to the trench occupied by westward-prograding deltaic systems fed by the denudation of the volcanic arc (Figs. 12A and 13A).

(2) In the late Bartonian–earliest Priabonian, around 39–38 Ma, the accretionary prism starts to emerge (Figs. 12B and 13B). The forearc basin is partitioned into two basins with varying subsidence rates likely due to pull-apart subsidence; the Minbu Basin in the south remains open to the proto–Bengal Bay to the west and the south, while in the north, quasi-closed estuarine conditions develop in the Chindwin Basin. Simultaneously, the metamorphic belts located to the east are progressively exhumed and start to feed the forearc.

(3) By 37 Ma, the Paleogene accretionary prism, that today forms the inner wedge of Indo-Burman Ranges, is completely emerged. The Chindwin Basin is temporarily overfilled and drainages in central Myanmar become southward directed (Fig. 12C). The modern geomorphology of central Myanmar is set up, with the central Myanmar low plains enclosed on the west and the east by topographic highs (Fig. 13C).

The 39–38 Ma window thus appears to be a period of significant change for the subduction margin, with the emergence of the inner wedge of the Indo-Burman Ranges, the first evidence of exhumation of the metamorphic belts, and the first indication of pull-apart partitioning of the forearc basin. Exhumation of the metamorphic belts could have sporadically started earlier in the middle Eocene, as discussed earlier, but the metamorphic belts became a prominent, continuous sediment supplier starting at 39–38 Ma. Similarly, pull-apart subsidence of the basin might have started earlier, but the forearc appears to be significantly partitioned during this time window.

Earlier onset of uplift and exhumation of the accretionary prism is also probable, as proposed by previous authors (as early as the Cretaceous; Socquet et al., 2002; Zhang et al., 2017a). However, the inner wedge lacks shallow-marine deposits and is dominated by marine turbidite sequences (Bender, 1983), indicating that depositional environments shifted very quickly from deep-sea deposition in the trench to sub-aerial deposition. It is thus likely that most of the uplift started only slightly before 39–38 Ma.

Contacts between sedimentary units exposed in the inner wedge provide a few more details about what happened after this early uplift of the accretionary prism. On the

eastern side of the inner wedge of the accretionary prism, Eocene marine rocks are unconformably overlain by a conglomeratic molasse, the Maw Gravels, which yield late middle Miocene fossil mammals (Bender, 1983). In places, a 10-m-thick, ferralitic paleosol profile with a 0.5–1-m-thick petroplinthic horizon made of continuous, thick iron crust developed in the Eocene rocks at the contact between both units (Fig. DR3 [see footnote 1]; Licht, 2013). The thickness of the lateritic profile and the presence of a petroplinthic horizon indicate that the development of the paleosol likely took a significant amount of time—up to several million years (Valeton, 1994). This finding indicates that there was a long period of tectonic quiescence between the initial uplift of the inner wedge during the late Eocene and the deposition of the late middle Miocene Molasse. The deposition of the Maw Gravels was likely related to the onset of the recent, Mio-Pliocene uplift of the Indo-Burman Ranges that exposed the outer wedge of the accretionary prism (Maurin and Rangin, 2009). The uplift of the Indo-Burman Ranges thus appears to have occurred in at least two steps: first, during the late Eocene when the inner wedge was exposed, and second, during the late Miocene–Pliocene when the outer wedge was formed.

Various mechanisms are proposed to explain the late Miocene-Pliocene uplift of the Indo-Burman Ranges, including the subduction of the large amount of Neogene sediments that fill up the Bengal Basin and the Sylhet Basin (Maurin and Rangin, 2009), and increased E-W shortening of the Burmese platelet due to the arrival of mid-crustal flow from the east following the late Miocene collapse of the Tibetan Plateau (Rangin et al., 2013). However, these mechanisms are only valid for the Neogene and cannot explain the late middle Eocene uplift of the inner wedge.

A temporary shift to flat slab subduction could explain the uplift of the accretionary prism, but would not explain the extremely high subsidence rates in the foreland basin or the high-grade metamorphism throughout the backarc areas (Finzel et al., 2011). The accretion of a small allochthonous terrane or volcanic arc, as proposed by others (i.e., Acharyya, 2007, 2015), could partly explain the uplift, but would also fail to explain the coeval shift to intense strike-slip deformation and subsidence in the forearc; there is also no clear evidence for such allochthonous blocks in the accretionary prism. A change of plate kinematics driving increased E-W convergence and upper plate shortening could also explain the shift to a more compressive regime and the resulting uplift of the accretionary prism; however, in the Paleogene, the convergence of the Indian plate

relative to Southeast Asia trended to lower velocities and increased obliquity, which would not favor this hypothesis (Lee and Lawver, 1995; Cande et al., 2010; van Hinsbergen et al., 2011b). Still others have proposed a collision of a northeast moving Indian plate with the Burmese margin slightly before 39–38 Ma followed by a change of convergence direction from NE to N (Morley, 2002; Aitchison et al., 2007; Vérard et al., 2017). The collision could have anchored the Burmese platelet to India and dragged it northward as the direction of convergence changed, providing an explanation for an episode of shortening in the accretionary prism followed by strike-slip deformation of the upper plate. However, it is remarkable that such a collision between a cold, thick continental plate and the weak, hot Burmese margin (Morley, 2009) did not result in more surface deformation and uplift; moreover, strike-slip deformation (and related pull-apart subsidence) seems coeval rather than posterior to accretionary wedge uplift.

Today, the obliquity ratio (ratio of the strike-slip velocity divided by the sum of strike-slip and normal velocity) of the convergence along the Burmese subduction margin is ~0.65 and so can be called "hyper-oblique" (Nielsen et al., 2004). The core of the inner wedge of the Indo-Burman Ranges displays a positive flower structure and is traversed by the Kabaw strike-slip Fault, which accommodates 1/4–1/3 of the N-S strike slip deformation of the Burma Terrane (Nielsen et al., 2004; Socquet et al., 2006; Maurin and Rangin, 2009). In this sense, the inner wedge of the Indo-Burman Ranges is very similar to retro-wedges formed along hyper-oblique convergence zones where the obliquity ratio r is > 0.5 (Burbidge and Braun, 1998; McClay et al., 2004). The Eocene uplift of the inner (retro-) wedge of the Indo-Burman Ranges can be explained in light of the known evolution of accretionary prisms formed by hyper-oblique convergence. Such systems go through a period of fast retro-wedge building and uplift via the transition from localized strain partitioning in the accretionary wedge to full strain partitioning, and all strike slip motion is eventually accommodated by one or several individual fault systems (McClay et al., 2004; Leever et al., 2011). Evidence of coeval pull-apart subsidence and partitioning in the forearc and of the onset of high-grade metamorphism associated with exhumation of the metamorphic belts corroborates intense shear and strike-slip faulting on the Burma platelet during that time. Thus, we interpret the late middle Eocene uplift of the Indo-Burman Ranges as reflecting localized strain partitioning and wedge build-up prefiguring the onset of a paleo-Kabaw Fault system ("oblique wedge stage" of Leever et al., 2011). The onset of full strain partitioning and of the paleo-Kabaw Fault

system would have been coeval or have shortly followed the late middle Eocene, eventually slowing the uplift of the accretionary wedge.

5.6. Implications for the History of India Asia Convergence

Our interpretations imply that the convergence of the Indian plate along the Burmese margin has been hyper-oblique since at least the late Bartonian, ca. 39–38 Ma, and that it resulted in the coeval uplift of the inner wedge of the accretionary prism, pull-apart subsidence and partitioning of the forearc basins, and high-grade metamorphism and exhumation along the metamorphic belts (Fig. 13). While the modern Burmese sliver fault system is commonly dated to the middle Miocene and the opening of the Andaman Sea (Khan and Chakraborty 2005; Socquet et al., 2006), our results suggest that a similar paleo-sliver system, with a paleo-Kabaw Fault in the accretionary prism and a paleo–Shan Scarp Fault in the metamorphic belts, was already set up by the late middle Eocene or shortly thereafter (Fig. 13B). These observations corroborate evidence for ca. Eocene to ca. Miocene syn-kinematic deposition in the backarc basin, indicating that a proto–"Shan Scarp" Fault was already active (Morley, 2017). Strike-slip deformation of the Burmese margin could have started even earlier, sometime in the middle Eocene, but would have been less substantial.

Our results thus suggest that the northward drag of the Burmese platelet pre-dates the opening of the Andaman Sea and the set-up of the modern sliver system in the middle Miocene by at least 20 million years. Central Myanmar has thus likely moved northward by much more than 400–500 km, which is the lower-end estimate of northward motion achieved by simply closing the Andaman Sea rift system (Maung, 1987). We suspect that the actual motion of Central Myanmar over this time period to be closer to Mitchell's (1993) upper estimate of ~1100 km, with 600–700 km of the motion occurring between the late middle Eocene and the middle Miocene; this movement was accommodated to the opening of the Eocene-Miocene Mergui and North Sumatra Basins south the Andaman Rift (Hall and Morley, 2004).

There is no clear evidence for shortening and surface uplift in central Myanmar before the late middle Eocene. Leading up to the shift in sedimentation regime 39–38 Ma, accumulation in the forearc basin was continuous and dominated by the denudation of the volcanic arc from the Paleocene to the late middle Eocene, as is seen in standard Andean-type margins, and thus rules out a collision with India. A collision of the Indian Plate with the Burmese margin sometime during the early to middle Eocene, as is

proposed by most of the kinematic models dominated by extrusion processes (Tapponnier et al., 1982; Replumaz and Tapponnier, 2003; Replumaz et al., 2010; Cogné et al., 2013), and more exotic scenarios (Aitchison et al., 2007; Vérard et al., 2017), seems thus unlikely. If such a collision had occurred, it would have been located in northernmost Myanmar, in the Eastern Himalayan Syntaxis—where forearc strata have not been preserved (Fig. 2), leaving most of the Burmese margin undeformed.

Our reconstruction of the history of the Burmese subduction margin validates geodynamic models that locate Myanmar east of the collision zone as early as the Paleocene, with Indochina already forming a narrow peninsula at the southeastward extremity of East Asia. This narrow peninsula must have had a similar-to-today N-S orientation since at least the late middle Eocene to explain hyper-oblique convergence along the Burmese margin. In this sense, our results are in agreement with models dominated by homogeneous thickening and continuous deformation of weaker Asian lithosphere that propose a conservative, similar-to-today pre-collisional paleogeography for SE Asia and argue that most of Myanmar and the Burma Terrane was not particularly shortened or thickened by the collision with India (Fig. 1C; e.g., England and Houseman, 1986; Molnar et al., 1993; Hallet and Molnar, 2001; Shen et al., 2001; van Hinsbergen et al., 2011a, 2012; Hall, 2012; Seton et al., 2012). However, our results do not completely exclude extrusion and rotation processes as active post-collisional processes in SE Asia; the shift to hyper-oblique convergence along the Burmese margin could be explained by an undetermined amount of post-collisional rotation of peninsular Indochina. Our reconstructions show that this rotation must have been achieved by 39–38 Ma to explain the onset of hyper-oblique convergence along the Burmese margin. The idealized extrusion-dominated reconstructions of van Hinsbergen et al. (2011a), adapted from Replumaz and Tapponnier (2003) and Royden et al. (2008) are the closest analogues to this scenario. Paleomagnetic estimates of post-collisional clockwise rotation in peninsular Indochina yield results of variable magnitude, with estimates of 20–30° for the whole of Indochina (Richter and Fuller, 1996; Charusiri et al., 2006; Li et al., 2017), and as much as >70° in some places (Sato et al., 2001; Tong et al., 2016). Yet, the lack of detailed geological data in peninsular Indochina (i.e., ages and origins of volcanism and metamorphism along shear zones) often precludes a robust age interpretation for this rotation, as evidenced by the recent synthesis of Li et al. (2017), and ultimately hinders a clear evaluation of the accuracy of this scenario.

We also see three additional mechanisms to possibly explain the shift to hyper-oblique convergence in the late middle Eocene, which are more controversial.

(1) A potential collision between the eastern tip of India and northernmost Myanmar shortly before 39 Ma could have anchored the Burmese margin to the Indian plate's northwards motion. However, this timing is at odds with many other studies along the India-Asia Suture that indicate a collision started ca. 55 Ma (see reviews in Najman, 2006; Najman et al., 2010).

(2) A late and poorly dated small rotation (~15° counterclockwise) of Indian convergence in the middle Eocene (Lee and Lawver, 1995; Cande et al., 2010) could have triggered the shift to strike-slip deformation. This late rotation would have slightly increased the convergence obliquity along the margin, but it seems too small to have alone triggered strain partitioning on the Burmese margin.

(3) A change in the properties of the subducting material may have favored the shift to strain partitioning on the Burmese margin. By the late Eocene, most of the old, Jurassic Tethyan oceanic crust had been subducted below the Asian subduction margin. The late Eocene would correspond roughly to the time when Cenozoic oceanic crust from the Indian Ocean reached the Burmese margin (Seton et al., 2012; Hall, 2012). This younger, less dense oceanic lithosphere could have acted as a giant sheet anchor increasing both the northward drag of the subduction margin and the shear on the Burmese plate.

Cretaceous–Paleogene paleomagnetic data from the Burmese platelet could potentially help us validate or reject these scenarios by reconstructing the amount and timing of paleo-rotation of the subduction margin; however, paleomagnetic data from central Myanmar are so far virtually nonexistent.

6. CONCLUSIONS

Our results show that the modern tectonic configuration of central Myanmar, today a sliver plate bounded to the west by the Indo-Burman Ranges and the Kabaw Fault, and to the east by the Burmese metamorphic belts and the Sagaing Fault, was actually first formed during a short time window in the late middle Eocene.

From the Paleocene to the middle Eocene, the Burmese margin displayed the regular morphology of an Andean-type margin, with a forearc basin developed on a nascent accretionary prism open to the trench, where westward-prograding deltaic systems were fed by the denudation of the Wuntho-Popa volcanic arc. In the late middle Eocene, around 39–38 Ma, the accretionary prism started emerging. Pull-apart subsidence

partitioned the forearc basin into two basins—the Chindwin Basin to the north and the Minbu Basin to the south. Quasi-closed estuarine conditions developed in the Chindwin Basin, whereas the Minbu Basin remained more open to the ocean. Simultaneously, increased shear stress in the backarc area led to metamorphism and exhumation of the Burma terrane basement. By 37 Ma, the Paleogene accretionary prism, forming today the inner wedge of Indo-Burman Ranges, had completely emerged. The main drainages in central Myanmar became southward directed, and the modern central Myanmar low plains were formed.

This tectonic evolution can be explained in light of the known evolution of accretionary prisms formed by hyper-oblique convergence. Coeval pull-apart subsidence and partitioning in the forearc, and onset of high-grade metamorphism associated with exhumation in the metamorphic belts indicate both intense shear and strike-slip faulting on the Burmese platelet during that time, and high obliquity of the convergence at the Burmese margin. We interpret the synchronous uplift of the Indo-Burman Ranges as reflecting accretionary wedge build-up marking the onset of a paleo–Kabaw Fault system. These interpretations imply that a similar-to-today sliver system, with a paleo–Kabaw Fault in the accretionary prism and a paleo–Sagaing shear zone (the paleo–Shan Scarp Fault) creating high-grade metamorphism in the metamorphic belts to the east, was already set up by the late middle Eocene. This evolution indicates that the Burmese sliver platelet is at least twice older than previously thought and that it has experienced a significant (>500 km), but yet to be determined, amount of northward motion. Finally, our results do not support any India-Asia convergence scenario involving a Paleogene collision of India with the Burmese subduction margin. Our reconstruction for the evolution of the Burmese margin is more in agreement with conservative geodynamic models for the India-Asia convergence arguing for a close-to-modern pre-collisional paleogeometry for the Indochina Peninsula, and indicates that any post-collisional rotation of Indochina, if it existed, must have been achieved by 39 Ma.

ACKNOWLEDGMENTS

This research was primarily funded by the European Research Council Consolidator Grant MAGIC 649081, the Marie Curie fellowship ECAMMETT 656731, and the University of Washington. We thank two anonymous reviewers, Chris Morley, Kyi Kyi Thein, Chit Sein, J.-J. Jaeger, O. Chavasseau, V. Lazarri, Andrew Schauer, D. Cowan, D. van

Hinsbergen, M. Mueller, M. Needle, M. Koehler, A. Gagnon, M. Pecha, G. Gehrels, D. Giesler, A. Pullen, B. Nelson, and F. Teng for prolific discussions, and assistance in the field and in the lab.

1GSA Data Repository item 2018336, including supplementary figures, geochronological data, sulfur isotope and grain counting results, is available at http://www.geosociety.org/datarepository/2018 or by request to editing@geosociety.org.

References

Acharyya, S.K., 2007, Collisional emplacement history of the Naga-Andaman ophiolites and the position of the eastern Indian suture: Journal of Asian Earth Sciences , v. 29, no. 2, p. 229–242, https://doi-org.insu.bib.cnrs.fr/10.1016/j.jseaes.2006.03.003.

Acharyya, S.K., 2015, Indo-Burma Range: a belt of accreted microcontinents, ophiolites and Mesozoic–Paleogene flyschoid sediments: International Journal of Earth Sciences , v. 104, no. 5, p. 1235–1251, https://doi-org.insu.bib.cnrs.fr/10.1007/s00531-015-1154-6.

Adnet, S., Cappetta, H., Beard, K.C., Marivaux, L., Marandat, B., Chaimanee, Y., et al, 2008, First myliobatiform teeth (Elasmobranchii, Neoselachii) from the pondaung formation (late middle Eocene) of central Myanmar: Neues Jahrbuch für Geologie und Palaontologie, Abhandlungen , v. 247, no. 3, p. 335–340, https://doi-org.insu.bib.cnrs.fr/10.1127/0077-7749/2008/0247-0335.

Aitchison, J.C., Ali, J.R., and Davis, A.M., 2007, When and where did India and Asia collide?: Journal of Geophysical Research. Solid Earth , v. 112, B5, https://doi-org.insu.bib.cnrs.fr/10.1029/2006JB004706.

Allègre, C.O., Courtillot, V., Tapponnier, P., Hirn, A., Mattauer, M., Coulon, C., et al, 1984, Structure and evolution of the Himalaya–Tibet orogenic belt: Nature , v. 307, no. 5946, p. 17–22, https://doi-org.insu.bib.cnrs.fr/10.1038/307017a0.

Allen, J.R., 2000, Morphodynamics of Holocene salt marshes: A review sketch from the Atlantic and Southern North Sea coasts of Europe: Quaternary Science Reviews , v. 19, no. 12, p. 1155–1231, https://doi-org.insu.bib.cnrs.fr/10.1016/S0277-3791(99)00034-7.

Allen, R., Najman, Y., Carter, A., Barfod, D., Bickle, M.J., Chapman, H.J., et al, 2008, Provenance of the Tertiary sedimentary rocks of the Indo-Burman Ranges, Burma (Myanmar): Burman arc or Himalayan-derived?: Journal of the Geological Society , v. 165, no. 6, p. 1045–1057, https://doi-org.insu.bib.cnrs.fr/10.1144/0016-76492007-143.

Anthony, E.J., Lang, J., and Oyédé, L.M., 1996, Sedimentation in a tropical, microtidal, wave-dominated coastal-plain estuary: Sedimentology , v. 43, no. 4, p. 665–675, https://doi-org.insu.bib.cnrs.fr/10.1111/j.1365-3091.1996.tb02019.x.

Anthony, E.J., Oyédé, L.M., and Lang, J., 2002, Sedimentation in a fluvially infilling, barrier-bound estuary on a wave-dominated, microtidal coast: The Ouémé River estuary, Benin, West Africa: Sedimentology , v. 49, no. 5, p. 1095–1112, https://doi-org.insu.bib.cnrs.fr/10.1046/j.1365-3091.2002.00491.x.

Bannert, D., Lyen, A.S., and Htay, T., 2011, The Geology of the Indoburman Ranges in Myanmar: Geologisches Jahrbuch , v. 101, p. 5–101.

Barley, M.E., Pickard, A.L., Zaw, K., Rak, P., and Doyle, M.G., 2003, Jurassic to Miocene magmatism and metamorphism in the Mogok metamorphic belt and the India-Eurasia collision in Myanmar: Tectonics , v. 22, no. 3, https://doi-org.insu.bib.cnrs.fr/10.1029/2002TC001398.

Bender, F., 1983, Geology of Burma: Berlin, Gebrüder Borntraeger, 293 p.

Bertrand, G., and Rangin, C., 2003, Tectonics of the western margin of the Shan plateau (central Myanmar): Implication for the India–Indochina oblique convergence since the Oligocene: Journal of Asian Earth Sciences , v. 21, no. 10, p. 1139–1157, https://doi-org.insu.bib.cnrs.fr/10.1016/S1367-9120(02)00183-9.

Bertrand, G., Rangin, C., Maluski, H., Bellon, H., and Party, G.S., 2001, Diachronous cooling along the Mogok Metamorphic Belt (Shan scarp, Myanmar): The trace of the northward migration of the Indian syntaxis: Journal of Asian Earth Sciences , v. 19, no. 5, p. 649–659, https://doi-org.insu.bib.cnrs.fr/10.1016/S1367-9120(00)00061-4.

Botev, Z.I., Grotowski, J.F., and Kroese, D.P., 2010, Kernel density estimation via diffusion: Annals of Statistics , v. 38, no. 5, p. 2916–2957, https://doi-org.insu.bib.cnrs.fr/10.1214/10-AOS799.

Brunnschweiler, R.O., 1966, On the Geology of the Indoburman Ranges: Journal of the Geological Society of Australia , v. 13, p. 137–194, https://doi-org.insu.bib.cnrs.fr/10.1080/00167616608728608.

Burbidge, D.R., and Braun, J., 1998, Analogue models of obliquely convergent continental plate boundaries: Journal of Geophysical Research. Solid Earth , v. 103, B7, p. 15,221–15,237, https://doi-org.insu.bib.cnrs.fr/10.1029/98JB00751.

Cande, S.C., Patriat, P., and Dyment, J., 2010, Motion between the Indian, Antarctic and African plates in the early Cenozoic: Geophysical Journal International , v. 183, no. 1, p. 127–149, https://doi-org.insu.bib.cnrs.fr/10.1111/j.1365-246X.2010.04737.x.

Casagrande, D.J., 1987, Sulphur in peat and coal, in Scott, A.C., ed., Coal and coal-bearing strata: Recent advances : Geological Society of London Special Publication 32, p. 87–105, https://doi-org.insu.bib.cnrs.fr/10.1144/GSL.SP.1987.032.01.07.

Chaimanee, Y., Chavasseau, O., Beard, K.C., Kyaw, A.A., Soe, A.N., Sein, C., et al, 2012, Late Middle Eocene primate from Myanmar and the initial anthropoid colonization of Africa: Proceedings of the National Academy of Sciences of the United States of America , v. 109, p. 10,293–10,297, https://doi-org.insu.bib.cnrs.fr/10.1073/pnas.1200644109.

Charusiri, P., Imsamut, S., Zhuang, Z., Ampaiwan, T., and Xu, X., 2006, Paleomagnetism of the earliest Cretaceous to early late Cretaceous sandstones, Khorat Group,

Northeast Thailand: Implications for tectonic plate movement of the Indochina block: Gondwana Research , v. 9, no. 3, p. 310–325, https://doi-org.insu.bib.cnrs.fr/10.1016/j.gr.2005.11.006.

Chavasseau, O., Chaimanee, Y., Coster, P., Emonet, E.G., Soe, A.N., Kyaw, A.A., Maung, A., Rugbumrung, M., Shwe, H., and Jaeger, J.-J., 2010, First record of a chalicothere from the Miocene of Myanmar: Acta Palaeontologica Polonica , v. 55, p. 13–22, https://doi-org.insu.bib.cnrs.fr/10.4202/app.2009.0033.

Chavasseau, O., Chaimanee, Y., Tun, S.T., Soe, A.N., Barry, J.C., Marandat, B., et al, 2006, Chaungtha, a new Middle Miocene mammal locality from the Irrawaddy Formation, Myanmar: Journal of Asian Earth Sciences , v. 28, no. 4, p. 354–362, https://doi-org.insu.bib.cnrs.fr/10.1016/j.jseaes.2005.10.012.

Chen, Y., Courtillot, V., Cogné, J.P., Besse, J., Yang, Z., and Enkin, R., 1993, The configuration of Asia prior to the collision of India: Cretaceous paleomagnetic constraints: Journal of Geophysical Research, Solid Earth , v. 98, B12, p. 21,927–21,941.

Chew, D.M., Petrus, J.A., and Kamber, B.S., 2014, U–Pb LA–ICPMS dating using accessory mineral standards with variable common Pb: Chemical Geology , v. 363, p. 185–199, https://doi-org.insu.bib.cnrs.fr/10.1016/j.chemgeo.2013.11.006.

Cogné, J.P., Besse, J., Chen, Y., and Hankard, F., 2013, A new Late Cretaceous to Present APWP for Asia and its implications for paleomagnetic shallow inclinations in Central Asia and Cenozoic Eurasian plate deformation: Geophysical Journal International , v. 192, no. 3, p. 1000–1024, https://doi-org.insu.bib.cnrs.fr/10.1093/gji/ggs104.

Collinson, J.D., Mountney, N.P., and Thompson, D.B., 2006, Sedimentary Structures: Terra Publishing, third edition, 292 p.

Dalrymple, R.W., Zaitlin, B.A., and Boyd, R., 1992, Estuarine facies models: conceptual basis and stratigraphic implications: perspective: Journal of Sedimentary Research , v. 62, no. 6, https://doi-org.insu.bib.cnrs.fr/10.1306/D4267A69-2B26-11D7-8648000102C1865D.

DeCelles, P.G., Kapp, P., Gehrels, G.E., and Ding, L., 2014, Paleocene-Eocene foreland basin evolution in the Himalaya of southern Tibet and Nepal: Implications for the age of initial India-Asia collision: Tectonics , v. 33, no. 5, p. 824–849, https://doi-org.insu.bib.cnrs.fr/10.1002/2014TC003522.

DeCelles, P.G., Robinson, D.M., and Zandt, G., 2002, Implications of shortening in the Himalayan fold-thrust belt for uplift of the Tibetan Plateau: Tectonics , v. 21, no. 6, https://doi-org.insu.bib.cnrs.fr/10.1029/2001TC001322.

Dickinson, W.R., 1985, Interpreting provenance relations from detrital modes of sandstones, in Zuma, G.G., ed., Provenance of Arenites: Cosenza, Italy , D. Reidel Publishing Company, p. 333–361, https://doi-org.insu.bib.cnrs.fr/10.1007/978-94-017-2809-6_15.

England, P., and Houseman, G., 1986, Finite strain calculations of continental deformation: 2. Comparison with the India-Asia collision zone: Journal of

Geophysical Research, Solid Earth , v. 91, B3, p. 3664–3676, https://doi-org.insu.bib.cnrs.fr/10.1029/JB091iB03p03664.

Finzel, E.S., Trop, J.M., Ridgway, K.D., and Enkelmann, E., 2011, Upper plate proxies for flat-slab subduction processes in southern Alaska: Earth and Planetary Science Letters , v. 303, no. 3-4, p. 348–360, https://doi-org.insu.bib.cnrs.fr/10.1016/j.epsl.2011.01.014.

Fry, B., Silva, S.R., Kendall, C., and Anderson, R.K., 2002, Oxygen isotope corrections for online δ34S analysis: Rapid Communications in Mass Spectrometry , v. 16, no. 9, p. 854–858, https://doi-org.insu.bib.cnrs.fr/10.1002/rcm.651.

Gardiner, N.J., Hawkesworth, C.J., Robb, L.J., Whitehouse, M.J., Roberts, N.M., Kirkland, C.L., and Evans, N.J., 2017, Contrasting Granite Metallogeny through the Zircon Record: A Case Study from Myanmar: Scientific Reports , v. 7, no. 1, p. 748, https://doi-org.insu.bib.cnrs.fr/10.1038/s41598-017-00832-2.

Gardiner, N.J., Searle, M.P., Robb, L.J., and Morley, C.K., 2015, Neo-Tethyan magmatism and metallogeny in Myanmar—An Andean analogue?: Journal of Asian Earth Sciences , v. 106, p. 197–215, https://doi-org.insu.bib.cnrs.fr/10.1016/j.jseaes.2015.03.015.

Garzanti, E., Wang, J.G., Vezzoli, G., and Limonta, M., 2016, Tracing provenance and sediment fluxes in the Irrawaddy River basin (Myanmar): Chemical Geology , v. 440, p. 73–90, https://doi-org.insu.bib.cnrs.fr/10.1016/j.chemgeo.2016.06.010.

Gibbons, A.D., Zahirovic, S., Müller, R.D., Whittaker, J.M., and Yatheesh, V., 2015, A tectonic model reconciling evidence for the collisions between India, Eurasia and intra-oceanic arcs of the central-eastern Tethys: Gondwana Research , v. 28, no. 2, p. 451–492, https://doi-org.insu.bib.cnrs.fr/10.1016/j.gr.2015.01.001.

Gingras, M.K., Pemberton, S.G., and Saunders, T., 2001, Bathymetry, sediment texture, and substrate cohesiveness; their impact on modern Glossifungites trace assemblages at Willapa Bay, Washington: Palaeogeography, Palaeoclimatology, Palaeoecology , v. 169, no. 1-2, p. 1–21, https://doi-org.insu.bib.cnrs.fr/10.1016/S0031-0182(01)00212-7.

Gough, A., and Hall, R., 2017, Oligocene Fluvio-Deltaic Depositional Environments Salin Sub-Basin, Central Myanmar [abs.]: American Geophysical Union Fall Meeting 2017, New Orleans, abstract #EP21F-1904.

Gradstein, F.M., Ogg, J.G., Schmitz, M., and Ogg, G., eds., 2012, The Geologic Time Scale 2012 : Elsevier, 1176 p.

Hall, R., 2012, Late Jurassic–Cenozoic reconstructions of the Indonesian region and the Indian Ocean: Tectonophysics , v. 570, p. 1–41, https://doi-org.insu.bib.cnrs.fr/10.1016/j.tecto.2012.04.021.

Hall, R., and Morley, C.K., 2004, Sundaland basins, in Clift, P., et al, eds., Continent-Ocean Interactions within the East Asian Marginal Seas: Washington, D.C. , American Geophysical Union, Geophysical Monograph, v. 149, p. 55–85.

Hallet, B., and Molnar, P., 2001, Distorted drainage basins as markers of crustal strain east of the Himalaya: Journal of Geophysical Research, Solid Earth , v. 106, B7, p. 13,697–13,709, https://doi-org.insu.bib.cnrs.fr/10.1029/2000JB900335.

Harrison, T.M., Yin, A., and Ryerson, F.J., 1998, Orographic evolution of the Himalaya and Tibetan plateau: Oxford Monographs on Geology and Geophysics , v. 39, p. 39–72.

Jaeger, J.-J., Thein, T., Benammi, M., Chaimanee, Y., Soe, A.N., Lwin, T., et al, 1999, A new primate from the middle Eocene of Myanmar and the Asian early origin of anthropoids: Science , v. 286, no. 5439, p. 528–530, https://doi-org.insu.bib.cnrs.fr/10.1126/science.286.5439.528.

Khan, P.K., and Chakraborty, P.P., 2005, Two-phase opening of Andaman Sea: A new seismotectonic insight: Earth and Planetary Science Letters , v. 229, no. 3, p. 259–271, https://doi-org.insu.bib.cnrs.fr/10.1016/j.epsl.2004.11.010.

Khin, K., and Myitta, 1999, Marine transgression and regression in Miocene sequences of northern Pegu (Bago) Yoma, Central Myanmar: Journal of Asian Earth Sciences , v. 17, no. 3, p. 369–393, http:/doi.org/10.1016/S0743-9547(98)00065-8.

Lee, H.Y., Chung, S.L., and Yang, H.M., 2016, Late Cenozoic volcanism in central Myanmar: Geochemical characteristics and geodynamic significance: Lithos , v. 245, p. 174–190, https://doi-org.insu.bib.cnrs.fr/10.1016/j.lithos.2015.09.018.

Lee, T.Y., and Lawver, L.A., 1995, Cenozoic plate reconstruction of Southeast Asia: Tectonophysics , v. 251, no. 1-4, p. 85–138, https://doi-org.insu.bib.cnrs.fr/10.1016/0040-1951(95)00023-2.

Leeder, M.R., 2009, Sedimentology and Sedimentary Basins: From Turbulence to Tectonics: John Wiley & Sons, 608 p.

Leever, K.A., Gabrielsen, R.H., Sokoutis, D., and Willingshofer, E., 2011, The effect of convergence angle on the kinematic evolution of strain partitioning in transpressional brittle wedges: Insight from analog modeling and high-resolution digital image analysis: Tectonics , v. 30, no. 2, https://doi-org.insu.bib.cnrs.fr/10.1029/2010TC002823.

Li, S., Advokaat, E.L., van Hinsbergen, D.J., Koymans, M., Deng, C., and Zhu, R., 2017, Paleomagnetic constraints on the Mesozoic-Cenozoic paleolatitudinal and rotational history of Indochina and South China: Review and updated kinematic reconstruction: Earth-Science Reviews , v. 171, p. 58–77, https://doi-org.insu.bib.cnrs.fr/10.1016/j.earscirev.2017.05.007.

Licht, A., 2013, Paléodrainage, paléoenvironnements et paléoclimats de l'Eocène birman: Implications sur l'origine et l'évolution précoce des anthropoïdes asiatiques [Ph.D. thesis]: France, University of Poitiers, 264 p.

Licht, A., Boura, A., De Franceschi, D., Ducrocq, S., Soe, A.N., and Jaeger, J.-J., 2014a, Fossil woods from the late middle Eocene Pondaung Formation, Myanmar: Review of Palaeobotany and Palynology, v. 202, p. 29–46, https://doi-org.insu.bib.cnrs.fr/10.1016/j.revpalbo.2013.12.002.

Licht, A., Boura, A., De Franceschi, D., Utescher, T., Sein, C., and Jaeger, J.-J., 2015, Late middle Eocene fossil wood of Myanmar: Implications for the landscape and the climate of the Eocene Bengal Bay: Review of Palaeobotany and Palynology , v. 216, p. 44–54, https://doi-org.insu.bib.cnrs.fr/10.1016/j.revpalbo.2015.01.010.

Licht, A., Cojan, I., Caner, L., Soe, A.N., Jaeger, J., and France-Lanord, C., 2014b, Influence of permeability barriers in alluvial hydromorphic palaeosols: The Eocene Pondaung Formation, Myanmar: Sedimentology , v. 61, p. 362–382.

Licht, A., France-Lanord, C., Reisberg, L., Fontaine, C., Soe, A.N., and Jaeger, J.-J., 2013, A palaeo Tibet–Myanmar connection? Reconstructing the Late Eocene drainage system of central Myanmar using a multi-proxy approach: Journal of the Geological Society , v. 170, no. 6, p. 929–939, https://doi-org.insu.bib.cnrs.fr/10.1144/jgs2012-126.

Licht, A., Reisberg, L., France-Lanord, C., Soe, A.N., and Jaeger, J.-J., 2016, Cenozoic evolution of the central Myanmar drainage system: Insights from sediment provenance in the Minbu Sub-Basin: Basin Research , v. 28, no. 2, p. 237–251, https://doi-org.insu.bib.cnrs.fr/10.1111/bre.12108.

Licht, A., van Cappelle, M., Abels, H. A., Ladant, J., Trabucho-Alexandre, J., France-Lanord, C., Donnadieu, Y., Vandenberghe, J., Rigaudier, T., Lecuyer, C., Terry Jr., D., Adriaens, R., Boura, A., Guo, Z., Soe, A.N., Dupont-Nivet, G., and Jaeger, J.-J., 2014c, Asian monsoons in a late Eocene greenhouse world: Nature , v. 513, p. 501–506, https://doi-org.insu.bib.cnrs.fr/10.1038/nature13704.

Liu, C.Z., Chung, S.L., Wu, F.Y., Zhang, C., Xu, Y., Wang, J.G., et al, 2016, Tethyan suturing in Southeast Asia: Zircon U-Pb and Hf-O isotopic constraints from Myanmar ophiolites: Geology , v. 44, no. 4, p. 311–314, https://doi-org.insu.bib.cnrs.fr/10.1130/G37342.1.

Ludwig, K.R., 2003, User's manual for Isoplot 3.00: A Geochronological Toolkit for Microsoft Excel: Berkeley Geochronological Center Special Publication 4.

Ma, L., Wang, Y., Fan, W., Geng, H., Cai, Y., Zhong, H., et al, 2014, Petrogenesis of the early Eocene I-type granites in west Yingjiang (SW Yunnan) and its implication for the eastern extension of the Gangdese batholiths: Gondwana Research , v. 25, no. 1, p. 401–419.

Ma, Y., Yang, T., Bian, W., Jin, J., Zhang, S., Wu, H., and Li, H., 2016, Early Cretaceous paleomagnetic and geochronologic results from the Tethyan Himalaya: Insights into the Neotethyan paleogeography and the India–Asia collision: Scientific Reports , v. 6, 21605, https://doi-org.insu.bib.cnrs.fr/10.1038/srep21605.

Maffione, M., van Hinsbergen, D.J., Koornneef, L.M., Guilmette, C., Hodges, K., Borneman, N., et al, 2015, Forearc hyperextension dismembered the south Tibetan ophiolites: Geology , v. 43, p. 475–478, https://doi-org.insu.bib.cnrs.fr/10.1130/G36472.1.

Maung, H., 1987, Transcurrent movements in the Burma–Andaman Sea region: Geology , v. 15, p. 911–912, https://doi-org.insu.bib.cnrs.fr/10.1130/0091-7613(1987)15<911:TMITBS>2.0.CO;2.

Maurin, T., and Rangin, C., 2009, Structure and kinematics of the Indo-Burmese Wedge: Recent and fast growth of the outer wedge: Tectonics , v. 28, no. 2, https://doi-org.insu.bib.cnrs.fr/10.1029/2008TC002276.

Maury, R.C., Pubellier, M., Rangin, C., Wulput, L., Cotten, J., Socquet, A., et al, 2004, Quaternary calc-alkaline and alkaline volcanism in an hyper-oblique convergence setting, central Myanmar and western Yunnan: Bulletin de la Société Géologique de

France , v. 175, no. 5, p. 461–472, https://doi-org.insu.bib.cnrs.fr/10.2113/175.5.461.

McClay, K.R., Whitehouse, P.S., Dooley, T., and Richards, M., 2004, 3D evolution of fold and thrust belts formed by oblique convergence: Marine and Petroleum Geology , v. 21, no. 7, p. 857–877, https://doi-org.insu.bib.cnrs.fr/10.1016/j.marpetgeo.2004.03.009.

McQuarrie, N., Tobgay, T., Long, S.P., Reiners, P.W., and Cosca, M.A., 2014, Variable exhumation rates and variable displacement rates: Documenting recent slowing of Himalayan shortening in western Bhutan: Earth and Planetary Science Letters , v. 386, p. 161–174, https://doi-org.insu.bib.cnrs.fr/10.1016/j.epsl.2013.10.045.

Metcalfe, I., 2013, Gondwana dispersion and Asian accretion: tectonic and palaeogeographic evolution of eastern Tethys: Journal of Asian Earth Sciences , v. 66, p. 1–33, https://doi-org.insu.bib.cnrs.fr/10.1016/j.jseaes.2012.12.020.

Miall, A.D., 2013, The geology of fluvial deposits: sedimentary facies, basin analysis, and petroleum geology: Springer, 582 p., https://doi-org.insu.bib.cnrs.fr/10.1007/978-3-662-03237-4.

Mitchell, A., Chung, S.L., Oo, T., Lin, T.H., and Hung, C.H., 2012, Zircon U–Pb ages in Myanmar: Magmatic–metamorphic events and the closure of a neo-Tethys ocean?: Journal of Asian Earth Sciences , v. 56, p. 1–23, https://doi-org.insu.bib.cnrs.fr/10.1016/j.jseaes.2012.04.019.

Mitchell, A.H.G., 1993, Cretaceous–Cenozoic tectonic events in the western Myanmar (Burma)–Assam region: Journal of the Geological Society , v. 150, no. 6, p. 1089–1102, https://doi-org.insu.bib.cnrs.fr/10.1144/gsjgs.150.6.1089.

Mitchell, A.H.G., Htay, M.T., Htun, K.M., Win, M.N., Oo, T., and Hlaing, T., 2007, Rock relationships in the Mogok metamorphic belt, Tatkon to Mandalay, central Myanmar: Journal of Asian Earth Sciences , v. 29, no. 5, p. 891–910, https://doi-org.insu.bib.cnrs.fr/10.1016/j.jseaes.2006.05.009.

Molnar, P., England, P., and Martinod, J., 1993, Mantle dynamics, uplift of the Tibetan Plateau, and the Indian monsoon: Reviews of Geophysics , v. 31, no. 4, p. 357–396.

Morley, C.K., 2002, A tectonic model for the Tertiary evolution of strike–slip faults and rift basins in SE Asia: Tectonophysics , v. 347, no. 4, p. 189–215, https://doi-org.insu.bib.cnrs.fr/10.1016/S0040-1951(02)00061-6.

Morley, C.K., 2009, Evolution from an oblique subduction back-arc mobile belt to a highly oblique collisional margin: the Cenozoic tectonic development of Thailand and eastern Myanmar, in Cawood, P.A., and Kröner, A., eds., Earth Accretionary Systems in Space and Time : Geological Society of London Special Publication 318, no. 1, p. 373–403, https://doi-org.insu.bib.cnrs.fr/10.1144/SP318.14.

Morley, C.K., 2012, Late Cretaceous–early Palaeogene tectonic development of SE Asia: Earth-Science Reviews , v. 115, no. 1-2, p. 37–75, https://doi-org.insu.bib.cnrs.fr/10.1016/j.earscirev.2012.08.002.

Morley, C.K., 2017, Syn-kinematic sedimentation at a releasing splay in the northern Minwun Ranges, Sagaing Fault zone, Myanmar: Significance for fault timing and

displacement: Basin Research , v. 29, S1, p. 684–700, https://doi-org.insu.bib.cnrs.fr/10.1111/bre.12201.

Mozley, P.S., and Wersin, P., 1992, Isotopic composition of siderite as an indicator of depositional environment: Geology , v. 20, no. 9, p. 817–820, https://doi-org.insu.bib.cnrs.fr/10.1130/0091-7613(1992)020<0817:ICOSAA>2.3.CO;2.

Myanmar Geosciences Society (MGS), 2014, Geological map of Myanmar, revised version: Myanmar Geosciences Society, Yangon.

Nagappa, Y., 1959, Foraminiferal biostratigraphy of the Cretaceous-Eocene succession in the India-Pakistan-Burma region: Micropaleontology , v. 5, no. 2, p. 145–177, https://doi-org.insu.bib.cnrs.fr/10.2307/1484208.

Najman, Y., 2006, The detrital record of orogenesis: A review of approaches and techniques used in the Himalayan sedimentary basins: Earth-Science Reviews , v. 74, no. 1–2, p. 1–72, https://doi-org.insu.bib.cnrs.fr/10.1016/j.earscirev.2005.04.004.

Najman, Y., Appel, E., Boudagher-Fadel, M., Bown, P., Carter, A., Garzanti, E., et al, 2010, Timing of India-Asia collision: Geological, biostratigraphic, and palaeomagnetic constraints: Journal of Geophysical Research, Solid Earth , v. 115, B12, https://doi-org.insu.bib.cnrs.fr/10.1029/2010JB007673.

Najman, Y., Jenks, D., Godin, L., Boudagher-Fadel, M., Millar, I., Garzanti, E., et al, 2017, The Tethyan Himalayan detrital record shows that India–Asia terminal collision occurred by 54 Ma in the Western Himalaya: Earth and Planetary Science Letters , v. 459, p. 301–310, https://doi-org.insu.bib.cnrs.fr/10.1016/j.epsl.2016.11.036.

Nichols, G., 2009, Sedimentology and stratigraphy: Oxford, John Wiley & Sons, 355 p.

Nielsen, C., Chamot-Rooke, N., and Rangin, C., 2004, From partial to full strain partitioning along the Indo-Burmese hyper-oblique subduction: Marine Geology , v. 209, no. 1–4, p. 303–327, https://doi-org.insu.bib.cnrs.fr/10.1016/j.margeo.2004.05.001.

Oo, K.L., Zaw, K., Meffre, S., Aung, D.W., and Lai, C.K., 2015, Provenance of the Eocene sandstones in the southern Chindwin Basin, Myanmar: Implications for the unroofing history of the Cretaceous–Eocene magmatic arc: Journal of Asian Earth Sciences , v. 107, p. 172–194, https://doi-org.insu.bib.cnrs.fr/10.1016/j.jseaes.2015.04.029.

Paton, C., Woodhead, J., Hellstrom, J., Hergt, J., Greig, A., and Maas, R., 2010, Improved laser ablation U-Pb zircon geochronology through robust down-hole fractionation correction: Geochemistry Geophysics Geosystems , v. 11, no. 3, https://doi-org.insu.bib.cnrs.fr/10.1029/2009GC002618.

Pivnik, D.A., Nahm, J., Tucker, R.S., Smith, G.O., Nyein, K., Nyunt, M., and Maung, P.H., 1998, Polyphase deformation in a fore-arc/back-arc basin, Salin subbasin, Myanmar (Burma): AAPG Bulletin , v. 82, no. 10, p. 1837–1856.

Pubellier, M., 2008, Structural Map of Eastern Eurasia: CCGM, Commission for the Geological Map of the World, Scale at equator 1:12,500,000, 1 sheet.

Rangin, C., Maurin, T., and Masson, F., 2013, Combined effects of Eurasia/Sunda oblique convergence and East-Tibetan crustal flow on the active tectonics of Burma:

Journal of Asian Earth Sciences , v. 76, p. 185–194, https://doi-org.insu.bib.cnrs.fr/10.1016/j.jseaes.2013.05.018.

Rangin, C., Maw, W., Lwin, S., Naing, W., Mouret, C., Bertrand, G., and the G.I.A.C. Scientific Party, 1999, Cenozoic Pull-Apart basins in Central Myanmar: the trace of the path of India along the Western Margin of Sundaland [abs.]: Terra Nova , v. 4, p. 59.

Replumaz, A., and Tapponnier, P., 2003, Reconstruction of the deformed collision zone between India and Asia by backward motion of lithospheric blocks: Journal of Geophysical Research , v. 108, https://doi-org.insu.bib.cnrs.fr/10.1029/2001JB000661.

Replumaz, A., Guillot, S., Villaseñor, A., and Negredo, A.M., 2013, Amount of Asian lithospheric mantle subducted during the India/Asia collision: Gondwana Research , v. 24, no. 3, p. 936–945, https://doi-org.insu.bib.cnrs.fr/10.1016/j.gr.2012.07.019.

Replumaz, A., Negredo, A.M., Guillot, S., and Villaseñor, A., 2010, Multiple episodes of continental subduction during India/Asia convergence: Insight from seismic tomography and tectonic reconstruction: Tectonophysics , v. 483, no. 1, p. 125–134, https://doi-org.insu.bib.cnrs.fr/10.1016/j.tecto.2009.10.007.

Richter, B., and Fuller, M., 1996, Palaeomagnetism of the Sibumasu and Indochina blocks: Implications for the extrusion tectonic model, in Hall, R., and Blundell, D., Tectonic Evolution of Southeast Asia : Geological Society of London, Special Publication 106, no. 1, p. 203–224, https://doi-org.insu.bib.cnrs.fr/10.1144/GSL.SP.1996.106.01.13.

Robinson, R.A., Brezina, C.A., Parrish, R.R., Horstwood, M.S., Oo, N.W., Bird, M.I., et al, 2014, Large rivers and orogens: The evolution of the Yarlung Tsangpo–Irrawaddy system and the eastern Himalayan syntaxis: Gondwana Research , v. 26, no. 1, p. 112–121, https://doi-org.insu.bib.cnrs.fr/10.1016/j.gr.2013.07.002.

Roy, P.S., Cowell, P.J., Ferland, M.A., Thom, B.G., Carter, R.W.G., and Woodroffe, C.D., 1994, Wave-dominated coasts, in Carter, R.W.G., and Woodroffe, C.D., eds., Coastal Evolution: Late Quaternary Shoreline Morphodynamics : Cambridge University Press, p. 121–186.

Royden, L.H., Burchfiel, B.C., and van der Hilst, R.D., 2008, The geological evolution of the Tibetan Plateau: Science , v. 321, p. 1054–1058, https://doi-org.insu.bib.cnrs.fr/10.1126/science.1155371.

Sato, K., Liu, Y., Zhu, Z., Yang, Z., and Otofuji, Y.I., 2001, Tertiary paleomagnetic data from northwestern Yunnan, China: Further evidence for large clockwise rotation of the Indochina block and its tectonic implications: Earth and Planetary Science Letters , v. 185, no. 1, p. 185–198, https://doi-org.insu.bib.cnrs.fr/10.1016/S0012-821X(00)00377-0.

Searle, M., Corfield, R.I., Stephenson, B.E.N., and McCarron, J.O.E., 1997, Structure of the North Indian continental margin in the Ladakh–Zanskar Himalayas: implications for the timing of obduction of the Spontang ophiolite, India–Asia collision and deformation events in the Himalaya: Geological Magazine , v. 134, no. 3, p. 297–316, https://doi-org.insu.bib.cnrs.fr/10.1017/S0016756897006857.

Searle, M.P., Morley, C.K., Waters, D.J., Gardiner, N.J., Htun, U.K., Nu, T.T., and Robb, L.J., 2017, Tectonic and metamorphic evolution of the Mogok Metamorphic and Jade Mines belts and ophiolitic terranes of Burma (Myanmar), in Barber, A.J., Zaw, K., and Crow, M.J., eds., Myanmar: Geology, Resources and Tectonics : Geological Society of London Memoir 48, p. 261–293.

Searle, M.P., Noble, S.R., Cottle, J.M., Waters, D.J., Mitchell, A.H.G., Hlaing, T., and Horstwood, M.S.A., 2007, Tectonic evolution of the Mogok metamorphic belt, Burma (Myanmar) constrained by U-Th-Pb dating of metamorphic and magmatic rocks: Tectonics , v. 26, no. 3, https://doi-org.insu.bib.cnrs.fr/10.1029/2006TC002083.

Searle, M.P., Whitehouse, M.J., Robb, L.J., Ghani, A.A., Hutchison, C.S., Sone, M., et al, 2012, Tectonic evolution of the Sibumasu–Indochina terrane collision zone in Thailand and Malaysia: Constraints from new U–Pb zircon chronology of SE Asian tin granitoids: Journal of the Geological Society , v. 169, no. 4, p. 489–500, https://doi-org.insu.bib.cnrs.fr/10.1144/0016-76492011-107.

Seton, M., Müller, R.D., Zahirovic, S., Gaina, C., Torsvik, T., Shephard, G., et al, 2012, Global continental and ocean basin reconstructions since 200 Ma: Earth–Scientific Review (Singapore) , v. 113, no. 3–4, p. 212–270.

Sevastjanova, I., Hall, R., Rittner, M., Paw, S.M.T.L., Naing, T.T., Alderton, D.H., and Comfort, G., 2016, Myanmar and Asia united, Australia left behind long ago: Gondwana Research , v. 32, p. 24–40, http://doi.org.insu.bib.cnrs.fr/10.1016/j.gr.2015.02.001.

Shen, F., Royden, L.H., and Burchfiel, B.C., 2001, Large-scale crustal deformation of the Tibetan Plateau: Journal of Geophysical Research , v. 106, B4, p. 6793–6816, https://doi-org.insu.bib.cnrs.fr/10.1029/2000JB900389.

Socquet, A., Goffé, B., Pubellier, M., and Rangin, C., 2002, Le métamorphisme Tardi-Crétacé à Éocène des zones internes de la chaîne Indo-Birmane (Myanmar occidental): implications géodynamiques: Comptes Rendus Geoscience , v. 334, no. 8, p. 573–580, https://doi-org.insu.bib.cnrs.fr/10.1016/S1631-0713(02)01796-0.

Socquet, A., Vigny, C., Chamot-Rooke, N., Simons, W., Rangin, C., and Ambrosius, B., 2006, India and Sunda plates motion and deformation along their boundary in Myanmar determined by GPS: Journal of Geophysical Research. Solid Earth , v. 111, B5, https://doi-org.insu.bib.cnrs.fr/10.1029/2005JB003877.

Tapponnier, P., Peltzer, G., Le Dain, A.Y., Armijo, R., and Cobbold, P., 1982, Propagating extrusion tectonics in Asia: New insights from simple experiments with plasticine: Geology , v. 10, no. 12, p. 611–616, https://doi-org.insu.bib.cnrs.fr/10.1130/0091-7613(1982)10<611:PETIAN>2.0.CO;2.

Tessier, B., Archer, A.W., Laniere, W., and Feldman, H.R., 1995, Comparison of ancient tidal rhythmites (Carboniferous of Kansas and Indiana, USA) with modern analogues (the Bay of Mont-Saint-Michel, France), in Flemming B.W., and Bartholomä, A., eds., Tidal Signatures in Modern and Ancient Sediments: Special Publication of the International Association of Sedimentologists 24 , p. 259–271.

Thein, M., and Maung, M., 2017, The Eastern (Back-arc) Basin of Central Myanmar: Basement rocks, lithostratigraphic units, palaeocurrents, provenance and developmental history, in Barber, A.J., Zaw, K., and Crow, M.J., eds., Myanmar: Geology, Resources and Tectonics: Geological Society of London Memoir 48, p. 169–183.

Tong, Y., Yang, Z., Jing, X., Zhao, Y., Li, C., Huang, D., and Zhang, X., 2016, New insights into the Cenozoic lateral extrusion of crustal blocks on the southeastern edge of Tibetan Plateau: Evidence from paleomagnetic results from Paleogene sedimentary strata of the Baoshan Terrane: Tectonics , v. 35, no. 11, p. 2494–2514, https://doi-org.insu.bib.cnrs.fr/10.1002/2016TC004221.

United Nations, 1978, Atlas of Stratigraphy Volume V: United Nations, ESCAP, New York.

Valeton, I., 1994, Element concentration and formation of ore deposits by weathering: Catena , v. 21, no. 2–3, p. 99–129, https://doi-org.insu.bib.cnrs.fr/10.1016/0341-8162(94)90006-X.

van Hinsbergen, D.J., Kapp, P., Dupont-Nivet, G., Lippert, P.C., DeCelles, P.G., and Torsvik, T.H., 2011a, Restoration of Cenozoic deformation in Asia and the size of Greater India: Tectonics , v. 30, no. 5. TC5003, https://doi-org.insu.bib.cnrs.fr/10.1029/2011TC002908.

van Hinsbergen, D.J., Lippert, P.C., Dupont-Nivet, G., McQuarrie, N., Doubrovine, P.V., Spakman, W., and Torsvik, T.H., 2012, Greater India Basin hypothesis and a two-stage Cenozoic collision between India and Asia: Proceedings of the National Academy of Sciences of the United States of America , v. 109, no. 20, p. 7659–7664.

van Hinsbergen, D.J., Steinberger, B., Doubrovine, P.V., and Gassmöller, R., 2011b, Acceleration and deceleration of India-Asia convergence since the Cretaceous: Roles of mantle plumes and continental collision: Journal of Geophysical Research, Solid Earth , v. 116, B6, https://doi-org.insu.bib.cnrs.fr/10.1029/2010JB008051.

Vérard, C., Stampfli, G., Borel, G., and Hochard, C., 2017, The Indian Promontory: A Bridge between Plate Tectonics and Life Evolution Models: Universal Journal of Geoscience , v. 5, no. 2, p. 25–32, https://doi-org.insu.bib.cnrs.fr/10.13189/ujg.2017.050202.

Vermeesch, P., 2013, Multi-sample comparison of detrital age distributions: Chemical Geology , v. 341, p. 140–146

Wang, J.G., Hu, X., Garzanti, E., An, W., and Liu, X.C., 2017, The birth of the Xigaze forearc basin in southern Tibet: Earth and Planetary Science Letters , v. 465, p. 38–47, https://doi-org.insu.bib.cnrs.fr/10.1016/j.epsl.2017.02.036.

Wang, J.G., Wu, F.Y., Tan, X.C., and Liu, C.Z., 2014, Magmatic evolution of the Western Myanmar Arc documented by U–Pb and Hf isotopes in detrital zircon: Tectonophysics , v. 612, p. 97–105, https://doi-org.insu.bib.cnrs.fr/10.1016/j.tecto.2013.11.039.

Yin, A., and Harrison, T.M., 2000, Geologic evolution of the Himalayan-Tibetan orogen: Annual Review of Earth and Planetary Sciences , v. 28, no. 1, p. 211–280, https://doi-org.insu.bib.cnrs.fr/10.1146/annurev.earth.28.1.211.

Yin, A., Harrison, T.M., Ryerson, F.J., Wenji, C., Kidd, W.S.F., and Copeland, P., 1994, Tertiary structural evolution of the Gangdese thrust system, southeastern Tibet: Journal of Geophysical Research, Solid Earth , v. 99, B9, p. 18,175–18,201, https://doi-org.insu.bib.cnrs.fr/10.1029/94JB00504.

Zaw, K., 1990, Geological, petrological and geochemical characteristics of granitoid rocks in Burma: With special reference to the associated W-Sn mineralization and their tectonic setting: Journal of Southeast Asian Earth Sciences , v. 4, no. 4, p. 293–335, https://doi-org.insu.bib.cnrs.fr/10.1016/0743-9547(90)90004-W.

Zhang, J.E., Xiao, W., Windley, B.F., Cai, F., Sein, K., and Naing, S., 2017b, Early Cretaceous wedge extrusion in the Indo-Burma Range accretionary complex: Implications for the Mesozoic subduction of Neotethys in SE Asia: International Journal of Earth Sciences , v. 106, no. 4, p. 1391–1408, https://doi-org.insu.bib.cnrs.fr/10.1007/s00531-017-1468-7.

Zhang, P., Mei, L., Hu, X., Li, R., Wu, L., Zhou, Z., and Qiu, H., 2017a, Structures, uplift, and magmatism of the Western Myanmar Arc: Constraints to mid-Cretaceous-Paleogene tectonic evolution of the western Myanmar continental margin: Gondwana Research , v. 52, p. 18–38, https://doi-org.insu.bib.cnrs.fr/10.1016/j.gr.2017.09.002.

GSA Data Repository Item 2018336

Alexis Licht, Guillaume Dupont-Nivet, Zaw Win, Hnin Hnin Swe, Myat Kaythi, Pierrick Roperch, Tamas Ugrai, Virginia Littell, Diana Park, Jan Westerweel, Dominic Jones, Fernando Poblete, Day Wa Aung, Huasheng Huang, Carina Hoorn, and Kyaing Sein, 2019, Paleogene evolution of the Burmese forearc basin and implications for the history of India-Asia convergence: GSA Bulletin, https://doi.org/10.1130/B35002.1.

U-Pb dating methods at the University of Washington

Figures DR1-DR3

Tables DR1–DR3

Supplementary methods - U-Pb dating methods at the University of Washington

Zircon crystals are extracted from 1 to 5 kg samples by traditional methods of crushing and grinding, followed by separation with a Wilfley table, heavy liquids, and a Frantz magnetic separator at the University of Washington. A split of 100 to 1000 zircon crystals, is separated to include all grain sizes, is incorporated into a 1" epoxy mount together with fragments of the Plesovice International standard zircon (Slama et al., 2008) and fragment of our internal standard zircon, GHB, coming from the Hypersolvus granite of the Golden Horn Batholith of the North Cascades (Eddy et al., 2016). The mounts are polished, imaged with a backscattered electron detector (BSE) with our in-house, JEOL 733 Superprobe microprobe to distinguish zircons from other remaining heavy minerals, and polished again prior to isotopic analysis.

U-Pb geochronology of zircons was conducted by laser ablation inductively coupled plasma mass spectrometry (LA–ICPMS) at the University of Washington. The analyses involve ablation of zircon with an Analyte G2 excimer laser (operating at a wavelength of 193 nm) using a spot diameter of 25 microns, 10 Hz pulse repetition rate and an energy fluence of 4.12 J cm^{-2}. The ablated material is carried in helium and mixed with nitrogen into the plasma source of an iCAP RQ Quadrupole ICP-MS. Analyzed masses include ^{238}U, ^{235}U, ^{232}Th, ^{207}Pb, ^{206}Pb, and ^{204}Pb, with a total, combined dwell time of ~0.4 s. Each analysis consists of a 10 s integration on peaks with the laser off (for background), 38 s of acquisition with the laser firing, and a 17 s delay to purge the previous sample and prepare for the next analysis.

Data reduction is conducted with *Iolite*, using their Geochron Data Reduction Scheme to get U-Pb ages uncorrected for common lead (Paton et al., 2010), and the Andersen Routine of the *Vizualage* Data Reduction scheme (Chew et al., 2014), for U-Pb ages corrected for common lead. To ensure grains with a complex history (e.g., inheritance, Pb loss, or overgrowths, detectable amount of ^{204}Pb) do not compromise data quality, the time-resolved pattern of $^{206}Pb/^{238}U$ is monitored closely during data reduction, and any analyses that show abnormal patterns (e.g., different fractionation from standards or jumps in value) are rejected (Gehrels et al., 2011).

Data are provided in three formats: measured isotopic ratios (already corrected for downhole fraction and instrument bias with *Iolite*), U-Pb ages uncorrected for common lead, and U-Pb ages corrected for common lead with the Andersen routine. For each analysis, the errors in determining $^{206}Pb/^{238}U$ result in a measurement error of ~1–3% (at 2-sigma) in the $^{206}Pb/^{238}U$ age. The errors in measurement of $^{206}Pb/^{207}Pb$ also result in ~1–3% uncertainty (at 2-sigma) in age for grains that are >1.0 Ga, but are substantially larger for younger grains due to low intensity of the ^{207}Pb signal. The crossover in precision of $^{206}Pb/^{238}U$ and $^{206}Pb/^{207}Pb$ ages occurs at ~1.2 Ga. The best age for every analysis is thus determined from $^{206}Pb/^{238}U$ age for analyses with $^{206}Pb/^{238}U$ age < 1.2 Ga and from $^{206}Pb/^{207}Pb$ age for analyses with $^{206}Pb/^{238}U$ age > 1.2 Ga. 7. Analyses with >20% discordance (<80% concordance), as well with >5% reverse discordance (<105% concordance) are included but are marked as 'discordant' if the grains are older than 500 Ma and should be used with caution.

The accuracy of our protocol is regularly tested with our secondary standard GHB and a set of 8 international standards provided by the Arizona Laserchron facility, including FCT, Temora2, OG1, R33, TarBra, Oracle, 91500, and 9435 (contact the Laserchron for more information about ages and origin). Over one year of analysis, the average offset to the TIMS U-Pb age value for our determined ages uncorrected for common lead is less than 0.5 % for half of them (FCT, oracle, Tarbra, OG1) less than 1.5% for others (R33, 91500, Temora2, GHB); only the Paleogene 9435 standard displays a higher average offset (2.3 %), but this standard also displays high age variability when analyzed with a Multi-collector ICP-MS (Mark Pecha, Laserchron, pers. com; Gehrels et al., 2008). Ages corrected for common lead with the Andersen routine display a commonly bigger offset (~1.5%, but up to 3-5% for Proterozoic grains). We thus recommend to use the ages uncorrected for common lead.

The uncertainty resulting from the calibration correction is generally 1-2% (2-sigma) for both $^{206}Pb/^{207}Pb$ and $^{206}Pb/^{238}U$ ages. Uncertainties from this calibration correction are not included in the age uncertainties provided in the supplementary material and should be combined (quadratically) with the uncertainty of the age of the standard to yield an external uncertainty for each sample. This external uncertainty is reported in the auxiliary material table with our data and provides a minimum uncertainty for each set of analyses.

References:

Chew, D.M., Petrus, J.A. and Kamber, B.S. (2014), U–Pb LA–ICPMS dating using accessory mineral standards with variable common Pb. Chemical Geology, 363: 185-199

Eddy, M. P., Bowring, S. A., Miller, R. B., & Tepper, J. H. (2016). Rapid assembly and crystallization of a fossil large-volume silicic magma chamber. Geology, 44(4), 331-334.

Gehrels, G. E., Valencia, V. A., & Ruiz, J. (2008). Enhanced precision, accuracy, efficiency, and spatial resolution of U-Pb ages by laser ablation–multicollector–inductively coupled plasma–mass spectrometry. Geochemistry, Geophysics, Geosystems, 9(3).

Gehrels, G., Kapp, P., DeCelles, P., Pullen, A., Blakey, R., Weislogel, A., ... & Yin, A. (2011). Detrital zircon geochronology of pre-Tertiary strata in the Tibetan-Himalayan orogen. Tectonics, 30(5).

Paton, C., Woodhead, J., Hellstrom, J., Hergt, J., Greig, A. and Maas, R (2010) Improved laser ablation U-Pb zircon geochronology through robust down-hole fractionation correction. Geochemistry, Geophysics, Geosystems, 11(3), doi:10.1029/2009GC002618

Sláma, J., Košler, J., Condon, D. J., Crowley, J. L., Gerdes, A., Hanchar, J. M., ... & Schaltegger, U. (2008). Plešovice zircon—a new natural reference material for U–Pb and Hf isotopic microanalysis. Chemical Geology, 249(1-2), 1-35.

Paleogene evolution of the Burmese forearc basin and implications for the history of India-Asia convergence

Alexis Licht , Guillaume Dupont-Nivet, Zaw Win, Hnin Hnin Swe, Myat Kaythi, Pierrick Roperch, Tamas Ugrai, Virginia Littell, Diana Park, Jan Westerweel, Dominic Jones, Fernando Poblete, Day Wa Aung, Huasheng Huang, Carina Hoorn, and Kyaing Sein

Supplementary Figures

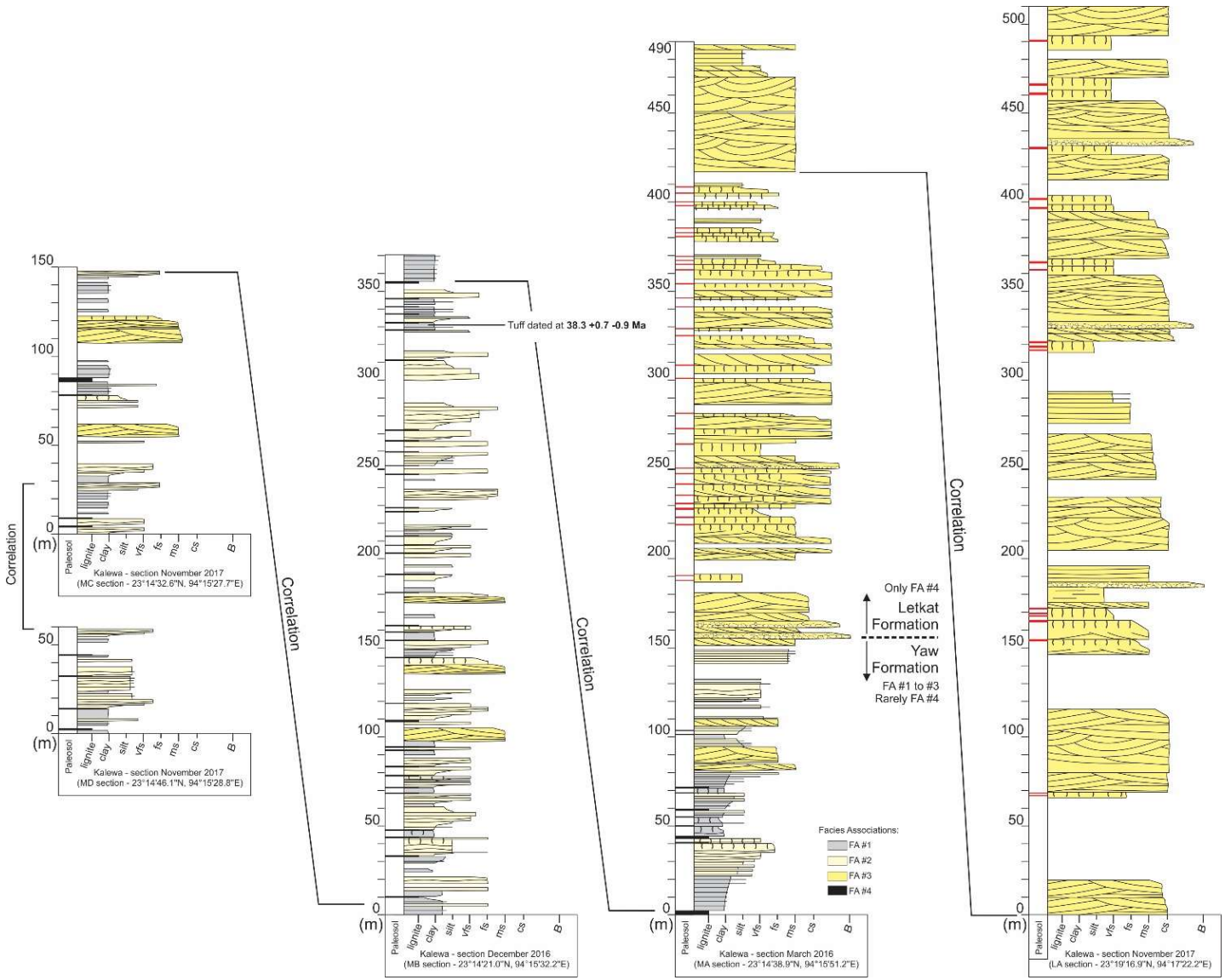

Supplementary Figure DR1: Detailed logs of the Yaw and Letkat Formations, with associated facies associations, and their correlations (correlations were made in the field by following marker beds, distance between sections is ~200 to 2000 m). Stratigraphic sections MA to MD were measured at the 10-cm scale using a Jacob Staff, stratigraphic section LA weas measured at the 1-m scale. The base of MD section is approximatively ~500 m above the transition between the Pondaung and the Yaw Formation, marked by the appearance of the first lignites. The top of LA section is ~700 m below the transition from the Letkat to the Natma Formation, which is gradual and marked by an increased in fine-grained, pedogenised deposits.

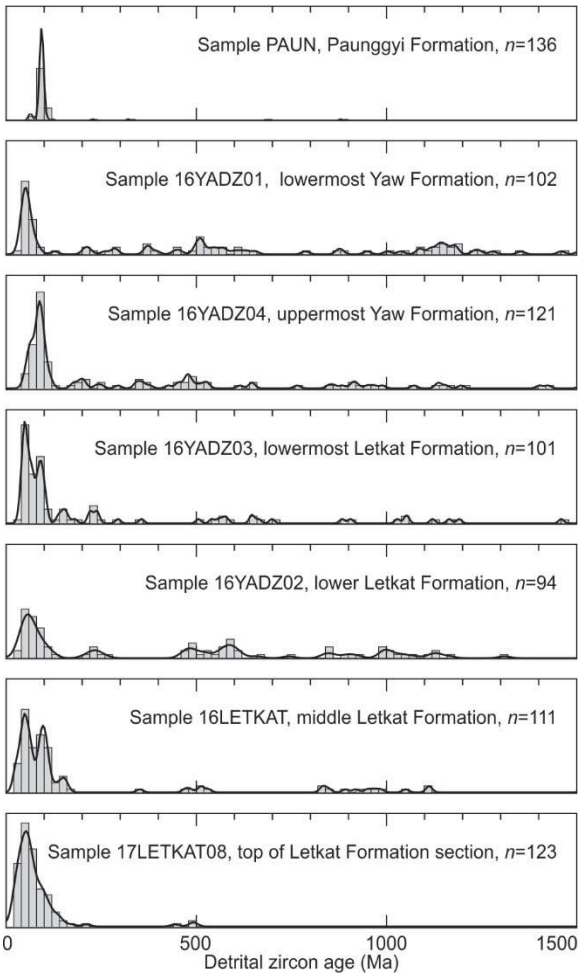

Supplementary Figure DR2: Kernel density estimators (KDE) and histograms (20 Myr bins) for the seven detrital sandstones presented in this study. The kernel density bandwidth of each plot was determined with plug-in bandwidth selection method of Botev et al. (2010). Stratigraphic and geographic location of the samples is given in supplementary table 2.

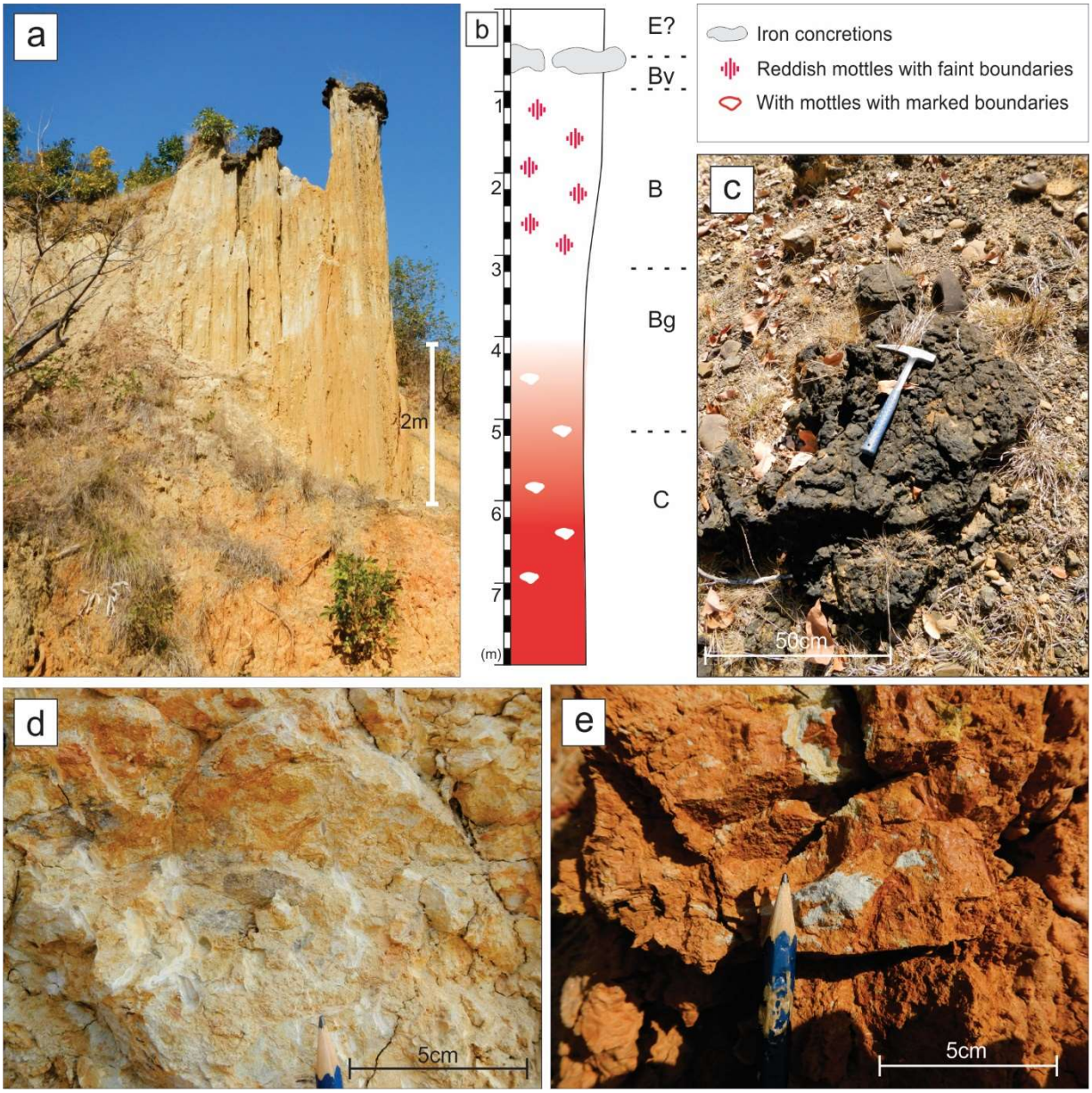

Supplementary Figure DR3: (a) Ferralitic paleosol developed in Eocene clastics below the Maw Gravels near Gangaw, eastern edge of the Indo-Burman Ranges (After Licht, 2013). **(b)** interpreted profile with pedogenic horizons. **(c)** Iron concretions in petroplinthic horizon Bv. **(d)** red mottles in the Bg horizon; **(e)** White mottles in the C horizon.

Table DR1 - Lignite Sulfur results

Sample	Strati	PeakArea (Vs)	Percent S	Percent S Accuracy	Percent S Precision	d34S vs VCDT (permil)	d34S Accuracy	d34S Precision
16MBOM48	48m in MB section	18.949	0.4683	-0.044993	0.12518	1.7094	-0.26587	0.071155
YA16OM68	68m in MA section	241.482	5.1633	-0.044993	0.12518	5.4165	-0.26587	0.071155
16MBOM355	355m in MB section	16.785	0.42264	-0.044993	0.12518	3.5212	-0.26587	0.071155
16MBOM93	93m in MB section	26.372	0.64143	-0.044993	0.12518	-0.66048	-0.26587	0.071155
16MBOM329	329m in MB section	50.436	1.1414	-0.044993	0.12518	-2.7313	-0.26587	0.071155
16MBOM266	266m in MB section	23.151	0.56195	-0.044993	0.12518	1.3519	-0.26587	0.071155
16MBOM247	247m in MB section	15.086	0.39296	-0.044993	0.12518	0.054964	-0.26587	0.071155
16MBOM163	163m in MB section	18.983	0.46828	-0.044993	0.12518	0.92713	-0.26587	0.071155
YA16OM01	1m in MB section	14.848	0.37859	-0.044993	0.12518	1.104	-0.26587	0.071155
16MBOM44	44m in MB section	50.378	1.1458	-0.044993	0.12518	-2.9935	-0.26587	0.071155
16MBOM311	311m in MB section	26.982	0.65299	-0.044993	0.12518	0.19105	-0.26587	0.071155
16MBOM345	345m in MB section	47.902	1.0841	-0.044993	0.12518	1.7831	-0.26587	0.071155
YA16OM54	54m in MB section	113.778	2.5238	-0.044993	0.12518	0.33143	-0.26587	0.071155
YA16OM33	33m in MB section	29.272	0.68432	-0.044993	0.12518	-6.4483	-0.26587	0.071155
16LIG01	~350m below MD section	2.444	0.11841	-0.044993	0.12518	1.2883	-0.26587	0.071155
17MCOM04	4 m in MC section	7.314	0.3721	-0.32544	0.13916	2.0312	-0.16738	0.17854
17MCOM09	9 m in MC section	20.937	0.81862	-0.32544	0.13916	-9.1345	-0.16738	0.17854
17MCOM79	79 m in MC section	43.148	1.6095	-0.32544	0.13916	-5.9663	-0.16738	0.17854
17MCOM87	87 m in MC section	48.237	1.8406	-0.32544	0.13916	4.9545	-0.16738	0.17854
17MDOM02	2 m in MD section	18.389	0.71656	-0.32544	0.13916	-0.29152	-0.16738	0.17854
17MDOM13	13 m in MD section	63.577	2.2279	-0.32544	0.13916	15.4724	-0.16738	0.17854
17MDOM23	23 m in MD section	8.82	0.38212	-0.32544	0.13916	-0.47639	-0.16738	0.17854
17MDOM31	21 m in MD section	79.852	2.6932	-0.32544	0.13916	7.0634	-0.16738	0.17854
17MDOM35	35 m in MD sction	36.295	1.4328	-0.32544	0.13916	19.3023	-0.16738	0.17854
17MDOM44	44 m in MD section	4.724	0.23827	-0.32544	0.13916	11.0702	-0.16738	0.17854

Table DR2 - Grain-counting results

Sample	Stratigraphic location	Qm	Qp	Phylo	Heavy M	Opaque	F	Lmeta	Lsed	Lcarb	Lvolc	Total
16LETKAT	Letkat Fm, along the road, level ~80m in LA section (sample for DZ U-Pb dating as well)	194	20	14	14	4	12	14	41	0	7	320
PAUN	Paunggyi Formation, along the road (sample for DZ U-Pb dating as well)	142	24	0	2	5	35	23	28	1	54	314
YA16DZ01	Very most base of the Yaw Formation, out of the log (sample for DZ U-Pb dating as well)	87	58	6	5	13	26	22	42	2	49	310
YA16DZ02	Level 271, MA section, middle of Letkat Fm (sample for DZ U-Pb dating as well)	186	17	6	4	4	13	26	42	0	23	321
YA16DZ03	Level 181, MA section, base of Letkat Fm (sample for DZ U-Pb dating as well)	182	19	7	8	5	17	34	40	0	36	348
YA16DZ04	Level 85, MA section, sandstone below letkat Fm (sample for DZ U-Pb dating as well)	137	40	2	15	8	11	31	34	4	59	341
YA16QFL01	Level 87, MA section (Yaw Fm)	159	24	0	1	2	11	31	56	0	27	311
YA16QFL02	level 34, MA section (Yaw Fm)	131	26	0	6	11	29	29	56	0	57	345
YA16QFL03	Level 371, MA section (Letkat Fm)	213	21	5	7	6	27	19	26	0	21	345
YA16QFL05	Level 321, MA section (Letkat Fm)	216	44	0	3	3	12	18	27	0	17	340
YA16QFL06	Level 221, MA section (Letkat Fm)	203	9	5	14	3	10	22	46	1	28	341
YA16QFL09	Level 486, MA section (Letkat Fm)	186	25	7	7	6	33	15	29	1	4	313
16MBQFL217	Level 217, MB section (Yaw Fm)	169	12	0	2	12	23	17	58	1	44	338

Q	F	L	Lm	Ls	Lv
74.3	1.4	21.5	22.6	66.1	11.3
54.1	1.6	34.5	21.9	26.7	51.4
50.7	4.5	40.2	19.5	37.2	43.4
66.1	1.3	29.6	28.6	46.2	25.3
61.3	1.5	33.5	30.9	36.4	32.7
56.0	2.5	40.5	25.0	27.4	47.6
59.4	0.6	37.0	27.2	49.1	23.7
47.9	3.4	43.3	20.4	39.4	40.1
71.6	1.8	20.2	28.8	39.4	31.8
77.8	0.9	18.6	29.0	43.5	27.4
66.5	0.9	30.4	22.9	47.9	29.2
72.0	2.0	16.7	31.3	60.4	8.3
55.9	3.7	37.0	14.3	48.7	37.0

Table DR3 - U-Pb results

Sample name	Location	Description
YA16DZ01	23°13'06.6"N, 94°14'52.2"E	Very most base of the Yaw Formation, out of the log
YA16DZ02	23°13'42.6"N, 94°15'58.7"E	Level 271, MA section, middle of Letkat Fm
YA16DZ03	23°13'42.6"N, 94°15'58.7"E	Level 181, MA section, base of Letkat Fm
YA16DZ04	23°13'42.6"N, 94°15'58.7"E	Level 85, MA section, sandstone below letkat Fm
LETKAT	23°11'32.1"N, 94°16'07.4"E	Letkat Fm, along the road, level ~80m in LA section
17LETKAT08	23°19'10.7"N, 94°17'54.3"E	Letkat Fm, level 476m in LA section
PAUN	23°13'27.4"N, 94°09'07.7"E	Paunggyi Formation
16MBV01	23°14'23.3"N, 94°15'48.3"E	Tuff layer, level 332 in MB section

1. Measured ratios corrected for downhole fraction and instrument bias.
2. Ages are given uncorrected for common lead, and corrected following Andersen's method. We recommend the use of uncorrected ages (Andersen's method sometimes fails to accurately reproduce the age of international standards with our set up).
3. Best age is determined from 206Pb/238U age for analyses with 206Pb/238U age <1200 Ma and from 206Pb/207Pb age for analyses with 206Pb/238U age > 1200 Ma.
4. All uncertainties include only measurement errors and are given in 2 s.
5. additionnal systematic uncertainty during the sessions: ~1.3%.
6. Accuracy: observed offset for the ages of our secondary standards (R33 and GHB) during the sessions is in most of cases < 2%, and in rare cases up to 4 %.
7. Analyses with 206Pb/238U age > 500 Ma and with >20% discordance (<80% concordance) are included but are noted as discordant
8. Analyses with 206Pb/238U age > 500 Ma and with >5% reverse discordance (<105% concordance) are included but are noted as discordant
9. concordance is calculated between 206Pb/238U and 206Pb/207Pb ages;

Sample 16YADZ01

	Ratios						U-Pb ages uncorrected for common lead									Corrected for common lead using Andersen's routine					
Grain	Final207_235	Final207_235_2s	Final206_238	Final206_238_2s	Final207_206	Final207_206_2s	FinalAge 207_235	FinalAge 207_235_2s	FinalAge 206_238	FinalAge 206_238_2s	FinalAge 207_206	FinalAge 207_206_2s	Concordance (%)	Best age	Best age 2s	FinalAgeAnd207_235	FinalAgeAnd207_235_2s	FinalAgeAnd206_238	FinalAgeAnd206_238_2s	FinalAgeAnd207_206	FinalAgeAnd207_206_2s
Z001	0.754	0.018	0.0929	0.001	0.0591	0.0014	570	10	572.7	6	561	53	-2.1	572.7	6.0	552.6	6.1	571.2	6.4	488	30
Z002	0.057	0.01	0.0078	0.00028	0.0472	0.0051	55.5	9.5	50.1	1.8	120	230	58.3	50.1	1.8	50	1.9	49.9	1.9	50.1	1.8
Z003	0.484	0.018	0.05982	0.00093	0.0591	0.0028	400	12	374.5	5.6	539	97	30.5	374.5	5.6	366.5	6.2	371.9	6.3	334	23
Z004	0.34	0.016	0.0456	0.00084	0.0534	0.0028	297	12	287.4	5.2	320	110	10.2	287.4	5.2	283.5	6.1	286.5	5.7	245	26
Z005	1.688	0.071	0.159	0.0025	0.0754	0.0036	1002	26	951	14	1063	92	10.5	951.0	14.0	941	15	944	16	913	33
Z006	7.16	0.28	0.3902	0.007	0.1312	0.0051	2127	36	2123	32	2122	60	0.0	2122.0	60.0	2086	34	2112	36	2054	39
Z007	0.0612	0.0064	0.00794	0.0002	0.0542	0.0052	60.1	6.1	51	1.3	350	200	85.4	51.0	1.3	50.5	1.3	50.4	1.4	50.9	1.3
Z008	2.229	0.062	0.2015	0.0031	0.0806	0.0016	1188	20	1183	17	1206	40	1.9	1183.0	17.0	1166	19	1180	17	1139	23
Z009	0.938	0.051	0.1034	0.0017	0.0661	0.0037	668	26	634.3	9.6	760	110	16.5	634.3	9.6	612	12	629	11	566	36
Z010	0.0383	0.0048	0.0065	0.00015	0.0428	0.0056	38.1	4.7	41.79	0.95	-100	220	141.8	41.8	1.0	42	1.1	42	1.1	41.79	0.95
Z011	0.0767	0.0033	0.01218	0.00081	0.0453	0.0018	75.1	3.1	78	5.1	-15	75	620.0	78.0	5.1	78.3	5.3	78.2	5.3	73.4	7.2
Z012	0.133	0.01	0.0203	0.0003	0.0477	0.0037	126.1	9	129.5	1.9	90	150	-43.9	129.5	1.9	129.5	2.1	129.7	2.1	127.6	3.8
Z014	0.0526	0.0061	0.0084	0.00025	0.0451	0.0056	51.9	5.9	53.9	1.6	-20	220	369.5	53.9	1.6	54	1.7	54.1	1.8	53.8	1.7
Z015	0.32	0.049	0.0416	0.0013	0.0552	0.0087	274	37	262.5	8.1	330	290	20.5	262.5	8.1	260.6	9.4	261	9.7	257.7	9.7
Z016	2.19	0.14	0.1945	0.0054	0.0804	0.0045	1171	45	1145	29	1180	110	3.0	1145.0	29.0	1119	37	1138	30	1074	58
Z017	0.0487	0.0073	0.00792	0.00027	0.0443	0.0066	48.1	7	50.8	1.7	-60	250	184.7	50.8	1.7	50.9	1.8	51	1.8	50.6	1.7
Z018	0.0425	0.0069	0.00722	0.00025	0.0436	0.0074	42.1	6.8	46.4	1.6	-100	270	146.4	46.4	1.6	46.6	1.8	46.6	1.8	46.5	1.6
Z019	2.691	0.096	0.235	0.0051	0.0815	0.0032	1324	27	1361	27	1221	78	-11.5	discordant	discordant	1304	23	1357	28	1184	61
Z020	0.64	0.13	0.013	0.0013	0.328	0.048	468	80	83	8	3300	320	97.5	83.0	8.0	57.6	6.4	51.7	3.7	270	170
Z021	2.26	0.13	0.2011	0.0037	0.0801	0.005	1194	42	1181	20	1170	120	-0.9	1181.0	20.0	1144	27	1174	21	1059	81
Z022	3.917	0.088	0.2826	0.0044	0.0991	0.0018	1616	18	1604	22	1605	35	0.1	1605.0	35.0	1595	21	1600	23	1573	22
Z023	3.99	0.15	0.2801	0.0058	0.1015	0.002	1629	31	1591	29	1649	36	3.5	1649.0	36.0	1588	28	1584	29	1579	24
Z024	0.732	0.022	0.0888	0.0014	0.0589	0.0013	557	13	548.4	8.4	558	48	1.7	548.4	8.4	539	10	547.1	8.6	493	26
Z025	0.0495	0.0039	0.00684	0.00019	0.0525	0.0045	49	3.7	43.9	1.2	270	160	83.7	43.9	1.2	43.6	1.3	43.6	1.3	43.8	1.3
Z027	0.903	0.021	0.1076	0.0012	0.061	0.0014	653	11	658.5	7.2	629	51	-4.7	658.5	7.2	643.4	8.3	657.4	7.4	577	36
Z028	2.075	0.06	0.1899	0.0049	0.0779	0.0014	1139	20	1120	26	1141	34	1.8	1120.0	26.0	1120	27	1118	28	1086	27
Z029	4.89	0.19	0.3255	0.0065	0.1083	0.0035	1797	32	1816	32	1760	61	-3.2	1760.0	61.0	1769	35	1810	34	1706	51
Z030	1.327	0.052	0.1237	0.0033	0.078	0.0044	855	23	751	19	1130	110	33.5	discordant	discordant	734	19	739	21	723	23
Z031	4.51	0.097	0.3033	0.0058	0.1062	0.0014	1732	18	1707	29	1734	24	1.6	1734.0	24.0	1704	27	1702	31	1683	25
Z032	0.098	0.04	0.00825	0.00062	0.081	0.029	91	33	52.9	4	690	520	92.3	52.9	4.0	49.5	3.7	49.4	3.7	52.9	4
Z033	0.35	0.033	0.04575	0.00099	0.0542	0.0048	303	25	288.4	6.1	340	180	15.2	288.4	6.1	286.1	6.1	287	5.8	276	16
Z034	0.66	0.013	0.0804	0.0012	0.0588	0.0011	514.4	8	498.4	7.4	556	41	10.4	498.4	7.4	495.3	6.6	496.8	7.5	471	19
Z035	13.99	0.23	0.5112	0.0075	0.199	0.0031	2747	16	2661	32	2816	25	5.5	2816.0	25.0	2645	34	2620	42	2671	32
Z036	2.092	0.052	0.194	0.003	0.0783	0.0012	1145	17	1143	16	1152	30	0.8	1143.0	16.0	1128	16	1140	17	1107	17
Z037	1.752	0.05	0.1692	0.0025	0.0752	0.0016	1026	18	1007	14	1068	45	5.7	1007.0	14.0	994	16	1003	14	968	26
Z038	0.805	0.029	0.099	0.001	0.0589	0.002	598	16	608.6	6	546	75	-11.5	discordant	discordant	585	11	607.4	6	490	47
Z039	0.079	0.014	0.00953	0.00099	0.0619	0.0072	77	13	61.1	6.3	580	230	89.5	61.1	6.3	57.5	3.8	57.5	3.8	61.1	6.3
Z040	0.082	0.016	0.0094	0.00038	0.063	0.011	79	15	60.3	2.4	540	360	88.8	60.3	2.4	59.1	2.8	59.1	2.8	60.1	2.5
Z041	0.326	0.063	0.01062	0.00061	0.211	0.035	274	48	68.1	3.9	2490	380	97.3	68.1	3.9	53.2	2.3	52.8	2.3	68.1	3.9
Z042	2.427	0.097	0.2085	0.0058	0.0819	0.0031	1249	29	1220	31	1235	78	1.2	1235.0	78.0	1207	31	1214	33	1162	58
Z043	0.058	0.012	0.008	0.00034	0.052	0.011	56	12	51.4	2.2	160	360	67.9	51.4	2.2	51	2.4	51	2.4	51.4	2.2
Z044	1.953	0.067	0.1838	0.0032	0.0754	0.0023	1098	23	1088	17	1072	61	-1.5	1088.0	17.0	1075	19	1085	18	1020	39
Z045	0.675	0.019	0.08435	0.00084	0.0581	0.0017	523	12	522	5	522	61	0.0	522.0	5.0	504.2	6.4	520.5	5.2	433	30
Z046	0.0619	0.0063	0.0095	0.00024	0.0476	0.0049	60.8	6	61	1.5	80	190	23.8	61.0	1.5	61	1.6	61	1.6	61	1.5
Z047	0.0474	0.0069	0.00779	0.00025	0.0458	0.0072	46.8	6.7	50	1.6	-30	250	266.7	50.0	1.6	50.1	1.6	50.1	1.6	50	1.6
Z048	2.165	0.082	0.1973	0.0032	0.0799	0.0033	1166	27	1161	17	1171	83	0.9	1161.0	17.0	1117	19	1154	19	1047	51
Z049	0.564	0.024	0.0718	0.0018	0.057	0.0019	453	16	447	11	474	73	5.7	447.0	11.0	435	11	446	11	377	32

Z050	0.268	0.033	0.03325	0.00044	0.0587	0.007	238	23	210.9	2.8	480	200	56.1	210.9	2.8	206.2	2.7	208.7	2.5	182	20
Z051	2.034	0.061	0.1895	0.0033	0.0777	0.0012	1125	20	1118	18	1135	31	1.5	1118.0	18.0	1108	20	1116	18	1087	22
Z053	1.787	0.041	0.1753	0.003	0.0741	0.0015	1040	15	1041	17	1039	41	-0.2	1041.0	17.0	1021	14	1039	17	992	25
Z054	0.104	0.015	0.0114	0.00034	0.0662	0.009	99	13	73.1	2.2	670	260	89.1	73.1	2.2	70.6	1.9	70.6	1.9	73.2	2.2
Z055	7.34	0.11	0.3759	0.0065	0.1417	0.0018	2153	13	2056	31	2247	21	8.5	2247.0	21.0	2043	34	2027	37	2073	37
Z056	2.037	0.052	0.1939	0.0042	0.0755	0.0018	1127	17	1142	23	1076	48	-6.1	discordant	discordant	1112	16	1140	23	1045	35
Z058	0.678	0.019	0.0831	0.001	0.0591	0.0018	525	12	514.8	6.1	558	65	7.7	514.8	6.1	505.3	7.3	513.2	6.3	458	26
Z059	1.969	0.047	0.1848	0.0044	0.0757	0.0014	1104	16	1093	24	1083	37	-0.9	1093.0	24.0	1086	22	1091	25	1040	24
Z060	3.317	0.05	0.2559	0.0026	0.0942	0.0014	1484	12	1469	13	1509	28	2.7	1509.0	28.0	1459	12	1464	14	1447	14
Z061	0.2477	0.0087	0.03352	0.00046	0.0538	0.002	224.4	7.1	212.5	2.9	342	81	37.9	212.5	2.9	210.4	2.9	211.6	3	201.6	9.5
Z063	3.96	0.14	0.2798	0.0062	0.1004	0.0031	1624	27	1590	31	1624	58	2.1	1624.0	58.0	1566	24	1579	34	1529	27
Z064	2.752	0.097	0.226	0.0057	0.0872	0.0024	1340	26	1313	30	1357	52	3.2	1357.0	52.0	1300	29	1307	32	1267	32
Z065	16.19	0.5	0.509	0.013	0.2248	0.0053	2886	29	2650	54	3013	38	12.0	3013.0	38.0	2609	74	2531	77	2662	64
Z066	0.074	0.02	0.0079	0.00042	0.062	0.015	71	18	50.7	2.7	450	440	88.7	50.7	2.7	49.3	2.7	49.3	2.8	50.4	3.2
Z068	0.821	0.016	0.1006	0.0014	0.05955	0.00098	610.4	9.8	618.1	8.2	583	35	-6.0	discordant	discordant	602.9	9	617.6	8.4	548	23
Z071	0.833	0.031	0.1003	0.0018	0.0605	0.0024	614	17	616	11	598	83	-3.0	616.0	11.0	593	11	614	11	512	39
Z072	3.89	0.2	0.2742	0.0088	0.1001	0.0041	1607	43	1561	45	1617	77	3.5	1617.0	77.0	1555	50	1552	49	1521	54
Z073	3.138	0.08	0.2468	0.0029	0.0921	0.0021	1440	20	1422	15	1463	43	2.8	1463.0	43.0	1398	15	1415	16	1378	23
Z074	0.769	0.023	0.0931	0.0016	0.0591	0.0012	579	13	573.6	9.4	567	45	-1.2	573.6	9.4	565	11	572.4	9.5	525	24
Z075	1.187	0.054	0.1302	0.0017	0.066	0.0026	791	25	789	10	785	80	-0.5	789.0	10.0	760	16	785.8	9.9	697	43
Z076	1.435	0.055	0.1462	0.0023	0.071	0.0017	901	23	880	13	949	49	7.3	880.0	13.0	868	16	876	13	856	20
Z077	1.409	0.071	0.1462	0.0029	0.068	0.0025	890	31	879	17	886	61	0.8	879.0	17.0	875	19	877	16	831	39
Z078	0.801	0.017	0.0977	0.0012	0.0594	0.0012	597	9.7	601	6.9	576	45	-4.3	601.0	6.9	582.8	7	599.8	7.1	523	30
Z079	0.233	0.096	0.0109	0.0013	0.131	0.042	186	68	69.9	8.2	1130	520	93.8	69.9	8.2	60.8	4.7	59.5	3.4	70.1	8.3
Z080	0.104	0.014	0.00925	0.0002	0.0805	0.0096	100	13	59.3	1.3	1030	230	94.2	59.3	1.3	56.7	1.2	56.7	1.2	59.4	1.3
Z082	0.07	0.011	0.00803	0.00032	0.067	0.013	68	11	51.5	2	540	340	90.5	51.5	2.0	50.8	2.5	50.8	2.5	51.5	2
Z083	0.153	0.033	0.0102	0.00032	0.102	0.019	140	29	65.4	2	1200	390	94.6	65.4	2.0	60.4	1.2	60.3	1.2	65.4	2
Z084	10.53	0.24	0.4567	0.0085	0.1674	0.0029	2480	21	2424	38	2529	29	4.2	2529.0	29.0	2395	32	2395	44	2411	31
Z085	2.078	0.047	0.1957	0.0029	0.0758	0.0016	1141	16	1152	16	1084	43	-6.3	discordant	discordant	1133	14	1151	16	1066	34
Z086	0.653	0.027	0.0826	0.0015	0.0576	0.0026	509	17	511.6	9	490	100	-4.4	511.6	9.0	496.9	9.7	508.5	8.8	456	30
Z087	0.0663	0.0075	0.00882	0.0002	0.0549	0.0064	64.9	7.2	56.6	1.3	320	230	82.3	56.6	1.3	56	1.5	56	1.5	56.4	1.3
Z088	2.337	0.096	0.2108	0.0029	0.0806	0.0034	1219	30	1233	15	1185	88	-4.1	1185.0	88.0	1185	23	1228	16	1113	55
Z090	0.75	0.054	0.0926	0.0018	0.0593	0.0047	563	32	571	10	510	170	-12.0	discordant	discordant	555	13	569	12	501	41
Z091	0.05	0.011	0.00752	0.00032	0.05	0.011	49	10	48.3	2	30	360	-61.0	48.3	2.0	48.3	2.4	48.3	2.4	48.3	2
Z092	0.0594	0.0081	0.00817	0.00019	0.053	0.0072	58.3	7.7	52.5	1.2	240	250	78.1	52.5	1.2	52.1	1.4	52.1	1.4	52.5	1.2
Z093	0.49	0.014	0.06367	0.00081	0.0558	0.0016	404.7	9.8	397.9	4.9	432	65	7.9	397.9	4.9	390.2	7.2	396.8	5.1	342	30
Z094	2.47	0.1	0.2122	0.0037	0.0846	0.0036	1258	29	1240	19	1283	82	3.4	1283.0	82.0	1197	17	1232	21	1168	31
Z095	0.0665	0.0057	0.01034	0.00023	0.048	0.0046	65.2	5.4	66.3	1.4	90	170	26.3	66.3	1.4	66.2	1.6	66.3	1.6	66.4	1.5
Z096	0.073	0.011	0.00948	0.00036	0.0549	0.0077	71	11	60.8	2.3	310	270	80.4	60.8	2.3	60.1	2.2	60.1	2.2	60.8	2.3
Z097	0.75	0.026	0.0872	0.0011	0.0625	0.0024	567	15	539	6.6	668	84	19.3	539.0	6.6	527.2	7.2	535.5	7	486	33
Z098	3.84	0.13	0.2809	0.0056	0.0992	0.003	1596	28	1595	28	1597	57	0.1	1597.0	57.0	1560	27	1588	30	1518	31
Z099	0.43	0.015	0.05992	0.0007	0.0519	0.0018	363	11	375.1	4.3	270	75	-38.9	375.1	4.3	367.9	4.9	375.4	4.4	303	30
Z100	0.082	0.042	0.00896	0.00093	0.058	0.019	73	33	57.5	5.9	150	510	61.7	57.5	5.9	56.1	4.8	56.4	4.7	57.5	5.9
Z102	2.19	0.19	0.1958	0.0046	0.0816	0.0071	1158	62	1152	25	1130	190	-1.9	1152.0	25.0	1096	30	1142	28	1017	63
Z103	0.622	0.03	0.0738	0.0025	0.0607	0.0032	489	18	459	15	620	120	26.0	459.0	15.0	444	11	455	16	405	31
Z104	0.2537	0.0096	0.03479	0.00047	0.0528	0.0019	229.2	7.8	220.5	2.9	303	79	27.2	220.5	2.9	218	2.9	219.6	3	188	17
Z105	0.641	0.018	0.081	0.001	0.0573	0.0013	503	11	501.8	6.1	495	50	-1.4	501.8	6.1	488.3	8.7	500.6	6.3	432	30
Z106	0.0386	0.0026	0.00607	0.0001	0.0462	0.0031	38.5	2.6	39	0.64	30	120	-30.0	39.0	0.6	39.09	0.67	39.04	0.64	38.97	0.65
Z107	0.666	0.016	0.08267	0.00097	0.0584	0.001	517.6	9.7	512	5.7	539	40	5.0	512.0	5.7	504	7.4	510.8	5.9	476	20
Z108	0.0424	0.0048	0.00705	0.00017	0.0437	0.0052	42	4.7	45.3	1.1	-80	200	156.6	45.3	1.1	45.5	1.2	45.5	1.2	45.3	1.1
Z109	0.11	0.014	0.01386	0.00049	0.0598	0.0088	106	13	88.7	3.1	470	280	81.1	88.7	3.1	87.2	3.4	87.1	3.4	88.7	3.2
Z110	8.32	0.15	0.4175	0.0043	0.1439	0.0019	2265	17	2249	20	2273	23	1.1	2273.0	23.0	2245	22	2243	22	2234	22

Z111	11.7	0.17	0.4836	0.0038	0.1755	0.0025	2579	13	2543	17	2609	24	2.5	2609.0	24.0	2547	18	2530	22	2561	21
Z112	0.494	0.038	0.05953	0.00086	0.0614	0.005	410	27	372.7	5.2	570	150	34.6	372.7	5.2	367.2	5.3	369.2	4.8	350	20
Z113	0.0484	0.0036	0.00727	0.00016	0.0488	0.0036	47.9	3.4	46.7	1	130	140	64.1	46.7	1.0	46.6	1.1	46.6	1.1	46.5	1.2
Z114	0.736	0.035	0.0904	0.0011	0.0584	0.0026	558	20	558.2	6.5	540	100	-3.4	558.2	6.5	534.3	9	556	7	437	44
Z115	0.06	0.011	0.00841	0.00029	0.0521	0.0098	58	11	54	1.9	150	320	64.0	54.0	1.9	53.7	2.1	53.7	2.1	54.1	1.9
Z116	2.505	0.091	0.2174	0.0061	0.0823	0.0022	1271	27	1268	33	1246	51	-1.8	1246.0	51.0	1246	30	1264	34	1186	33
Z117	0.0621	0.0067	0.00782	0.00023	0.0563	0.0061	60.9	6.4	50.2	1.5	420	210	88.0	50.2	1.5	49.6	1.6	49.6	1.6	50.2	1.5
Z118	2.144	0.06	0.1979	0.003	0.0787	0.0022	1166	18	1164	16	1152	60	-1.0	1164.0	16.0	1133	15	1160	17	1096	33
Z119	2.082	0.052	0.1932	0.0026	0.0779	0.0018	1141	17	1138	14	1137	45	-0.1	1138.0	14.0	1113	11	1135	14	1090	23
Z120	0.653	0.033	0.0825	0.0011	0.0574	0.003	508	20	511.1	6.4	500	130	-2.2	511.1	6.4	497.3	9.1	509.6	7.3	444	37

Sample 16YADZ02

	Ratios						U-Pb ages uncorrected for common lead									Corrected for common lead using Andersen's routine					
Grains	Final207_235	Final207_235_2s	Final206_238	Final206_238_2s	Final207_206	Final207_206_2s	FinalAge 207_235	FinalAge 207_235_2s	FinalAge 206_238	FinalAge 206_238_2s	FinalAge 207_206	FinalAge 207_206_2s	Concordance (%)	Best age	Best age 2s	FinalAgeAnd207_235	FinalAgeAnd207_235_2s	FinalAgeAnd206_238	FinalAgeAnd206_238_2s	FinalAgeAnd207_206	FinalAgeAnd207_206_2s
Z001	0.832	0.02	0.09686	0.00098	0.0625	0.0015	614	11	595.9	5.8	682	51	12.6	595.9	5.8	585.6	6.2	593.4	6	557	21
Z002	0.794	0.026	0.097	0.001	0.0596	0.0021	592	14	597.1	5.9	569	76	-4.9	597.1	5.9	576.6	7.4	595.6	6.3	512	37
Z003	0.085	0.0068	0.01277	0.00026	0.0486	0.0037	82.7	6.4	81.8	1.7	130	150	37.1	81.8	1.7	81.7	1.7	81.8	1.7	81.9	1.7
Z004	0.774	0.025	0.0925	0.0013	0.0601	0.0018	581	14	570.5	7.6	609	69	6.3	570.5	7.6	556.1	9.6	568.2	8	498	34
Z005	1.699	0.035	0.1672	0.0026	0.074	0.0017	1007	13	996	15	1035	45	3.8	996.0	15.0	978	11	993	15	950	22
Z006	1.396	0.047	0.1401	0.0028	0.0729	0.0026	886	20	845	16	1001	69	15.6	845.0	16.0	833	15	839	17	820	21
Z007	4.635	0.097	0.2928	0.0051	0.1151	0.0014	1754	17	1655	25	1880	22	12.0	1880.0	22.0	1646	28	1634	28	1661	28
Z008	1.216	0.027	0.1175	0.0021	0.0758	0.0027	807	12	716	12	1075	70	33.4	discordant	discordant	708	14	706	14	714	13
Z009	0.968	0.032	0.081	0.0025	0.087	0.002	686	16	502	15	1354	45	62.9	discordant	discordant	487	15	484	15	502	15
Z010	5.9	0.19	0.2951	0.0085	0.1455	0.0023	1957	27	1665	42	2291	28	27.3	discordant	discordant	1623	44	1592	45	1665	42
Z011	0.704	0.039	0.0858	0.0014	0.0599	0.0034	539	23	530.8	8.2	570	120	6.9	530.8	8.2	511	12	528.3	8.8	438	51
Z012	0.768	0.03	0.0928	0.0026	0.0601	0.0015	577	17	572	15	597	54	4.2	572.0	15.0	559	15	570	15	525	25
Z013	1.95	0.12	0.174	0.0028	0.0818	0.0048	1090	41	1034	15	1200	120	13.8	1034.0	15.0	999	20	1019	14	968	51
Z014	0.062	0.01	0.00879	0.00026	0.0506	0.0078	60.9	9.5	56.4	1.6	200	290	71.8	56.4	1.6	56.1	2	56.1	2	56.4	1.6
Z015	12.29	0.21	0.468	0.0064	0.191	0.0028	2625	16	2474	28	2748	25	10.0	2748.0	25.0	2450	35	2410	38	2485	33
Z016	0.414	0.043	0.04151	0.00082	0.0728	0.0077	347	31	262.1	5.1	860	210	69.5	262.1	5.1	254.7	5.9	256.6	5.3	256.2	9.1
Z017	1.484	0.025	0.1515	0.0014	0.0712	0.0011	923	10	909.6	7.7	960	30	5.3	909.6	7.7	901.8	7.9	907.1	8	893	13
Z019	1.718	0.031	0.1675	0.002	0.0744	0.0014	1014	12	998	11	1046	40	4.6	998.0	11.0	987	12	995	12	963	23
Z020	0.092	0.011	0.01272	0.00041	0.0531	0.007	89	11	81.4	2.6	250	250	67.4	81.4	2.6	80.9	2.8	81	2.8	81.1	2.7
Z021	0.812	0.062	0.1011	0.0021	0.059	0.0049	613	42	621	13	520	180	-19.4	discordant	discordant	606	17	621	15	552	43
Z022	0.0642	0.0045	0.01004	0.00021	0.0464	0.0031	63.1	4.3	64.4	1.3	40	120	-61.0	64.4	1.3	64.1	1.2	64.2	1.2	64.5	1.3
Z023	0.0704	0.0099	0.0109	0.0003	0.0473	0.0069	68.6	9.3	69.9	1.9	30	250	-133.0	69.9	1.9	69.9	2.1	70	2.1	69.9	1.9
Z024	0.615	0.024	0.0752	0.0022	0.0595	0.002	485	15	467	13	569	73	17.9	467.0	13.0	453	12	465	13	401	30
Z026	0.095	0.021	0.00984	0.00032	0.069	0.014	91	18	63.1	2	620	360	89.8	63.1	2.0	61.5	2.4	61.6	2.4	63.5	2.4
Z027	0.779	0.026	0.09496	0.00088	0.0597	0.0019	584	15	584.8	5.2	573	73	-2.1	584.8	5.2	562.4	9.5	582.8	5.2	479	50
Z028	0.743	0.022	0.0922	0.001	0.0586	0.0017	563	13	568.7	6.2	538	64	-5.7	discordant	discordant	548.2	8.8	567.3	6.3	469	43
Z029	0.061	0.0083	0.00893	0.00023	0.0498	0.0069	59.8	7.9	57.3	1.5	120	250	52.3	57.3	1.5	57.1	1.6	57.1	1.6	57.3	1.5
Z030	0.811	0.025	0.097	0.0014	0.0608	0.0017	602	14	596.8	8.2	620	62	3.7	596.8	8.2	579.7	9.2	594.8	8.3	530	32
Z031	0.1011	0.0087	0.01642	0.00035	0.0448	0.004	97.4	8	105	2.2	-20	160	625.0	105.0	2.2	105.3	2.5	105.4	2.5	104.3	3
Z032	0.0663	0.0079	0.01048	0.00032	0.0458	0.005	65	7.4	67.2	2	0	190	#DIV/0!	67.2	2.0	67.3	2	67.4	2	67.3	2
Z033	0.602	0.02	0.076	0.0012	0.0576	0.0021	477	13	472.4	7.5	496	80	4.8	472.4	7.5	462.2	9.1	471.2	8	433	24
Z035	0.0651	0.0088	0.00974	0.00023	0.0486	0.0067	63.7	8.4	62.5	1.4	90	240	30.6	62.5	1.4	62.4	1.5	62.4	1.6	62.5	1.4
Z036	0.619	0.02	0.0788	0.00087	0.057	0.0018	489	13	488.9	5.2	474	71	-3.1	488.9	5.2	476.8	6.6	487.8	5.2	433	28
Z038	0.663	0.022	0.0829	0.0015	0.0584	0.0022	516	13	513.1	9.2	524	80	2.1	513.1	9.2	499	10	511.7	9.8	440	33
Z039	2.184	0.063	0.1918	0.0036	0.0831	0.0027	1174	20	1131	20	1260	64	10.2	1131.0	20.0	1114	16	1122	22	1090	26
Z040	0.1054	0.007	0.01549	0.00039	0.0509	0.0042	101.5	6.4	99.1	2.5	190	150	47.8	99.1	2.5	98.6	2.8	98.8	2.8	97.6	3.3
Z041	1.716	0.04	0.167	0.0019	0.0748	0.002	1013	15	995	11	1053	54	5.5	995.0	11.0	975	11	991	12	941	27
Z042	3.67	0.18	0.2585	0.007	0.102	0.0029	1557	37	1481	36	1663	55	10.9	1663.0	55.0	1470	37	1466	37	1477	37
Z043	0.752	0.057	0.0903	0.0019	0.0608	0.0048	564	34	557	11	560	170	0.5	557.0	11.0	537	13	554	12	462	48
Z044	2.156	0.054	0.1927	0.0023	0.0814	0.0021	1165	17	1136	12	1221	51	7.0	1136.0	12.0	1120	14	1130	13	1102	23
Z045	0.095	0.013	0.01425	0.00046	0.0492	0.0069	91	12	91.2	2.9	100	250	8.8	91.2	2.9	91.2	3.3	91.2	3.3	91.2	2.9
Z046	1.368	0.048	0.1398	0.0032	0.0707	0.0018	873	21	843	18	950	57	11.3	843.0	18.0	830	18	838	19	810	24
Z047	0.273	0.012	0.03634	0.00058	0.0547	0.0025	244.5	9.3	230.1	3.6	375	98	38.6	230.1	3.6	227.2	4.3	228.9	3.9	218	11
Z048	1.729	0.075	0.1703	0.0027	0.0739	0.0032	1015	28	1013	15	1010	90	-0.3	1013.0	15.0	971	19	1008	16	913	42
Z049	0.0669	0.0056	0.01001	0.00031	0.049	0.0044	65.6	5.3	64.2	2	170	180	62.2	64.2	2.0	63.9	2.1	64	2.1	63.7	2.1
Z050	0.077	0.012	0.01048	0.0004	0.0542	0.0093	75	12	67.2	2.6	290	330	76.8	67.2	2.6	66.7	3.1	66.7	3.1	67.2	2.6
Z051	0.889	0.054	0.1008	0.0024	0.0642	0.003	642	26	619	14	724	80	14.5	619.0	14.0	612	13	615	12	606	21

Z052	1.732	0.072	0.1684	0.0057	0.0753	0.0029	1018	27	1003	31	1063	79	5.6	1003.0	31.0	974	26	998	33	944	36
Z053	0.119	0.012	0.01821	0.00043	0.0464	0.0047	113	11	116.3	2.7	60	190	-93.8	116.3	2.7	116.1	3	116.5	3	114.1	4.7
Z054	0.728	0.02	0.09131	0.0009	0.0585	0.002	554	12	563.2	5.3	530	75	-6.3	discordant	discordant	542.9	8.3	561.9	5.6	461	45
Z055	10.35	0.2	0.4579	0.0074	0.1637	0.002	2465	17	2429	33	2493	20	2.6	2493.0	20.0	2413	28	2412	37	2417	24
Z056	0.0539	0.0091	0.00861	0.00027	0.0451	0.0072	52.8	8.8	55.3	1.7	-40	260	238.3	55.3	1.7	55.4	1.7	55.4	1.7	55.3	1.8
Z057	0.101	0.02	0.01068	0.00043	0.069	0.013	96	18	68.5	2.7	630	380	89.1	68.5	2.7	66.2	3.1	66.2	3.1	68.2	2.8
Z058	0.075	0.011	0.0083	0.00015	0.0652	0.0085	73	10	53.32	0.96	600	240	91.1	53.3	1.0	52.06	0.91	52.03	0.91	53.32	0.96
Z059	0.079	0.011	0.01022	0.00023	0.0558	0.0072	76	10	65.5	1.5	370	240	82.3	65.5	1.5	64.7	1.5	64.6	1.5	65.2	1.6
Z060	0.776	0.025	0.0938	0.0012	0.0601	0.002	582	14	578.2	7	591	70	2.2	578.2	7.0	558.7	6.4	576.2	7.3	499	33
Z061	0.0699	0.009	0.00735	0.00016	0.0717	0.0096	68.2	8.4	47.2	1	770	260	93.9	47.2	1.0	45.8	1.2	45.7	1.2	47.2	1
Z062	0.2686	0.0085	0.03841	0.00043	0.0508	0.0016	241.3	6.8	242.9	2.7	224	69	-8.4	242.9	2.7	240.2	3.4	242.8	2.8	215	17
Z064	11.02	0.18	0.4807	0.0069	0.1668	0.0031	2524	15	2530	30	2522	31	-0.3	2522.0	31.0	2492	24	2519	36	2474	27
Z065	0.085	0.012	0.00991	0.00038	0.0611	0.0072	82	11	63.6	2.4	480	210	86.8	63.6	2.4	62.3	2.2	62.3	2.2	62	2.9
Z067	0.0538	0.0048	0.00762	0.00015	0.0516	0.0048	53.1	4.6	48.93	0.94	220	170	77.8	48.9	0.9	48.6	1.1	48.7	1.1	49.13	0.92
Z068	0.0427	0.0023	0.00636	0.00011	0.0488	0.0026	42.4	2.2	40.84	0.68	140	110	70.8	40.8	0.7	40.75	0.72	40.74	0.72	40.75	0.71
Z069	2.266	0.081	0.1986	0.0038	0.0832	0.0031	1198	25	1167	21	1253	76	6.9	1167.0	21.0	1133	20	1158	22	1100	36
Z070	1.413	0.049	0.1426	0.0029	0.072	0.0023	892	20	859	16	973	63	11.7	859.0	16.0	842	15	854	17	811	22
Z071	0.1216	0.0078	0.0174	0.0011	0.0508	0.0016	116.2	7.2	111.4	7.1	223	67	50.0	111.4	7.1	110.7	7.1	111	7.1	105.3	8.1
Z074	1.865	0.046	0.1763	0.0019	0.0769	0.002	1067	16	1047	10	1108	52	5.5	1047.0	10.0	1028	12	1042	11	1004	25
Z075	1.522	0.067	0.1542	0.006	0.0717	0.0016	935	27	924	33	969	45	4.6	924.0	33.0	905	29	920	34	875	28
Z076	0.256	0.013	0.03687	0.00056	0.0504	0.0025	231	10	233.4	3.5	230	110	-1.5	233.4	3.5	230.6	3.9	233.1	3.6	204	19
Z078	1.27	0.14	0.1092	0.0037	0.0855	0.0098	814	59	668	22	1170	200	42.9	discordant	discordant	644	23	649	25	633	29
Z079	0.764	0.032	0.0795	0.0027	0.0719	0.0035	576	19	493	16	966	94	49.0	493.0	16.0	486	16	484	16	493	16
Z080	4.68	0.17	0.3075	0.0043	0.1101	0.0034	1759	29	1728	21	1789	55	3.4	1789.0	55.0	1703	21	1717	22	1692	34
Z081	0.038	0.0046	0.00557	0.00014	0.0489	0.0054	37.8	4.5	35.78	0.89	150	220	76.1	35.8	0.9	35.67	0.86	35.7	0.87	36.1	1.1
Z082	2.17	0.14	0.1894	0.0037	0.0828	0.0051	1160	44	1118	20	1280	120	12.7	1118.0	20.0	1087	20	1111	24	1069	34
Z083	3.84	0.12	0.2656	0.0049	0.1057	0.0029	1597	26	1518	25	1718	50	11.6	1718.0	50.0	1503	25	1499	26	1509	26
Z084	0.1329	0.0044	0.01967	0.00052	0.0488	0.0013	126.6	3.9	125.5	3.3	152	60	17.4	125.5	3.3	125.2	3.3	125.5	3.4	122.5	4.3
Z085	0.093	0.011	0.01355	0.00027	0.05	0.0059	90	10	86.8	1.7	150	210	42.1	86.8	1.7	86.4	1.8	86.5	1.9	85.8	2.1
Z086	0.834	0.038	0.1	0.001	0.0608	0.0028	613	21	614.2	6.1	600	97	-2.4	614.2	6.1	585	11	611.5	6.6	489	49
Z087	9.93	0.19	0.3925	0.0059	0.1836	0.0022	2426	18	2134	27	2684	20	20.5	discordant	discordant	2080	29	2027	31	2134	27
Z088	12.79	0.28	0.4964	0.0063	0.1871	0.0041	2662	20	2598	27	2712	36	4.2	2712.0	36.0	2575	27	2564	35	2586	26
Z089	0.726	0.026	0.0839	0.0019	0.0623	0.0015	553	15	520	11	674	50	22.8	discordant	discordant	514	11	516	11	510	14
Z090	0.252	0.014	0.03316	0.00058	0.0555	0.0033	228	11	210.3	3.6	390	130	46.1	210.3	3.6	208	4	208.9	4.1	206.2	6
Z091	0.0521	0.006	0.00799	0.0002	0.0464	0.0052	51.4	5.7	51.3	1.3	50	200	-2.6	51.3	1.3	51.2	1.4	51.3	1.4	51.1	1.2
Z093	0.091	0.013	0.01322	0.00043	0.0508	0.0078	88	12	84.7	2.7	140	260	39.5	84.7	2.7	84.3	3	84.4	3.1	83.1	3.5
Z094	0.629	0.034	0.0781	0.0023	0.0582	0.0021	493	21	485	14	515	79	5.8	485.0	14.0	472	14	483	13	421	32
Z095	0.739	0.048	0.0916	0.0018	0.0577	0.0034	558	27	565	10	500	130	-13.0	discordant	discordant	544	12	563	11	460	49
Z096	0.0554	0.0088	0.00754	0.00035	0.0527	0.0054	54.4	8	48.4	2.3	250	150	80.6	48.4	2.3	47.8	1.9	47.8	1.9	47.9	2.5
Z097	0.099	0.013	0.01448	0.00043	0.0503	0.0068	95	12	92.7	2.7	140	240	33.8	92.7	2.7	92.4	3	92.4	3	92.7	2.8
Z098	1.728	0.086	0.1743	0.0031	0.0723	0.0039	1013	33	1036	17	950	120	-9.1	discordant	discordant	979	22	1031	18	858	77
Z099	0.676	0.018	0.0849	0.001	0.0578	0.0016	523	11	525.1	6.2	510	63	-3.0	525.1	6.2	510.1	7.6	524	6.5	458	29
Z100	0.0895	0.0053	0.01339	0.00023	0.0487	0.0031	86.9	5	85.7	1.4	130	120	34.1	85.7	1.4	85.3	1.6	85.6	1.6	80.8	4.4
Z101	0.051	0.0039	0.00783	0.00019	0.0475	0.0036	50.5	3.8	50.3	1.2	80	140	37.1	50.3	1.2	50.2	1.3	50.2	1.3	50.3	1.2
Z102	0.0394	0.0061	0.00584	0.0002	0.0498	0.0083	39	6	37.5	1.3	100	290	62.5	37.5	1.3	37.4	1.4	37.4	1.4	37.4	1.3
Z103	0.952	0.041	0.1082	0.0012	0.0638	0.0026	677	21	662.4	7.1	711	86	6.8	662.4	7.1	638.2	9.8	658.6	7.3	567	42
Z104	5.03	0.22	0.334	0.011	0.11	0.0031	1818	36	1855	55	1792	51	-3.5	1792.0	51.0	1790	40	1849	56	1734	42
Z106	1.856	0.075	0.1813	0.0032	0.0745	0.0032	1062	27	1074	18	1027	89	-4.6	1074.0	18.0	1023	20	1069	19	943	49
Z107	0.745	0.086	0.094	0.0031	0.0581	0.0067	557	52	579	18	470	250	-23.2	discordant	discordant	577	21	580	20	565	27
Z108	0.697	0.033	0.0878	0.0015	0.0576	0.0025	535	19	542.7	9.1	486	92	-11.7	discordant	discordant	515	11	541	9.1	399	51
Z109	2.687	0.048	0.2304	0.0029	0.0852	0.002	1327	14	1336	15	1312	46	-1.8	1312.0	46.0	1305	14	1333	16	1260	31
Z110	1.16	0.061	0.1224	0.004	0.0687	0.0028	777	28	744	23	865	82	14.0	744.0	23.0	727	24	739	23	696	32

Z111	0.882	0.016	0.10654	0.00093	0.0599	0.0012	641.5	8.8	652.6	5.4	594	43	-9.9	discordant	discordant	633.1	7.2	651.8	5.6	567	28
Z113	0.0482	0.0059	0.00735	0.00018	0.0464	0.0054	47.6	5.7	47.2	1.2	60	220	21.3	47.2	1.2	47.2	1.3	47.2	1.3	47.2	1.2
Z114	0.0531	0.0053	0.00791	0.00019	0.0492	0.0052	52.4	5.1	50.8	1.2	130	190	60.9	50.8	1.2	50.7	1.4	50.7	1.4	50.8	1.3
Z115	0.0624	0.006	0.00938	0.00035	0.0484	0.0043	61.3	5.7	60.2	2.3	120	170	49.8	60.2	2.3	60.1	2.3	60.1	2.3	60.3	2.3
Z116	0.796	0.02	0.0971	0.0011	0.0595	0.0016	594	11	597.6	6.5	574	57	-4.1	597.6	6.5	577.3	7	596.2	6.8	505	32
Z117	1.49	0.12	0.1484	0.0051	0.0731	0.0054	914	47	891	29	940	150	5.2	891.0	29.0	848	30	883	30	770	55
Z118	0.605	0.016	0.0773	0.00098	0.0569	0.0017	480	10	480	5.9	473	66	-1.5	480.0	5.9	464.9	5.9	478.8	6.2	397	35
Z119	0.0489	0.0072	0.00727	0.00026	0.0488	0.0074	48.2	7	46.7	1.7	100	270	53.3	46.7	1.7	46.6	1.8	46.6	1.8	46.7	2
Z120	0.251	0.011	0.03645	0.00073	0.0502	0.0022	227.3	8.7	230.8	4.6	196	90	-17.8	230.8	4.6	228.1	4.6	230.8	4.8	200	18

Sample 16YADZ03

	Ratios						U-Pb ages uncorrected for common lead									Corrected for common lead using Andersen's routine					
Grains	Final207_235	Final207_235_2s	Final206_238	Final206_238_2s	Final207_206	Final207_206_2s	FinalAge 207_235	FinalAge 207_235_2s	FinalAge 206_238	FinalAge 206_238_2s	FinalAge 207_206	FinalAge 207_206_2s	Concordance (%)	Best age	Best age 2s	FinalAgeAnd207_235	FinalAgeAnd207_235_2s	FinalAgeAnd206_238	FinalAgeAnd206_238_2s	FinalAgeAnd207_206	FinalAgeAnd207_206_2s
Z001	0.1544	0.0077	0.02247	0.00036	0.05	0.0027	145.5	6.8	143.2	2.3	190	110	24.6	143.2	2.3	142.8	2.4	143.1	2.5	141.3	3
Z002	0.21	0.03	0.0286	0.0012	0.0539	0.0083	190	25	181.6	7.4	290	290	37.4	181.6	7.4	180.6	8.1	180.9	8.1	179.5	8.4
Z003	0.091	0.019	0.00829	0.00023	0.079	0.015	87	16	53.2	1.5	980	350	94.6	53.2	1.5	51.3	1.4	51.2	1.4	52.9	1.7
Z004	0.0511	0.0032	0.00797	0.00014	0.0466	0.003	50.5	3.1	51.15	0.89	70	130	26.9	51.2	0.9	51.06	0.94	51.12	0.97	50.81	0.89
Z005	0.084	0.011	0.01055	0.00028	0.0577	0.0071	82	10	67.6	1.8	450	240	85.0	67.6	1.8	66.5	1.8	66.5	1.8	67.3	2
Z006	0.0549	0.0099	0.00725	0.00015	0.0563	0.0095	54	9.2	46.57	0.95	420	310	88.9	46.6	1.0	45.8	1.1	45.8	1.1	46.63	0.98
Z007	0.067	0.011	0.00791	0.00032	0.0617	0.0099	68	11	50.8	2	520	310	90.2	50.8	2.0	49.1	2.5	49.1	2.5	50.3	2.3
Z008	0.775	0.033	0.0929	0.0012	0.0606	0.0025	581	19	572.6	6.9	598	90	4.2	572.6	6.9	553.3	9.7	570.1	7.3	490	41
Z009	0.094	0.011	0.01344	0.00035	0.0518	0.0067	91	10	86	2.2	190	230	54.7	86.0	2.2	85.5	2.5	85.7	2.5	85.3	2.3
Z010	0.107	0.0096	0.0159	0.00053	0.049	0.0043	102.8	8.8	101.7	3.4	130	160	21.8	101.7	3.4	101.5	3.4	101.6	3.5	101	3.2
Z011	0.056	0.01	0.00832	0.00026	0.0499	0.0092	55.3	9.5	53.4	1.6	70	290	23.7	53.4	1.6	53.3	1.8	53.3	1.9	53.4	1.6
Z012	0.148	0.012	0.01681	0.00036	0.0637	0.0045	140	10	107.5	2.3	660	140	83.7	107.5	2.3	105.3	2.3	105.3	2.2	107.5	2.4
Z013	0.1653	0.0042	0.02393	0.00021	0.0501	0.0013	155.3	3.7	152.4	1.3	197	55	22.6	152.4	1.3	152	1.4	152.2	1.4	150.3	3
Z014	0.066	0.0086	0.01073	0.00029	0.0435	0.0054	64.5	8.1	68.8	1.9	-50	220	237.6	68.8	1.9	69.1	2	69	2	68.5	2
Z015	0.065	0.014	0.00962	0.0005	0.049	0.01	63	13	61.7	3.2	30	340	-105.7	61.7	3.2	61.5	3.3	61.6	3.3	61.6	3.2
Z016	11.85	0.17	0.4783	0.0055	0.1798	0.0018	2595	12	2519	24	2650	17	4.9	2650.0	17.0	2526	30	2496	31	2548	31
Z017	0.647	0.04	0.083	0.0017	0.0576	0.0035	504	24	514	10	480	130	-7.1	discordant	discordant	495	13	513	11	428	46
Z018	0.737	0.017	0.09116	0.00097	0.0587	0.0011	560	10	562.4	5.7	551	42	-2.1	562.4	5.7	549.1	8	561.4	5.9	509	23
Z019	0.648	0.029	0.0818	0.0011	0.0575	0.0024	506	18	506.9	6.5	484	85	-4.7	506.9	6.5	489.2	8.7	505.5	6.2	403	37
Z020	0.103	0.011	0.01532	0.00042	0.0488	0.0048	99	10	98	2.7	160	200	38.8	98.0	2.7	97.7	2.7	97.7	2.7	98.4	2.6
Z021	0.248	0.021	0.03521	0.00084	0.0511	0.0043	223	17	223.1	5.2	200	160	-11.6	223.1	5.2	219.5	4.6	222.7	5.3	192	20
Z022	0.263	0.018	0.03836	0.00054	0.0501	0.0034	236	14	242.7	3.3	180	130	-34.8	242.7	3.3	240.3	3.3	242.9	3.6	225	12
Z024	0.107	0.017	0.01427	0.00042	0.0527	0.008	102	15	92	3	270	280	65.9	92.0	3.0	90.4	3.1	90.4	3.2	92	3
Z025	1.727	0.042	0.1732	0.002	0.0723	0.0016	1017	15	1030	11	988	47	-4.3	1030.0	11.0	1004	12	1028	11	951	30
Z026	0.0437	0.0046	0.00692	0.00019	0.0452	0.0048	43.3	4.5	44.4	1.2	20	190	-122.0	44.4	1.2	44.4	1.4	44.5	1.4	44	1.5
Z027	2.23	0.075	0.2036	0.0026	0.0794	0.0024	1188	24	1195	14	1170	60	-2.1	1195.0	14.0	1155	17	1190	15	1107	34
Z028	0.1	0.041	0.00775	0.00062	0.087	0.028	93	36	49.8	4	910	540	94.5	49.8	4.0	46.9	2.5	46.8	2.5	49.8	4
Z029	0.0608	0.0059	0.00847	0.00016	0.0522	0.005	59.8	5.6	54.4	1	250	190	78.2	54.4	1.0	54	1.2	54	1.1	54	1.5
Z030	0.0578	0.0034	0.00963	0.00025	0.0442	0.0024	57	3.2	61.8	1.6	-50	100	223.6	61.8	1.6	61.8	1.8	62	1.7	61.4	2.3
Z031	0.144	0.024	0.01447	0.00043	0.071	0.01	135	20	92.6	2.8	810	260	88.6	92.6	2.8	90.1	3	89.9	3	92.6	2.8

Z032	0.753	0.026	0.0956	0.0019	0.0572	0.0019	568	15	588	11	481	72	-22.2	discordant	discordant	558	13	587	11	440	48
Z033	0.348	0.017	0.04688	0.00076	0.054	0.0028	302	13	295.3	4.7	350	110	15.6	295.3	4.7	290.7	5.1	294.4	5.2	262	20
Z034	0.0444	0.0049	0.00671	0.00019	0.0486	0.0058	44	4.7	43.1	1.2	80	210	46.1	43.1	1.2	43	1.4	43	1.4	43	1.2
Z035	0.091	0.013	0.01467	0.0004	0.0463	0.0066	88	12	93.9	2.5	20	250	-369.5	93.9	2.5	94.2	2.9	94.2	2.9	93.9	2.5
Z036	0.167	0.0069	0.02464	0.00031	0.0491	0.0019	156.6	6	156.9	2	152	81	-3.2	156.9	2.0	156	2	156.9	2	146.6	9.1
Z038	0.0722	0.0068	0.01106	0.00019	0.0471	0.0043	70.6	6.4	70.9	1.2	60	170	-18.2	70.9	1.2	70.9	1.3	71	1.3	70.9	1.6
Z039	0.1032	0.0067	0.0156	0.00023	0.048	0.0032	99.5	6.2	99.8	1.5	100	130	0.2	99.8	1.5	99.5	1.6	99.8	1.6	96.7	4.8
Z040	0.152	0.03	0.00675	0.00034	0.163	0.03	140	26	43.3	2.2	2060	370	97.9	43.3	2.2	37	2.4	36.9	2.4	43.3	2.2
Z041	0.108	0.012	0.01494	0.00035	0.0526	0.0058	103	11	95.6	2.2	250	210	61.8	95.6	2.2	94.8	2.3	95	2.4	95.2	2.1
Z042	0.0662	0.007	0.0105	0.00048	0.047	0.0048	66.5	7.3	67.3	3	50	180	-34.6	67.3	3.0	67.4	3.1	67.4	3.1	67.6	3.1
Z043	0.128	0.016	0.01507	0.00041	0.0616	0.0067	122	14	96.4	2.6	590	220	83.7	96.4	2.6	94.3	2.3	94.3	2.3	96.3	2.6
Z044	0.0768	0.0054	0.01155	0.00021	0.0474	0.0032	74.9	5	74	1.4	100	130	26.0	74.0	1.4	74.3	1.7	74.4	1.6	74.4	1.6
Z045	0.0512	0.0061	0.00773	0.00017	0.0483	0.0058	50.5	5.9	49.7	1.1	90	220	44.8	49.7	1.1	49.6	1.2	49.6	1.2	49.5	1.1
Z046	0.0953	0.0061	0.01533	0.0003	0.0452	0.003	92.3	5.7	98.1	1.9	-10	120	1081.0	98.1	1.9	98	1.9	98.4	2	91	5.6
Z047	0.062	0.014	0.00694	0.00025	0.061	0.011	61	13	44.6	1.6	540	330	91.7	44.6	1.6	42.8	1.6	42.8	1.6	44.6	1.6
Z049	0.885	0.025	0.106	0.0014	0.061	0.0021	643	14	649.2	8	620	74	-4.7	649.2	8.0	623.4	8.8	646.9	8.5	558	33
Z050	6.336	0.073	0.3672	0.0038	0.1245	0.0012	2023	10	2016	18	2021	17	0.2	2021.0	17.0	2009	13	2011	20	1999	15
Z051	0.297	0.016	0.03769	0.00045	0.0571	0.0026	263	12	238.5	2.8	468	93	49.0	238.5	2.8	235.3	3	236.5	2.7	236.4	3.8
Z053	0.998	0.028	0.1151	0.0014	0.063	0.0018	702	15	702	7.9	694	63	-1.2	702.0	7.9	680	11	700	8.3	620	33
Z054	0.0678	0.0085	0.00904	0.0003	0.057	0.008	66.2	8	58	1.9	350	250	83.4	58.0	1.9	57.3	2.1	57.3	2.1	58.1	1.9
Z055	0.79	0.05	0.0967	0.0018	0.0594	0.0038	587	28	595	10	530	140	-12.3	discordant	discordant	577	14	594	12	512	45
Z056	3.396	0.052	0.2688	0.0026	0.0917	0.0013	1503	12	1535	13	1458	28	-5.3	discordant	discordant	1495	12	1533	14	1443	22
Z057	0.67	0.26	0.0118	0.0024	0.282	0.07	420	140	76	15	2700	490	97.2	76.0	15.0	55	11	43.4	3.8	390	230
Z058	1.381	0.032	0.1471	0.0026	0.0689	0.0015	880	13	885	14	891	43	0.7	885.0	14.0	862	15	883	15	835	26
Z059	2.271	0.064	0.2141	0.0035	0.0772	0.0012	1201	20	1250	19	1124	31	-11.2	discordant	discordant	1199	19	1250	19	1117	28
Z060	0.0545	0.0041	0.00816	0.0002	0.0484	0.0034	53.8	3.9	52.4	1.3	120	130	56.3	52.4	1.3	52.2	1.3	52.3	1.3	52.2	1.5
Z061	0.0634	0.0079	0.00882	0.00018	0.0527	0.0065	62.1	7.5	56.6	1.2	230	230	75.4	56.6	1.2	55.9	1.4	56	1.4	55.8	1.4
Z062	0.131	0.017	0.01694	0.0005	0.0562	0.0073	123	15	108.3	3.2	340	240	68.1	108.3	3.2	107.8	3.1	108	3.1	107.4	3.2
Z064	0.945	0.026	0.1092	0.0022	0.063	0.002	674	14	668	13	692	67	3.5	668.0	13.0	642	10	665	14	574	33
Z065	0.1386	0.0096	0.02161	0.00043	0.0465	0.003	131.4	8.5	137.8	2.7	40	120	-244.5	137.8	2.7	137.8	2.7	138.2	2.8	135.2	3.9
Z066	0.413	0.021	0.05725	0.00093	0.0525	0.0032	349	15	358.8	5.7	280	120	-28.1	358.8	5.7	352.2	6.4	358.9	6.6	304	30
Z067	0.1081	0.0087	0.01615	0.00035	0.0488	0.0037	103.9	8	103.2	2.2	130	150	20.6	103.2	2.2	103	2.2	103.1	2.3	101.9	2.7
Z068	0.777	0.02	0.0944	0.0014	0.0598	0.0016	583	11	581.2	8.3	585	58	0.6	581.2	8.3	563.2	8.1	579.4	8.6	511	30
Z069	0.803	0.053	0.0994	0.0017	0.0587	0.0038	594	30	610.7	9.7	500	140	-22.1	discordant	discordant	586	15	610	10	487	50

Z070	0.0461	0.0052	0.00713	0.00016	0.0458	0.0048	45.7	5	45.8	1.1	40	190	-14.5	45.8	1.1	46.1	1	46.1	1	45.8	1.1
Z071	0.073	0.005	0.01116	0.00022	0.0478	0.0035	71.4	4.7	71.5	1.4	90	140	20.6	71.5	1.4	71.5	1.6	71.5	1.5	71.1	1.5
Z072	0.96	0.044	0.1058	0.0016	0.0652	0.0024	681	23	648.2	9.1	764	83	15.2	648.2	9.1	637	11	643.7	9	612	31
Z073	0.082	0.01	0.01428	0.00035	0.0422	0.0053	79.6	9.4	91.4	2.2	-140	200	165.3	91.4	2.2	91.7	2.5	92	2.5	90.1	3
Z075	0.1615	0.0086	0.02423	0.00032	0.0485	0.0027	151.7	7.5	154.3	2	120	110	-28.6	154.3	2.0	152.9	2.3	154.4	2.2	134	13
Z076	0.153	0.026	0.01034	0.00023	0.104	0.015	142	22	66.3	1.5	1390	300	95.2	66.3	1.5	61.2	1.1	61.2	1.1	66.3	1.6
Z077	1.788	0.065	0.1776	0.0045	0.0734	0.0012	1039	24	1053	25	1022	34	-3.0	1053.0	25.0	1030	25	1052	25	989	30
Z078	0.0508	0.0054	0.00823	0.00016	0.0439	0.0043	50.2	5.2	52.8	1	-20	180	364.0	52.8	1.0	53	1.1	53	1.1	52.8	1
Z079	1.472	0.04	0.1512	0.0025	0.0707	0.0019	917	17	908	14	938	55	3.2	908.0	14.0	887	16	904	15	839	28
Z080	0.06	0.011	0.00824	0.00027	0.0514	0.0079	58.5	9.9	52.9	1.7	200	260	73.6	52.9	1.7	52.8	1.6	52.8	1.6	52.6	1.9
Z081	0.0457	0.0045	0.00734	0.00017	0.0451	0.0043	45.3	4.4	47.2	1.1	-10	170	572.0	47.2	1.1	47.3	1.1	47.3	1.1	47.1	1
Z082	0.056	0.0095	0.00796	0.00017	0.0538	0.0092	54.9	9	51.1	1.1	210	290	75.7	51.1	1.1	50.7	1.3	50.7	1.3	50.7	1.3
Z083	0.0748	0.0062	0.01092	0.00022	0.05	0.0043	73.1	5.8	70	1.4	160	160	56.3	70.0	1.4	69.8	1.6	69.8	1.6	70	1.4
Z086	1.902	0.069	0.1783	0.0034	0.0782	0.0023	1079	24	1058	18	1143	58	7.4	1058.0	18.0	1043	19	1053	19	1035	26
Z087	0.0909	0.0082	0.01269	0.00025	0.0519	0.0044	88	7.6	81.3	1.6	230	160	64.7	81.3	1.6	80.9	1.7	80.8	1.7	81.3	1.6
Z088	1.752	0.027	0.1774	0.0021	0.072	0.001	1030	11	1053	12	982	29	-7.2	discordant	discordant	1023.9	9.9	1052	12	967	24
Z089	0.072	0.017	0.01148	0.00039	0.047	0.011	70	15	73.6	2.5	-70	330	205.1	73.6	2.5	73.6	3.1	73	2.8	72.4	3.5
Z090	0.152	0.069	0.01319	0.0009	0.088	0.033	154	64	84.4	5.7	810	480	89.6	84.4	5.7	79	2.3	79	2.3	84.2	5.9
Z091	0.0918	0.0097	0.01329	0.00028	0.0505	0.0055	88.8	8.9	85.1	1.8	170	200	49.9	85.1	1.8	84.6	2	84.8	2	83.5	2.7
Z092	0.0675	0.0095	0.01084	0.00032	0.0461	0.0071	65.9	9	69.5	2.1	-20	250	447.5	69.5	2.1	69.7	2.3	69.7	2.3	69.2	2.1
Z093	0.115	0.012	0.01444	0.00037	0.0593	0.0064	110	11	92.4	2.4	460	210	79.9	92.4	2.4	90.8	2.5	91	2.5	89.4	3.7
Z095	0.087	0.017	0.01345	0.00048	0.0462	0.0087	83	16	86.1	3.1	-40	300	315.3	86.1	3.1	86.2	3	86.2	3	86.1	3.1
Z096	0.0532	0.004	0.0079	0.00022	0.0491	0.0038	52.5	3.9	50.7	1.4	140	140	63.8	50.7	1.4	50.2	1.4	50.2	1.4	50.7	1.4
Z097	0.131	0.018	0.01516	0.00043	0.0614	0.0074	123	16	97	2.7	500	210	80.6	97.0	2.7	95	2.6	95.2	2.6	96.8	2.8
Z098	0.082	0.014	0.00792	0.0002	0.074	0.012	79	13	50.9	1.3	750	300	93.2	50.9	1.3	49.5	1.5	49.5	1.5	50.7	1.3
Z099	0.741	0.033	0.0876	0.0012	0.0613	0.0022	561	19	541.1	7.1	627	77	13.7	541.1	7.1	526	10	538	7.1	491	32
Z101	0.247	0.031	0.00871	0.00026	0.204	0.023	221	26	55.9	1.6	2730	220	98.0	55.9	1.6	44.8	1.7	44.6	1.7	55.9	1.6
Z103	0.1734	0.004	0.0258	0.00031	0.04868	0.00097	162.3	3.4	164.2	2	131	44	-25.3	164.2	2.0	162.2	2.2	164.2	2	131	16
Z104	0.0571	0.0061	0.00841	0.0002	0.0499	0.0057	56.2	5.8	54	1.3	150	210	64.0	54.0	1.3	53.8	1.5	53.8	1.5	54	1.3
Z105	0.063	0.0084	0.00996	0.00032	0.0471	0.0069	61.7	8	63.9	2	20	250	-219.5	63.9	2.0	64	2.3	64	2.3	63.7	2
Z106	0.0519	0.0037	0.00768	0.00019	0.049	0.003	51.4	3.5	49.3	1.2	140	120	64.8	49.3	1.2	49.1	1.2	49.2	1.2	48.9	1.5
Z107	1.968	0.051	0.1909	0.0029	0.0759	0.002	1103	17	1126	16	1084	55	-3.9	1126.0	16.0	1088	14	1124	16	1037	41
Z108	2.229	0.052	0.2061	0.0029	0.0789	0.0012	1189	16	1208	16	1167	30	-3.5	1167.0	30.0	1180	16	1207	16	1138	22
Z109	0.0919	0.0068	0.01358	0.00024	0.0489	0.0033	89	6.3	87	1.5	140	130	37.9	87.0	1.5	86.8	1.6	86.8	1.6	86.9	1.6

Z110	0.264	0.017	0.03788	0.00064	0.0506	0.0031	237	14	239.7	4	200	120	-19.9	239.7	4.0	238.4	4.3	239.7	4.1	229	11
Z111	0.771	0.018	0.0952	0.0011	0.0585	0.001	580	10	586.3	6.5	554	41	-5.8	discordant	discordant	569.7	7.9	585.4	6.6	511	26
Z112	0.0887	0.008	0.0141	0.0003	0.0459	0.0042	86	7.4	90.3	1.9	0	160	#DIV/0!	90.3	1.9	90.3	2.1	90.5	2.1	89.3	2.5
Z113	0.0913	0.0074	0.01386	0.00029	0.0482	0.0042	88.5	6.9	88.7	1.8	100	160	11.3	88.7	1.8	88.6	2	88.7	2	88.6	1.9
Z114	0.066	0.0061	0.00799	0.00018	0.06	0.0054	64.7	5.8	51.3	1.2	520	180	90.1	51.3	1.2	50.5	1.2	50.5	1.2	51.2	1.2
Z115	0.0439	0.0052	0.0055	0.00026	0.0604	0.008	43.5	5.1	35.3	1.7	470	250	92.5	35.3	1.7	34.7	1.7	34.7	1.7	35.3	1.7
Z116	0.093	0.015	0.00849	0.0003	0.081	0.014	89	14	54.5	1.9	900	360	93.9	54.5	1.9	52.3	2.3	52.2	2.3	54.5	1.9
Z117	0.0473	0.0039	0.00737	0.00024	0.0464	0.0032	46.9	3.8	47.3	1.6	40	130	-18.3	47.3	1.6	47.4	1.6	47.4	1.5	47.2	1.7
Z118	0.256	0.013	0.03594	0.00051	0.0517	0.0025	231	10	227.6	3.2	260	100	12.5	227.6	3.2	225.8	3.4	227.2	3.3	211	14
Z119	0.2475	0.0083	0.03488	0.00038	0.0517	0.0017	224.3	6.8	221	2.3	261	73	15.3	221.0	2.3	217.2	2.8	220.4	2.5	192	16
Z120	3.42	0.12	0.2685	0.0039	0.0925	0.0031	1506	27	1533	20	1463	65	-4.8	1463.0	65.0	1482	17	1528	20	1406	49

Sample 16YADZ04

	Ratios						U-Pb ages uncorrected for common lead									Corrected for common lead using Andersen's routine					
Grains	Final207_235	Final207_235_2s	Final206_238	Final206_238_2s	Final207_206	Final207_206_2s	FinalAge 207_235	FinalAge 207_235_2s	FinalAge 206_238	FinalAge 206_238_2s	FinalAge 207_206	FinalAge 207_206_2s	Concordance (%)	Best age	Best age 2s	FinalAgeAnd207_235	FinalAgeAnd207_235_2s	FinalAgeAnd206_238	FinalAgeAnd206_238_2s	FinalAgeAnd207_206	FinalAgeAnd207_206_2s
Z001	0.1024	0.0039	0.01534	0.00028	0.049	0.0019	98.9	3.6	98.1	1.8	147	78	33.3	98.1	1.8	98	1.8	98.1	1.9	97.7	1.8
Z002	0.0899	0.0081	0.01382	0.00038	0.0476	0.0045	86.9	7.5	88.5	2.4	60	170	-47.5	88.5	2.4	88.5	2.6	88.6	2.6	89.3	2.7
Z003	0.106	0.018	0.01563	0.00054	0.0493	0.0081	100	16	100	3.4	40	270	-150.0	100.0	3.4	99.9	3.6	99.9	3.6	100	3.4
Z004	0.0988	0.0071	0.01509	0.00038	0.0482	0.0037	95.3	6.6	96.6	2.4	120	150	19.5	96.6	2.4	96.4	2.6	96.5	2.6	96.6	2.5
Z005	0.0993	0.0076	0.01321	0.00038	0.0551	0.0042	95.7	7	84.6	2.4	350	150	75.8	84.6	2.4	83.8	2.5	83.8	2.5	83.9	2.4
Z006	1.221	0.069	0.1264	0.0043	0.0696	0.0025	802	34	767	25	889	76	13.7	767.0	25.0	752	26	761	24	723	39
Z007	0.427	0.012	0.0572	0.0012	0.0545	0.0014	360.7	8.9	358.4	7.4	378	58	5.2	358.4	7.4	348.3	6.9	357.4	7.5	290	25
Z008	2.996	0.066	0.2413	0.004	0.0905	0.0018	1404	17	1393	21	1428	38	2.5	1428.0	38.0	1367	17	1387	22	1343	22
Z009	22.25	0.42	0.597	0.012	0.2715	0.0038	3192	18	3015	49	3312	22	9.0	3312.0	22.0	2956	53	2891	69	3005	43
Z010	0.619	0.023	0.0769	0.0013	0.0586	0.0019	487	15	477.7	8	547	78	12.7	477.7	8.0	461	8.8	474.2	7.8	394	32
Z011	1.293	0.052	0.1434	0.0028	0.0656	0.0024	839	23	864	16	761	79	-13.5	discordant	discordant	814	18	861	16	683	58
Z012	0.187	0.011	0.02768	0.00053	0.0492	0.0028	173.5	9.1	176	3.4	150	110	-17.3	176.0	3.4	175.5	3.6	176.1	3.6	176.2	3.5
Z013	3.511	0.068	0.266	0.004	0.0959	0.0015	1528	15	1520	20	1541	30	1.4	1541.0	30.0	1497	18	1515	22	1478	19
Z014	0.677	0.027	0.0834	0.0022	0.0586	0.0019	523	16	516	13	532	68	3.0	516.0	13.0	498	13	514	13	423	38
Z015	3.526	0.083	0.2484	0.006	0.103	0.0015	1531	19	1430	31	1676	27	14.7	1676.0	27.0	1418	32	1411	33	1430	31
Z016	0.0914	0.0069	0.01407	0.00032	0.0474	0.0036	88.5	6.4	90	2	90	140	0.0	90.0	2.0	89.9	2.1	90	2.2	89.3	2.3
Z017	0.1009	0.0046	0.01508	0.00024	0.0484	0.002	97.5	4.2	96.5	1.5	122	84	20.9	96.5	1.5	96.2	1.5	96.4	1.5	93.4	3.3
Z018	0.1204	0.0071	0.01838	0.00037	0.0483	0.0033	116.6	6.9	117.4	2.3	120	130	2.2	117.4	2.3	117	2.5	117.3	2.5	115.7	2.8
Z019	1.755	0.031	0.1663	0.0028	0.0762	0.0012	1028	11	991	16	1096	32	9.6	991.0	16.0	981	15	986	17	959	16
Z020	0.1393	0.0089	0.01629	0.0005	0.0628	0.0037	133.5	8.4	104.1	3.1	640	130	83.7	104.1	3.1	102.1	3.2	102.2	3.2	103.2	3.8
Z022	1.381	0.026	0.1353	0.0025	0.0742	0.001	882	12	818	14	1043	27	21.6	discordant	discordant	812	15	810	15	818	15
Z023	0.0675	0.0033	0.01079	0.00023	0.0452	0.002	66.2	3.2	69.2	1.5	-10	84	792.0	69.2	1.5	69.3	1.5	69.3	1.5	69	1.5
Z024	0.215	0.041	0.01075	0.00044	0.138	0.019	192	31	68.9	2.8	2020	240	96.6	68.9	2.8	60.1	1.4	59.9	1.4	68.9	2.8
Z025	0.1053	0.0061	0.01574	0.00028	0.0481	0.0026	101.4	5.6	100.6	1.8	110	110	8.5	100.6	1.8	100.5	1.9	100.6	1.9	99.4	3.1
Z027	0.154	0.02	0.01388	0.00049	0.0809	0.0093	143	17	88.8	3.1	1070	230	91.7	88.8	3.1	84.9	2.8	84.7	2.8	88.8	3.1
Z028	0.0706	0.0074	0.01062	0.00053	0.0478	0.005	68.9	7	68.1	3.4	80	180	14.9	68.1	3.4	68	3.5	68	3.5	67.2	3.7
Z029	0.166	0.014	0.01584	0.00037	0.0768	0.0066	154	12	101.3	2.3	980	170	89.7	101.3	2.3	97.7	2.4	97.6	2.4	101.3	2.3
Z030	1.666	0.028	0.1592	0.0019	0.0754	0.0011	995	11	952	11	1075	29	11.4	952.0	11.0	947	10	947	11	945.1	9.9
Z031	0.415	0.018	0.0552	0.0011	0.0543	0.0024	353	12	346.2	6.9	354	92	2.2	346.2	6.9	338.9	7	345.2	7.2	289	24
Z032	4.485	0.075	0.2681	0.0044	0.1204	0.0016	1727	14	1531	22	1959	23	21.8	discordant	discordant	1506	24	1488	25	1531	22

Z033	0.0647	0.0098	0.0082	0.00049	0.0585	0.0095	63	9.3	52.6	3.2	360	300	85.4	52.6	3.2	51.8	3.3	51.8	3.3	51.2	3.4
Z034	3.467	0.077	0.2472	0.0052	0.1009	0.0017	1517	18	1423	27	1635	32	13.0	1635.0	32.0	1411	28	1405	29	1415	24
Z035	3.74	0.056	0.2762	0.0036	0.0973	0.0014	1579	12	1572	18	1574	26	0.1	1574.0	26.0	1552	15	1567	19	1523	19
Z037	0.608	0.016	0.0736	0.0013	0.0589	0.0012	481	10	457.4	8	553	46	17.3	457.4	8.0	451.4	7.6	455.1	8.2	426	15
Z038	0.1133	0.0075	0.01384	0.00034	0.0589	0.0039	108.6	6.8	88.6	2.1	490	140	81.9	88.6	2.1	87.3	2.2	87.3	2.2	87.9	2.1
Z039	0.937	0.024	0.1061	0.0017	0.0632	0.0016	670	13	650	10	711	54	8.6	650.0	10.0	634	10	647	10	590	24
Z040	0.0668	0.0058	0.00934	0.00027	0.0517	0.0047	65.4	5.5	60	1.7	220	170	72.7	60.0	1.7	59.6	1.9	59.6	1.9	60	1.8
Z041	0.546	0.023	0.0606	0.0016	0.0643	0.0025	441	15	379.4	9.8	723	80	47.5	379.4	9.8	373.2	9.6	374	10	368	12
Z042	0.445	0.013	0.0553	0.0017	0.0576	0.0011	373.3	9.3	347	11	506	43	31.4	347.0	11.0	343	10	345	11	330	12
Z043	0.704	0.024	0.0859	0.0015	0.0584	0.0019	539	14	531.3	8.9	522	72	-1.8	531.3	8.9	515.5	9.5	529.2	9.2	432	36
Z044	0.0805	0.0099	0.00903	0.00031	0.0658	0.009	77.9	9.3	57.9	2	620	280	90.7	57.9	2.0	56.5	2.4	56.5	2.4	57.7	2
Z046	1.48	0.03	0.1518	0.0024	0.0693	0.0013	921	12	911	13	902	37	-1.0	911.0	13.0	895	12	908	14	836	22
Z047	1.448	0.037	0.1475	0.0023	0.0698	0.0016	910	14	887	13	909	50	2.4	887.0	13.0	875	12	883	13	833	27
Z048	6.47	0.11	0.3386	0.0061	0.1359	0.0019	2040	14	1879	29	2172	25	13.5	2172.0	25.0	1861	34	1836	35	1884	31
Z049	0.129	0.01	0.01811	0.00044	0.051	0.0041	122.8	9.4	115.7	2.8	210	150	44.9	115.7	2.8	115.3	3	115.2	3	114.7	3.3
Z050	0.0863	0.0084	0.0123	0.00032	0.0509	0.0053	83.6	7.8	78.8	2	170	180	53.6	78.8	2.0	78.5	2.2	78.4	2.2	78.9	2.4
Z051	0.0954	0.0091	0.01318	0.00038	0.0519	0.0051	93.6	8.8	84.4	2.4	250	190	66.2	84.4	2.4	83.8	2.6	83.8	2.6	83.9	2.6
Z052	0.185	0.018	0.01498	0.00034	0.0871	0.0077	170	15	95.9	2.2	1290	180	92.6	95.9	2.2	90.4	2	90.2	2	95.9	2.2
Z053	0.078	0.0078	0.00987	0.00023	0.0562	0.0057	75.8	7.3	63.3	1.5	350	190	81.9	63.3	1.5	62.6	1.6	62.5	1.6	63.5	1.6
Z054	0.4416	0.0095	0.0582	0.001	0.0538	0.0012	371	6.7	364.9	6.1	353	49	-3.4	364.9	6.1	356.7	5.8	363.8	6.3	283	27
Z055	0.1167	0.0098	0.01556	0.00038	0.0536	0.0046	111.5	8.9	99.5	2.4	310	170	67.9	99.5	2.4	98.6	2.6	98.6	2.6	99.4	2.7
Z057	2.934	0.059	0.1446	0.0022	0.1438	0.0022	1389	15	871	12	2269	26	61.6	discordant	discordant	812	13	791	12	871	12
Z058	13.86	0.2	0.533	0.0084	0.1845	0.0023	2739	14	2753	35	2692	20	-2.3	2692.0	20.0	2727	18	2742	40	2656	21
Z059	0.69	0.016	0.0815	0.0017	0.0599	0.0014	532	9.9	505	10	597	57	15.4	505.0	10.0	496.6	9.8	502	11	460	22
Z060	0.748	0.032	0.0787	0.0013	0.0681	0.0032	568	19	488.4	7.6	829	92	41.1	488.4	7.6	478.6	7.4	480.6	8.2	474	13
Z061	0.2391	0.0075	0.03161	0.00056	0.0539	0.0016	217.4	6.2	200.6	3.5	349	66	42.5	200.6	3.5	199	3.5	199.4	3.6	193.7	6.5
Z062	0.704	0.017	0.0855	0.0012	0.0585	0.0015	540	10	529	7.3	536	55	1.3	529.0	7.3	517.6	7.2	527.1	7.6	455	25
Z063	0.85	0.02	0.1003	0.0014	0.06	0.0012	623	11	616.3	8.3	602	41	-2.4	616.3	8.3	605.7	9.7	614.7	8.5	544	28
Z064	0.2502	0.0094	0.03281	0.00059	0.0545	0.0023	226.3	7.6	208.1	3.7	361	90	42.4	208.1	3.7	205.6	3.9	206.7	3.9	183	15
Z065	0.17	0.016	0.01417	0.00043	0.0843	0.0073	158	14	90.7	2.7	1160	170	92.2	90.7	2.7	86.6	2.6	86.4	2.6	90.7	2.7
Z067	2.39	0.13	0.2099	0.0067	0.0815	0.0041	1235	39	1228	36	1200	110	-2.3	1200.0	110.0	1183	37	1216	38	1126	67
Z069	0.0678	0.0026	0.01002	0.00032	0.0486	0.0016	66.6	2.5	64.2	2	125	70	48.6	64.2	2.0	64.1	2.1	64.1	2.1	62.3	2.9
Z070	1.023	0.069	0.0691	0.0012	0.1064	0.0076	707	33	430.7	7.4	1650	130	73.9	430.7	7.4	407.3	8.9	403.3	9.2	430.7	7.4
Z071	1.537	0.028	0.1543	0.0021	0.0714	0.0012	944	11	925	11	961	35	3.7	925.0	11.0	912	10	921	12	878	17

Z073	2.157	0.045	0.1973	0.0031	0.0784	0.0014	1166	15	1161	16	1150	35	-1.0	1161.0	16.0	1140	14	1157	17	1092	20
Z075	6.9	0.11	0.3731	0.0044	0.1329	0.002	2098	14	2043	21	2134	26	4.3	2134.0	26.0	2037	21	2028	24	2036	21
Z076	0.1166	0.0058	0.01414	0.00028	0.059	0.0027	111.7	5.3	90.5	1.8	530	100	82.9	90.5	1.8	89.2	1.8	89.2	1.8	91	2
Z077	0.112	0.011	0.01348	0.00039	0.0602	0.0058	107.1	9.7	86.3	2.5	490	190	82.4	86.3	2.5	85	2.6	84.9	2.6	85.7	2.7
Z078	0.0972	0.0049	0.01465	0.00031	0.0476	0.0021	94	4.6	93.7	2	106	90	11.6	93.7	2.0	93.6	2	93.6	2	93.6	2.2
Z079	1.356	0.027	0.1435	0.0022	0.0684	0.00098	869	12	864	12	876	30	1.4	864.0	12.0	850	12	862	13	823	16
Z080	1.557	0.027	0.1533	0.0023	0.0736	0.0013	954	11	919	13	1025	36	10.3	919.0	13.0	909	12	914	14	893	13
Z081	0.113	0.011	0.01195	0.00029	0.0686	0.0063	108.3	9.8	76.6	1.8	750	180	89.8	76.6	1.8	74.2	2.1	74.1	2.1	76.6	1.8
Z082	0.284	0.034	0.03252	0.00086	0.064	0.0076	254	29	206.3	5.4	610	250	66.2	206.3	5.4	201.9	5.3	201.7	5.3	205.6	6.2
Z083	1.396	0.037	0.1416	0.0023	0.0716	0.0017	886	15	853	13	961	50	11.2	853.0	13.0	841	13	849	14	827	22
Z084	0.959	0.026	0.1134	0.0021	0.0614	0.0016	681	13	692	12	650	53	-6.5	discordant	discordant	668	11	691	13	588	37
Z085	0.0712	0.009	0.01029	0.00027	0.0505	0.0064	69.3	8.5	66	1.7	150	220	56.0	66.0	1.7	65.7	1.9	65.7	1.9	65.6	1.8
Z086	0.926	0.024	0.1056	0.0017	0.0642	0.0016	664	12	647	10	733	53	11.7	647.0	10.0	632.1	9.5	644	10	603	19
Z087	1.653	0.084	0.1627	0.0032	0.0747	0.0037	996	35	972	17	1031	97	5.7	972.0	17.0	933	20	963	18	883	36
Z088	2.389	0.075	0.2209	0.0055	0.0786	0.0015	1236	22	1286	29	1164	36	-10.5	discordant	discordant	1230	22	1285	29	1146	30
Z089	0.1144	0.0069	0.01449	0.00035	0.0576	0.0033	109.7	6.2	92.7	2.2	460	120	79.8	92.7	2.2	91.6	2.2	91.6	2.2	92.5	2.3
Z090	4.317	0.062	0.3014	0.0048	0.1045	0.0017	1696	12	1698	24	1701	29	0.2	1701.0	29.0	1667	17	1691	25	1634	22
Z091	2.27	0.1	0.193	0.0052	0.0859	0.0031	1197	32	1137	28	1325	67	14.2	1137.0	28.0	1110	28	1125	29	1096	33
Z092	0.242	0.023	0.01883	0.00034	0.0955	0.009	222	19	120.2	2.2	1440	160	91.7	120.2	2.2	113.6	2.4	113.3	2.4	120.2	2.2
Z093	0.073	0.0054	0.01079	0.00023	0.0494	0.0038	71.3	5.1	69.2	1.5	140	140	50.6	69.2	1.5	69	1.6	69	1.6	69.6	1.7
Z094	0.0924	0.0082	0.01372	0.00031	0.0499	0.0044	89.3	7.6	87.8	2	160	160	45.1	87.8	2.0	87.9	2.2	88	2.2	88	2.3
Z095	0.1024	0.0069	0.01343	0.00034	0.0556	0.0034	98.7	6.3	86	2.2	380	130	77.4	86.0	2.2	85.2	2.2	85.2	2.2	86	2.2
Z096	0.0855	0.0034	0.01276	0.00025	0.0491	0.0019	83.2	3.2	81.7	1.6	149	80	45.2	81.7	1.6	81.5	1.6	81.6	1.6	81.2	1.6
Z097	0.599	0.021	0.0761	0.0013	0.0576	0.0021	475	13	472.4	7.9	489	79	3.4	472.4	7.9	456.3	8.7	470.9	8.3	389	34
Z099	0.089	0.007	0.01326	0.00027	0.0491	0.0038	86.2	6.5	84.9	1.7	130	140	34.7	84.9	1.7	84.7	1.8	84.9	1.8	83.2	2.8
Z100	0.106	0.011	0.01079	0.00036	0.0729	0.0081	101	10	69.2	2.3	900	220	92.3	69.2	2.3	67	2.5	66.9	2.5	69.2	2.3
Z101	0.0963	0.0079	0.01299	0.00033	0.0544	0.0042	92.9	7.2	83.2	2.1	340	150	75.5	83.2	2.1	82.3	2.2	82.5	2.2	80.8	3.2
Z102	0.0951	0.0048	0.01371	0.00029	0.051	0.0025	92.1	4.5	87.8	1.8	230	100	61.8	87.8	1.8	87.4	1.9	87.5	1.9	87.8	1.9
Z103	0.0775	0.0079	0.01062	0.00039	0.0532	0.0049	75.4	7.4	68.1	2.5	260	170	73.8	68.1	2.5	67.5	2.4	67.6	2.4	67.2	2.8
Z104	0.1004	0.0068	0.01515	0.0003	0.0486	0.0032	96.9	6.3	97	1.9	130	130	25.4	97.0	1.9	96.8	2	96.9	2	97	1.9
Z105	2.936	0.069	0.2273	0.0037	0.0947	0.0022	1389	18	1320	19	1514	42	12.8	1514.0	42.0	1305	18	1307	21	1309	18
Z106	0.093	0.0089	0.01423	0.00049	0.0477	0.0044	89.8	8.2	91.1	3.1	80	170	-13.9	91.1	3.1	91.1	3.2	91.2	3.2	90	3.5
Z109	0.0638	0.004	0.0097	0.00028	0.0492	0.0033	62.7	3.8	62.2	1.8	140	130	55.6	62.2	1.8	62.1	1.9	62.1	1.9	62.1	1.8
Z110	0.272	0.014	0.03805	0.00085	0.0527	0.0028	244	11	240.7	5.2	280	110	14.0	240.7	5.2	237.3	5.1	240.3	5.5	233.4	7.7

Z111	0.199	0.017	0.0287	0.001	0.0501	0.0046	182	14	182.6	6.4	190	170	3.9	182.6	6.4	183	7.1	182.6	6.8	177.2	8.6
Z112	0.317	0.04	0.01594	0.00061	0.143	0.016	275	31	101.9	3.9	2110	220	95.2	101.9	3.9	89.9	3.4	89.4	3.4	101.9	3.9
Z113	0.353	0.013	0.04723	0.00075	0.0546	0.002	305.9	9.9	297.5	4.6	372	76	20.0	297.5	4.6	291.6	4.3	296.4	4.7	270	13
Z114	0.244	0.02	0.03056	0.00087	0.0588	0.0052	219	16	194	5.4	450	180	56.9	194.0	5.4	191.4	5.6	192.1	5.8	189.6	6.5
Z115	3.326	0.096	0.2538	0.0047	0.0959	0.0027	1487	24	1457	24	1542	57	5.5	1542.0	57.0	1424	24	1446	27	1398	32
Z116	0.0867	0.007	0.01365	0.00037	0.0465	0.004	84.1	6.5	87.4	2.4	30	150	-191.3	87.4	2.4	87.5	2.5	87.6	2.5	87.5	2.9
Z117	0.727	0.025	0.0729	0.0016	0.073	0.0021	553	14	453.4	9.5	996	59	54.5	453.4	9.5	445.2	9.5	444	9.6	452.6	9.3
Z118	0.0929	0.0081	0.01363	0.00031	0.0505	0.0048	89.8	7.5	87.3	2	170	170	48.6	87.3	2.0	87.1	2.3	87.1	2.3	87.2	2
Z119	0.615	0.021	0.0775	0.0014	0.0582	0.0019	486	13	481.2	8.5	514	70	6.4	481.2	8.5	464.1	9.1	477.6	9.3	400	30
Z120	0.0896	0.0086	0.0142	0.00034	0.0457	0.0044	86.6	8	90.9	2.1	30	180	-203.0	90.9	2.1	91	2.4	91.1	2.4	90.7	2.2
Z121	0.2832	0.0085	0.03972	0.00079	0.0519	0.0011	252.8	6.7	251.1	4.9	272	49	7.7	251.1	4.9	246.9	4.8	250.7	4.9	215	16
Z122	0.0592	0.0043	0.00878	0.0002	0.0495	0.0038	58.2	4.1	56.4	1.3	150	150	62.4	56.4	1.3	56.2	1.4	56.3	1.4	56	1.3
Z123	0.119	0.012	0.01503	0.00039	0.0581	0.0061	114	11	96.2	2.5	400	180	76.0	96.2	2.5	94.6	2.7	94.7	2.7	95.5	2.5
Z124	1.881	0.064	0.1816	0.0033	0.0755	0.0024	1071	22	1075	18	1060	64	-1.4	1075.0	18.0	1032	17	1069	19	957	37
Z125	0.0976	0.0034	0.01491	0.00032	0.0477	0.0015	94.4	3.1	95.4	2	88	64	-8.4	95.4	2.0	95	2.1	95.4	2.1	88.8	5.1
Z126	0.0662	0.0031	0.01035	0.00023	0.0467	0.0023	65	3	66.3	1.5	50	92	-32.6	66.3	1.5	66.4	1.6	66.4	1.6	66.3	1.5
Z127	0.828	0.03	0.0779	0.0028	0.0788	0.0038	615	18	483	17	1137	94	57.5	483.0	17.0	473	18	471	18	483	17
Z128	0.1056	0.0075	0.0155	0.00033	0.0496	0.0036	101.6	6.9	99.2	2.1	150	130	33.9	99.2	2.1	98.9	2.2	99	2.2	98.4	2.3
Z129	0.114	0.01	0.01705	0.00037	0.0497	0.0048	110.8	9.8	109	2.4	130	170	16.2	109.0	2.4	108.6	2.5	108.8	2.5	106.7	3.3
Z130	0.0925	0.0085	0.01363	0.00037	0.0494	0.0047	89.3	7.8	87.3	2.4	130	170	32.8	87.3	2.4	87.9	2.7	87.9	2.7	88	2.6
Z131	0.1	0.01	0.01359	0.00039	0.0525	0.0051	95.8	9.2	87	2.5	270	190	67.8	87.0	2.5	86.4	2.6	86.4	2.6	86.8	2.5
Z132	0.626	0.022	0.0775	0.0014	0.0592	0.0022	495	15	480.8	8.6	544	80	11.6	480.8	8.6	466.2	9	478.4	8.9	405	32
Z133	0.0775	0.0046	0.01049	0.0002	0.0545	0.0033	75.6	4.3	67.3	1.3	340	130	80.2	67.3	1.3	66.7	1.3	66.7	1.3	67	1.3
Z134	2.164	0.056	0.194	0.0032	0.0804	0.002	1171	17	1143	17	1202	53	4.9	1143.0	17.0	1120	17	1140	19	1090	24
Z135	0.0904	0.0052	0.01323	0.00029	0.0503	0.003	87.7	4.8	84.7	1.8	180	110	52.9	84.7	1.8	84.4	1.9	84.5	1.9	83.8	2.4
Z136	0.0515	0.0033	0.00756	0.00016	0.0496	0.0032	50.9	3.2	48.5	1	200	140	75.8	48.5	1.0	48.3	1	48.3	1	48.5	1
Z137	0.118	0.014	0.01689	0.0006	0.0512	0.0061	112	12	108	3.8	210	220	48.6	108.0	3.8	107.2	4.1	107.4	4.2	107.6	4.5
Z138	2.905	0.062	0.236	0.004	0.0893	0.0015	1381	16	1365	21	1406	33	2.9	1406.0	33.0	1343	17	1359	22	1322	20
Z140	0.0635	0.0027	0.00904	0.00025	0.0512	0.002	62.5	2.6	58	1.6	236	84	75.4	58.0	1.6	57.7	1.7	57.7	1.7	58	1.6

Sample 17LETKAT08

	Ratios						U-Pb ages uncorrected for common lead									Corrected for common lead using Andersen's routine					
Grains	Final207_235	Final207_235_2s	Final206_238	Final206_238_2s	Final207_206	Final207_206_2s	FinalAge 207_235	FinalAge 207_235_2s	FinalAge 206_238	FinalAge 206_238_2s	FinalAge 207_206	FinalAge 207_206_2s	Concordance (%)	Best age	Best age 2s	FinalAgeAnd207_235	FinalAgeAnd207_235_2s	FinalAgeAnd206_238	FinalAgeAnd206_238_2s	FinalAgeAnd207_206	FinalAgeAnd207_206_2s
Z001	0.096	0.014	0.01555	0.00046	0.0447	0.0067	92	13	99.5	2.9	-60	250	265.8	99.5	2.9	100	3.3	100	3.3	99.5	2.9
Z002	0.053	0.0041	0.00867	0.00019	0.0446	0.0036	52.3	4	55.7	1.2	-30	140	285.7	55.7	1.2	55.8	1.3	55.9	1.3	55.4	1.3
Z003	0.088	0.016	0.01639	0.0005	0.0391	0.007	84	15	104.8	3.2	-280	250	137.4	104.8	3.2	106	3.4	106.1	3.5	104.8	3.2
Z004	0.0331	0.005	0.00513	0.00042	0.0461	0.0057	33	4.8	33	2.7	0	210	#DIV/0!	33.0	2.7	32.9	2.7	32.9	2.7	32.8	2.7
Z005	0.059	0.016	0.00679	0.00029	0.063	0.014	58	14	43.6	1.8	600	460	92.7	43.6	1.8	42.9	1.7	42.8	1.7	43.6	1.8
Z006	0.187	0.042	0.01903	0.00067	0.07	0.014	166	34	121.5	4.2	570	380	78.7	121.5	4.2	118.4	4.6	118.3	4.6	121.8	5.3
Z007	0.0604	0.0085	0.00909	0.00028	0.0485	0.0068	59.1	8	58.4	1.8	50	230	-16.8	58.4	1.8	58.3	1.9	58.3	1.9	58.3	1.8
Z008	0.0557	0.0028	0.00869	0.00019	0.0471	0.0025	55	2.7	55.8	1.2	60	100	7.0	55.8	1.2	55.8	1.3	55.8	1.3	55.7	1.3
Z009	1.964	0.043	0.1942	0.0031	0.0734	0.0014	1102	15	1144	17	1019	38	-12.3	discordant	discordant	1096	14	1143	17	1004	33
Z010	0.087	0.013	0.01225	0.00044	0.0538	0.009	84	12	78.5	2.8	180	280	56.4	78.5	2.8	77.9	3.1	77.9	3.1	77.8	2.8
Z011	0.105	0.023	0.01193	0.00096	0.067	0.016	99	20	76.4	6.1	390	390	80.4	76.4	6.1	74.8	6.4	74.8	6.4	75	6.9
Z012	0.0656	0.009	0.00976	0.00045	0.0489	0.0063	64.1	8.5	62.6	2.9	90	220	30.4	62.6	2.9	62.5	3	62.5	3	62.3	3
Z013	0.31	0.1	0.0274	0.0011	0.069	0.012	251	55	173.9	7.1	620	260	72.0	173.9	7.1	184	37	193	57	171.3	9.1
Z014	0.072	0.013	0.00947	0.00041	0.056	0.01	70	12	60.8	2.6	280	330	78.3	60.8	2.6	60.1	2.8	60.1	2.9	60.6	2.7
Z015	0.1074	0.0072	0.01682	0.00083	0.047	0.0021	103.3	6.6	107.5	5.3	60	85	-79.2	107.5	5.3	107.5	5.4	107.7	5.4	103.4	7.6
Z016	0.0612	0.003	0.0093	0.00015	0.0477	0.0023	60.2	2.8	59.65	0.98	93	94	35.9	59.7	1.0	59.6	1	59.6	1	59.6	1
Z017	10.13	0.18	0.4759	0.0079	0.1543	0.0016	2445	17	2508	35	2393	17	-4.8	2393.0	17.0	2438	20	2506	36	2382	18
Z018	0.0343	0.0022	0.00502	0.00011	0.0494	0.003	34.3	2.1	32.28	0.72	150	120	78.5	32.3	0.7	32.16	0.74	32.17	0.74	32.28	0.88
Z019	0.605	0.022	0.0799	0.0017	0.0544	0.0016	479	14	496	10	372	64	-33.3	496.0	10.0	474	11	495	11	366	38
Z020	0.109	0.024	0.01037	0.00043	0.072	0.013	102	21	66.5	2.8	650	310	89.8	66.5	2.8	63.7	1.9	63.6	1.9	66.6	2.8
Z021	0.0348	0.0017	0.00532	0.00019	0.0472	0.0018	34.7	1.7	34.2	1.2	67	76	49.0	34.2	1.2	34.2	1.3	34.2	1.3	34.1	1.3
Z022	0.09	0.31	0.0122	0.0057	-0.03	0.24	-30	330	78	36	-8200	7000	101.0	78.0	36.0	65	27	59	26	380	270
Z023	0.0529	0.0041	0.00823	0.00016	0.0461	0.0034	52.3	4	52.8	1	20	130	-164.0	52.8	1.0	52.9	1.1	53.2	1.2	53.4	1.3
Z024	0.069	0.013	0.01077	0.00033	0.0464	0.0086	67	13	69.1	2.1	-20	310	445.5	69.1	2.1	69.2	2.3	69.2	2.3	69	2.1
Z025	0.0546	0.0088	0.00791	0.00027	0.0498	0.0078	53.5	8.5	50.8	1.8	150	280	66.1	50.8	1.8	50.5	1.8	50.5	1.8	50.8	1.8
Z026	0.0432	0.0033	0.00649	0.00012	0.0485	0.0038	42.9	3.2	41.7	0.77	110	150	62.1	41.7	0.8	41.62	0.84	41.62	0.84	41.72	0.79
Z027	0.0302	0.0014	0.00463	0.00022	0.0474	0.0018	30.2	1.4	29.8	1.4	63	82	52.7	29.8	1.4	29.7	1.4	29.7	1.4	29.8	1.4
Z028	1.919	0.089	0.1896	0.0045	0.0733	0.0028	1083	30	1119	24	1001	77	-11.8	discordant	discordant	1065	25	1116	24	987	41
Z029	0.0397	0.0038	0.00616	0.00022	0.0467	0.0043	39.4	3.7	39.6	1.4	30	160	-32.0	39.6	1.4	39.6	1.4	39.6	1.4	39.6	1.4
Z030	0.0871	0.0079	0.012	0.00022	0.0525	0.0045	84.4	7.3	76.9	1.4	250	170	69.2	76.9	1.4	76.4	1.4	76.4	1.4	76.9	1.4

Z033	0.026	0.002	0.0041	0.00013	0.0475	0.004	26	2	26.35	0.83	60	150	56.1	26.4	0.8	26.33	0.89	26.33	0.89	26.16	0.98
Z034	0.0704	0.0025	0.01096	0.00018	0.0466	0.0017	69	2.3	70.3	1.2	45	72	-56.2	70.3	1.2	70.3	1.2	70.4	1.2	69.5	1.7
Z035	1.431	0.047	0.1541	0.0043	0.0673	0.0012	899	20	923	24	841	37	-9.8	discordant	discordant	890	22	922	24	811	32
Z036	0.0453	0.003	0.00739	0.00021	0.0453	0.0031	44.9	3	47.5	1.3	-10	120	575.0	47.5	1.3	47.3	1.3	47.3	1.3	47.6	1.3
Z037	0.0499	0.004	0.00764	0.00018	0.0472	0.0037	49.4	3.9	49	1.2	70	150	30.0	49.0	1.2	49	1.2	49	1.2	49.3	1.3
Z038	0.0431	0.0051	0.00683	0.00021	0.046	0.0055	42.6	5	43.9	1.3	0	200	#DIV/0!	43.9	1.3	43.9	1.4	43.9	1.4	43.7	1.3
Z039	0.0521	0.0082	0.00738	0.00023	0.0512	0.0074	51.2	7.7	47.4	1.4	150	210	68.4	47.4	1.4	46.5	1.1	46.5	1.1	47.4	1.4
Z040	2.009	0.062	0.1917	0.0031	0.0759	0.0024	1115	22	1130	17	1075	66	-5.1	discordant	discordant	1090	18	1129	17	1021	39
Z041	0.0864	0.0049	0.01343	0.00024	0.0464	0.0025	84	4.6	86	1.5	40	100	-115.0	86.0	1.5	85.9	1.6	86.1	1.5	85.3	2.9
Z042	0.084	0.011	0.01407	0.00033	0.0429	0.0056	81	10	90.1	2.1	-80	220	212.6	90.1	2.1	90.4	2.3	90.5	2.3	90.1	2.1
Z043	0.0313	0.003	0.0048	0.00011	0.0469	0.0044	31.3	3	30.89	0.73	40	170	22.8	30.9	0.7	30.87	0.75	30.87	0.75	30.89	0.73
Z044	0.0571	0.0055	0.00834	0.00023	0.0496	0.005	56.2	5.3	53.6	1.5	170	190	68.5	53.6	1.5	53.3	1.6	53.3	1.6	53.5	1.5
Z047	0.152	0.025	0.0203	0.0012	0.0536	0.009	140	22	129.8	7.7	210	290	38.2	129.8	7.7	130.8	8.6	130.9	8.6	131.9	8.5
Z048	0.0311	0.0025	0.00501	0.00026	0.0457	0.0035	31.1	2.4	32.2	1.7	10	140	-222.0	32.2	1.7	32.3	1.7	32.3	1.7	32.1	1.7
Z049	0.1012	0.0058	0.01498	0.00032	0.0485	0.0024	97.7	5.4	95.9	2.1	125	98	23.3	95.9	2.1	95.7	2.1	95.8	2.1	96.4	2.4
Z050	0.0627	0.0041	0.01037	0.00025	0.0439	0.0027	61.7	3.9	66.5	1.6	-60	110	210.8	66.5	1.6	66.8	1.6	66.8	1.6	65.9	1.8
Z051	0.117	0.022	0.01007	0.0004	0.088	0.016	109	20	64.6	2.6	960	390	93.3	64.6	2.6	60.6	2.5	60.6	2.5	63.9	2.6
Z052	0.1044	0.0062	0.01584	0.00024	0.0476	0.0027	100.6	5.7	101.3	1.5	90	110	-12.6	101.3	1.5	101.4	1.6	101.4	1.6	101.3	1.5
Z053	0.0434	0.0068	0.00816	0.00029	0.0393	0.0065	42.9	6.6	52.4	1.9	-220	250	123.8	52.4	1.9	52.8	2.1	52.8	2.1	52	1.9
Z054	0.027	0.002	0.004122	0.000096	0.0474	0.0034	27	2	26.52	0.61	80	140	66.9	26.5	0.6	26.49	0.63	26.49	0.63	26.39	0.66
Z055	0.117	0.0028	0.01835	0.00038	0.04625	0.00072	112.3	2.6	117.2	2.4	20	32	-486.0	117.2	2.4	116.5	2.5	117.4	2.4	95.1	9.9
Z056	0.0341	0.0017	0.005486	0.00009	0.0453	0.0026	34	1.7	35.27	0.58	-10	110	452.7	35.3	0.6	35.34	0.64	35.34	0.64	35.27	0.58
Z057	0.1439	0.0048	0.02172	0.00076	0.04795	0.00098	136.4	4.3	138.5	4.8	98	44	-41.3	138.5	4.8	136.8	4.7	138.5	4.9	107	13
Z058	0.062	0.0062	0.01005	0.00027	0.0441	0.0037	60.8	5.9	64.5	1.7	-20	160	422.5	64.5	1.7	64.6	1.7	64.7	1.7	63.8	2.1
Z059	0.0644	0.0071	0.01126	0.00057	0.0418	0.0044	63	6.8	72.2	3.6	-150	170	148.1	72.2	3.6	72.7	3.7	72.7	3.7	71.1	3.6
Z060	0.0486	0.0041	0.00762	0.00015	0.0465	0.0041	48.1	4	48.94	0.96	40	160	-22.4	48.9	1.0	49	1	49	1	48.76	0.97
Z061	0.068	0.011	0.0109	0.0011	0.0443	0.005	67	11	70	6.9	-50	190	240.0	70.0	6.9	70.1	6.8	70.2	6.9	68	6.8
Z062	3.132	0.065	0.2348	0.0044	0.0968	0.0014	1440	16	1360	23	1562	27	12.9	1562.0	27.0	1352	24	1345	25	1363	24
Z063	0.0335	0.0045	0.0058	0.00042	0.0436	0.005	33.3	4.5	37.2	2.7	-90	190	141.3	37.2	2.7	38.1	2.9	38.1	2.9	37.2	2.7
Z064	0.0827	0.0066	0.01346	0.00036	0.0443	0.0031	80.4	6.2	86.2	2.3	-20	130	531.0	86.2	2.3	86.4	2.2	86.5	2.2	85.4	2.7
Z065	0.097	0.017	0.01421	0.00051	0.0499	0.0088	93	16	90.9	3.3	110	300	17.4	90.9	3.3	90.6	3.6	90.7	3.6	89.5	4.7
Z066	0.0527	0.0022	0.00834	0.0002	0.0458	0.0014	52.2	2.1	53.5	1.3	6	58	-791.7	53.5	1.3	53.6	1.3	53.6	1.3	53.4	1.4
Z067	0.0214	0.0027	0.003601	0.000068	0.0434	0.0056	21.5	2.7	23.17	0.44	-100	200	123.2	23.2	0.4	23.39	0.58	23.39	0.58	23.17	0.44
Z068	0.0567	0.0086	0.0095	0.00032	0.0421	0.0063	55.6	8.2	61	2	-120	240	150.8	61.0	2.0	61.2	2.2	61.2	2.2	61	2

Z069	0.0564	0.0043	0.00832	0.00021	0.0484	0.0033	55.6	4.1	53.4	1.3	110	130	51.5	53.4	1.3	53.3	1.3	53.3	1.3	52.6	1.6
Z070	0.092	0.0075	0.01436	0.00031	0.0473	0.0039	89	7	91.9	2	60	150	-53.2	91.9	2.0	91.9	2	92	2	91.5	2
Z071	0.098	0.018	0.01588	0.00054	0.045	0.0083	94	16	101.6	3.4	-40	290	354.0	101.6	3.4	102.3	3.4	102.5	3.4	101.5	3.5
Z072	1.837	0.053	0.1883	0.0033	0.0709	0.0021	1056	19	1112	18	937	62	-18.7	discordant	discordant	1043	16	1110	18	901	51
Z073	0.0698	0.0085	0.01069	0.00031	0.0473	0.0055	68.1	8	68.6	2	50	200	-37.2	68.6	2.0	68.6	2	68.6	2	68.6	2
Z074	0.0346	0.0049	0.005	0.00018	0.0499	0.0064	34.4	4.7	32.1	1.1	120	220	73.3	32.1	1.1	32	1.1	32	1.1	32.1	1.1
Z075	0.059	0.021	0.00895	0.0005	0.054	0.019	55	20	57.4	3.2	-50	530	214.8	57.4	3.2	57	4.1	57	4.1	57.4	3.2
Z076	0.0461	0.0036	0.00723	0.0002	0.0461	0.0032	45.7	3.5	46.4	1.3	20	120	-132.0	46.4	1.3	46.5	1.2	46.5	1.2	46.3	1.3
Z077	0.542	0.036	0.0716	0.0039	0.0545	0.0014	435	26	445	24	383	56	-16.2	445.0	24.0	430	23	445	24	350	34
Z078	0.11	0.015	0.01418	0.00067	0.0573	0.0074	108	15	90.7	4.2	370	230	75.5	90.7	4.2	89.5	4.2	89.6	4.2	89.3	4.8
Z079	0.164	0.063	0.01694	0.00079	0.057	0.011	126	27	108.3	5	250	200	56.7	108.3	5.0	105.2	2.5	105.3	2.5	102.2	7.4
Z080	0.818	0.037	0.1015	0.002	0.0584	0.0023	604	20	623	12	517	85	-20.5	discordant	discordant	595	15	622	12	482	49
Z081	0.0231	0.0019	0.003669	0.000096	0.0463	0.0041	23.2	1.9	23.61	0.61	50	160	52.8	23.6	0.6	23.59	0.64	23.59	0.64	23.62	0.63
Z082	0.0505	0.0066	0.00789	0.00027	0.0475	0.0066	49.8	6.4	50.7	1.7	40	240	-26.8	50.7	1.7	50.7	1.9	50.7	1.9	50.7	1.7
Z083	0.0253	0.0021	0.003645	0.000089	0.0502	0.0039	25.3	2	23.45	0.57	180	150	87.0	23.5	0.6	23.34	0.57	23.34	0.57	23.45	0.57
Z084	0.108	0.014	0.01609	0.00047	0.048	0.0072	103	13	102.9	3	70	270	-47.0	102.9	3.0	102.9	3.4	102.9	3.4	102.9	3
Z085	0.0621	0.004	0.01005	0.00032	0.0453	0.0022	61.1	3.9	64.4	2.1	-18	89	457.8	64.4	2.1	64.5	2.1	64.6	2.1	62.3	2.9
Z086	0.095	0.01	0.01466	0.00038	0.0474	0.0054	91.3	9.6	93.8	2.4	60	200	-56.3	93.8	2.4	93.9	2.7	94	2.7	94	2.4
Z087	0.069	0.011	0.01	0.0003	0.0473	0.0064	67	10	64.2	1.9	100	250	35.8	64.2	1.9	63.9	2	64	2	64.1	2
Z088	0.0356	0.0045	0.00519	0.00016	0.0509	0.0065	36.4	4.8	33.4	1	150	220	77.7	33.4	1.0	33.2	1	33.2	1	33.4	1
Z089	0.052	0.0046	0.00853	0.00052	0.0451	0.0035	51.3	4.4	54.7	3.3	-20	140	373.5	54.7	3.3	54.9	3.4	54.9	3.4	53.6	3.7
Z090	0.143	0.011	0.023	0.0014	0.0456	0.0025	135.5	9.4	146.4	8.6	0	100	#DIV/0!	146.4	8.6	146.5	8.8	147.1	8.8	137	12
Z091	0.0442	0.0065	0.00712	0.00037	0.0466	0.0071	43.7	6.3	45.7	2.4	-10	250	557.0	45.7	2.4	45.8	2.6	45.8	2.6	45.5	2.5
Z092	0.0533	0.0019	0.00861	0.00018	0.045	0.0015	52.7	1.9	55.2	1.1	-25	65	320.8	55.2	1.1	55.3	1.2	55.4	1.2	51.4	3.1
Z093	0.062	0.011	0.00886	0.00038	0.0506	0.009	60	10	56.9	2.4	90	300	36.8	56.9	2.4	56.6	2.5	56.6	2.5	56.9	2.4
Z094	1.002	0.04	0.1181	0.0033	0.0614	0.0016	702	20	719	19	641	54	-12.2	discordant	discordant	690	18	718	19	596	39
Z095	0.0733	0.0068	0.0111	0.00035	0.0484	0.0044	71.5	6.5	71.2	2.3	110	170	35.3	71.2	2.3	71	2.3	71.1	2.3	69.8	3.7
Z096	0.0578	0.0053	0.00987	0.00028	0.0427	0.0039	56.9	5.1	63.3	1.8	-110	160	157.5	63.3	1.8	63.6	1.9	63.7	1.9	63.2	1.8
Z097	0.0822	0.0051	0.01323	0.00063	0.046	0.002	80.1	4.8	84.7	4	22	85	-285.0	84.7	4.0	84.7	4	84.8	4	83.7	4.5
Z098	0.0789	0.0063	0.01094	0.00021	0.052	0.0037	76.9	5.8	70.2	1.3	230	130	69.5	70.2	1.3	69.6	1.2	69.8	1.3	67.8	2.9
Z099	0.0484	0.0047	0.00686	0.00016	0.052	0.0048	47.8	4.5	44.1	1	240	170	81.6	44.1	1.0	43.9	1.1	44	1.1	44.1	1.3
Z100	0.09	0.023	0.01586	0.00048	0.041	0.01	84	21	101.4	3.1	-260	360	139.0	101.4	3.1	102.2	3.4	102.3	3.4	101.2	3.1
Z101	0.0236	0.0024	0.003957	0.000078	0.0431	0.0041	23.6	2.4	25.46	0.5	-100	160	125.5	25.5	0.5	25.56	0.5	25.56	0.5	25.37	0.53
Z102	0.0625	0.0037	0.00998	0.00027	0.0454	0.0025	61.5	3.6	64	1.7	0	100	#DIV/0!	64.0	1.7	64.1	1.8	64.2	1.8	63.1	2.2

Z103	0.768	0.027	0.0974	0.0018	0.0569	0.0019	577	15	599	11	481	78	-24.5	discordant	discordant	569	11	598	11	452	44
Z104	0.0948	0.0058	0.01426	0.00037	0.0481	0.0026	91.7	5.3	91.3	2.3	110	110	17.0	91.3	2.3	91.1	2.4	91.2	2.4	91.9	2.4
Z105	0.069	0.011	0.00987	0.00027	0.0514	0.0085	67	10	63.3	1.8	130	280	51.3	63.3	1.8	63	2	63	2	63.3	1.8
Z106	1.614	0.054	0.1661	0.0022	0.0704	0.0022	973	21	991	12	936	61	-5.9	discordant	discordant	955	14	988	12	874	41
Z107	0.03	0.002	0.00433	0.00018	0.0495	0.0024	30	1.9	27.9	1.1	158	97	82.3	27.9	1.1	27.7	1.2	27.7	1.2	27.7	1.1
Z108	0.034	0.0012	0.005492	0.000097	0.0449	0.0016	33.9	1.2	35.31	0.62	-29	66	221.8	35.3	0.6	35.37	0.65	35.39	0.64	34.95	0.96
Z109	0.1178	0.0071	0.018	0.00038	0.0479	0.0033	112.8	6.5	115	2.4	90	120	-27.8	115.0	2.4	114.8	2.5	115.1	2.6	110.5	4.4
Z110	0.0692	0.0026	0.01119	0.00032	0.0448	0.001	67.9	2.4	71.7	2	-36	45	299.2	71.7	2.0	71.9	2	72	2	70.5	2.2
Z111	1.621	0.059	0.1759	0.0066	0.0668	0.0011	976	22	1044	36	829	34	-25.9	discordant	discordant	976	22	1044	36	828	33
Z112	0.129	0.038	0.0089	0.00067	0.098	0.031	117	31	57.1	4.3	900	440	93.7	57.1	4.3	55	5.4	53.9	5.6	59.7	5.5
Z113	0.063	0.015	0.00675	0.00038	0.065	0.016	60	14	43.4	2.4	360	440	87.9	43.4	2.4	42.3	2.3	42.2	2.3	43.4	2.4
Z114	0.0289	0.0045	0.00443	0.00011	0.0478	0.0077	28.8	4.4	28.52	0.72	30	270	4.9	28.5	0.7	28.5	0.82	28.5	0.82	28.59	0.72
Z115	0.0529	0.0067	0.00847	0.00083	0.0472	0.0056	52.1	6.5	54.3	5.3	40	200	-35.8	54.3	5.3	54.4	5.3	54.5	5.3	50.7	5.5
Z116	0.0452	0.0042	0.00692	0.00014	0.0484	0.0051	44.8	4.1	44.45	0.87	90	190	50.6	44.5	0.9	44.4	1	44.4	1	43.9	1
Z117	0.094	0.0092	0.01458	0.00037	0.0469	0.0045	92.6	9.1	93.3	2.3	90	180	-3.7	93.3	2.3	93.3	2.5	93.3	2.5	93.5	2.3
Z118	0.0805	0.0054	0.01245	0.00037	0.0471	0.0031	78.4	5.1	79.8	2.4	70	120	-14.0	79.8	2.4	79.7	2.5	79.8	2.5	78.6	3
Z120	0.168	0.031	0.02335	0.00076	0.0525	0.0093	153	27	148.8	4.8	140	310	-6.3	148.8	4.8	148.2	5.2	148.2	5.3	148.8	4.8
Z121	0.085	0.012	0.01086	0.00034	0.0571	0.0084	82	11	69.6	2.1	330	260	78.9	69.6	2.1	68.8	2.3	68.8	2.3	69.5	2.1
Z122	0.0455	0.0078	0.00831	0.00033	0.0403	0.0073	46.5	8.1	53.4	2.1	-200	270	126.7	53.4	2.1	53.7	2.3	53.8	2.3	53.4	2.1
Z123	0.591	0.013	0.0796	0.0014	0.0539	0.0011	471.4	8.2	493.5	8.3	359	45	-37.5	493.5	8.3	468.3	8.1	493.3	8.4	342	37
Z124	0.0567	0.0046	0.00792	0.00016	0.0516	0.0037	55.9	4.4	50.9	1.1	220	140	76.9	50.9	1.1	50.6	1	50.6	1	50.7	1
Z125	0.0411	0.0019	0.00653	0.00026	0.0457	0.001	40.9	1.9	42	1.7	0	44	#DIV/0!	42.0	1.7	42	1.7	42	1.7	41	2.3
Z126	0.114	0.021	0.01776	0.00063	0.0477	0.0088	107	20	113.5	4	20	320	-467.5	113.5	4.0	113.7	4.5	113.7	4.5	113.5	4
Z127	0.188	0.075	0.01342	0.00084	0.08	0.014	142	34	85.9	5.4	990	320	91.3	85.9	5.4	85	6.5	83.5	6.2	86	8.8
Z128	0.0186	0.0018	0.003134	0.000064	0.0432	0.0044	18.7	1.8	20.17	0.41	-100	170	120.2	20.2	0.4	20.22	0.47	20.22	0.47	20.17	0.41
Z129	2.313	0.091	0.1777	0.0057	0.0941	0.0016	1213	28	1054	31	1507	32	30.1	discordant	discordant	1038	32	1030	32	1054	31
Z130	0.0269	0.0021	0.00409	0.00008	0.0476	0.0037	27	2.1	26.31	0.51	110	150	76.1	26.3	0.5	26.37	0.58	26.37	0.59	26.31	0.51
Z131	0.643	0.025	0.0834	0.0016	0.056	0.0021	503	15	516.4	9.5	427	81	-20.9	discordant	discordant	499	11	516.1	9.9	419	38
Z132	0.0611	0.0046	0.01001	0.00018	0.0442	0.0031	60.1	4.4	64.2	1.1	-50	130	228.4	64.2	1.1	64.5	1.1	64.5	1.1	64.2	1.1
Z133	0.0561	0.0082	0.00686	0.00026	0.0596	0.0085	55	7.8	44.1	1.6	400	250	89.0	44.1	1.6	43.4	1.7	43.4	1.7	43.9	1.8
Z134	0.196	0.024	0.0214	0.0023	0.0663	0.0025	180	20	136	15	797	77	82.9	136.0	15.0	133	14	133	14	136	15
Z135	0.0556	0.0039	0.0089	0.00028	0.0454	0.003	54.9	3.8	57.1	1.8	0	120	#DIV/0!	57.1	1.8	57.2	1.8	57.2	1.8	57	1.8
Z136	0.041	0.002	0.006538	0.000094	0.0455	0.0022	40.8	2	42.01	0.6	2	90	-2000.5	42.0	0.6	42.06	0.61	42.08	0.62	41.52	0.76
Z137	0.0401	0.0025	0.0068	0.00011	0.0426	0.0024	39.8	2.4	43.71	0.7	-119	98	136.7	43.7	0.7	43.9	0.7	43.94	0.7	43.2	1.1

Z138	0.133	0.034	0.01803	0.00087	0.052	0.013	121	30	115.2	5.5	80	420	-44.0	115.2	5.5	114.3	5.9	114.4	5.9	113.5	5.5
Z139	0.367	0.052	0.0212	0.0026	0.121	0.0041	308	39	135	17	1954	63	93.1	135.0	17.0	123	15	122	15	135	17
Z140	0.2272	0.0099	0.03369	0.00053	0.0488	0.0018	207.5	8.1	213.6	3.3	137	77	-55.9	213.6	3.3	212	3.5	213.9	3.3	193	14

Sample 16LETKAT

	Ratios						U-Pb ages uncorrected for common lead									Corrected for common lead using Andersen's routine					
Grains	Final207_235	Final207_235_2s	Final206_238	Final206_238_2s	Final207_206	Final207_206_2s	FinalAge 207_235	FinalAge 207_235_2s	FinalAge 206_238	FinalAge 206_238_2s	FinalAge 207_206	FinalAge 207_206_2s	Concordance (%)	Best age	Best age 2s	FinalAgeAnd207_235	FinalAgeAnd207_235_2s	FinalAgeAnd206_238	FinalAgeAnd206_238_2s	FinalAgeAnd207_206	FinalAgeAnd207_206_2s
Z001	0.132	0.034	0.00821	0.0006	0.096	0.019	121	28	52.7	3.9	1320	410	96.0	52.7	3.9	49.6	3.9	47.9	4.1	55.7	5.5
Z002	0.0808	0.0081	0.00819	0.00028	0.0705	0.0062	78.5	7.6	52.6	1.8	820	180	93.6	52.6	1.8	51	1.6	51	1.6	52.6	1.8
Z003	0.0555	0.0036	0.00802	0.0003	0.05	0.0027	54.7	3.5	51.5	1.9	180	110	71.4	51.5	1.9	51.3	1.9	51.3	1.9	51.9	2.2
Z004	0.0706	0.0091	0.00847	0.0005	0.0631	0.0081	68.9	8.5	54.4	3.2	520	240	89.5	54.4	3.2	52.1	2.9	52.1	2.9	54.2	3.2
Z006	0.0952	0.0072	0.01513	0.00056	0.0473	0.0041	93.8	7.4	96.8	3.5	90	160	-7.6	96.8	3.5	95.8	3.4	96.8	3.7	95.6	4.1
Z007	10.98	0.34	0.407	0.012	0.1961	0.0058	2516	29	2196	57	2783	49	21.1	discordant	discordant	2148	68	2076	71	2206	58
Z008	0.0536	0.0019	0.00787	0.00022	0.0499	0.002	53	1.8	50.6	1.4	181	85	72.0	50.6	1.4	50.4	1.5	50.4	1.5	50.1	1.5
Z009	0.1089	0.0099	0.01521	0.00075	0.0536	0.005	104.4	9.1	97.3	4.8	290	180	66.4	97.3	4.8	94.8	4.1	94.9	4.1	96	5.4
Z010	0.0716	0.009	0.01102	0.00045	0.0466	0.0056	69.8	8.4	70.6	2.9	60	210	-17.7	70.6	2.9	70.7	3	70.7	3	70.6	2.9
Z011	0.0267	0.0036	0.00418	0.00026	0.0482	0.0073	26.7	3.5	26.9	1.7	130	270	79.3	26.9	1.7	26.8	1.8	26.8	1.8	26.5	1.7
Z012	0.228	0.041	0.01675	0.00074	0.096	0.015	202	33	107.1	4.7	1240	310	91.4	107.1	4.7	99.6	3.5	99.3	3.5	106.9	4.7
Z013	0.0987	0.0054	0.0152	0.00045	0.0477	0.0028	95.5	5	97.2	2.8	90	110	-8.0	97.2	2.8	97.2	3	97.3	3	94.7	3.6
Z015	0.75	0.052	0.0931	0.0027	0.0602	0.0047	569	32	573	16	530	160	-8.1	discordant	discordant	550	17	572	17	479	46
Z016	0.0489	0.0053	0.00687	0.00041	0.0513	0.0044	48.3	5.2	44.1	2.6	220	170	80.0	44.1	2.6	43.9	2.6	43.9	2.6	44.1	2.6
Z017	0.1647	0.0079	0.02423	0.00077	0.0497	0.0024	154.5	6.8	154.3	4.8	174	98	11.3	154.3	4.8	153.6	5	154.1	5.1	149.9	6.1
Z018	0.082	0.014	0.01025	0.00037	0.058	0.01	79	13	65.7	2.4	300	310	78.1	65.7	2.4	65.9	3.2	64.8	2.6	66.7	3
Z019	0.0585	0.0037	0.00899	0.00023	0.0476	0.0032	57.6	3.6	57.7	1.5	80	130	27.9	57.7	1.5	57.7	1.6	57.7	1.6	57.7	1.5
Z020	0.139	0.0042	0.02094	0.00051	0.0485	0.0013	132.1	3.7	133.6	3.2	121	57	-10.4	133.6	3.2	133.1	3.3	133.7	3.3	127.4	6.3
Z021	0.093	0.029	0.01088	0.0006	0.063	0.02	87	23	69.7	3.8	250	360	72.1	69.7	3.8	66.5	5	66.5	5	71	5.8
Z022	0.124	0.01	0.0181	0.00062	0.0503	0.0043	117.8	9.1	115.7	4	190	160	39.1	115.7	4.0	115.4	4.2	115.5	4.2	115.6	4
Z023	0.0333	0.0044	0.00454	0.00012	0.0532	0.0066	33.2	4.3	29.21	0.8	280	230	89.6	29.2	0.8	28.87	0.79	28.87	0.79	29.5	0.87
Z024	0.0549	0.0055	0.00818	0.00031	0.0507	0.0053	54.1	5.3	52.5	2	180	200	70.8	52.5	2.0	51.9	2.3	51.9	2.3	52.5	2
Z025	0.137	0.024	0.01519	0.00069	0.065	0.012	128	21	97.1	4.4	550	330	82.3	97.1	4.4	94.3	5.2	94.3	5.2	97.1	4.4
Z026	0.149	0.058	0.01675	0.00056	0.066	0.026	114	19	107.1	3.6	180	270	40.5	107.1	3.6	106.1	4	105.1	4.8	107.1	3.7
Z027	0.121	0.015	0.01656	0.00073	0.053	0.0062	115	14	105.8	4.6	280	230	62.2	105.8	4.6	104.8	4.8	104.9	4.8	107.3	5.5
Z028	1.294	0.05	0.1389	0.0041	0.0683	0.0028	845	21	838	23	870	81	3.7	838.0	23.0	801	19	834	24	717	46
Z029	0.643	0.025	0.083	0.0024	0.0578	0.0024	507	17	514	14	494	88	-4.0	514.0	14.0	494	15	512	15	411	45
Z030	0.109	0.015	0.01465	0.00039	0.0547	0.0077	104	14	93.8	2.5	270	260	65.3	93.8	2.5	93	2.8	93	2.8	93.6	2.5
Z031	0.0681	0.0034	0.01026	0.00032	0.0486	0.0024	66.8	3.2	65.8	2.1	150	110	56.1	65.8	2.1	65.6	2.1	65.7	2.1	63.2	3.3
Z032	0.0503	0.0043	0.00676	0.00016	0.0541	0.0048	49.8	4.1	43.5	1	310	180	86.0	43.5	1.0	43.3	1.2	43.3	1.3	43.8	1.4

Z033	0.131	0.022	0.0162	0.00068	0.0592	0.0095	122	19	103.6	4.3	370	280	72.0	103.6	4.3	102.1	4.5	100.8	4.7	99.5	5.8
Z034	2.39	0.13	0.1909	0.0083	0.0911	0.0032	1239	44	1124	45	1429	68	21.3	discordant	discordant	1105	45	1107	47	1107	45
Z035	1.594	0.06	0.1591	0.0046	0.073	0.002	964	23	951	26	1003	55	5.2	951.0	26.0	928	24	947	27	896	29
Z036	0.816	0.019	0.1004	0.0016	0.0593	0.0015	605	11	616.8	9.1	565	55	-9.2	discordant	discordant	590.8	8.9	615.5	9.4	501	33
Z037	1.89	0.04	0.1773	0.0032	0.078	0.0014	1076	14	1052	17	1142	35	7.9	1052.0	17.0	1038	16	1047	18	1026	20
Z038	0.132	0.0058	0.01905	0.00053	0.051	0.0022	125.7	5.2	121.6	3.3	223	87	45.5	121.6	3.3	119.7	3.7	120.4	3.8	112.9	6.6
Z039	1.481	0.06	0.1537	0.004	0.0704	0.0028	919	25	921	23	912	82	-1.0	921.0	23.0	879	24	917	24	786	53
Z040	0.085	0.016	0.01073	0.00036	0.059	0.01	82	14	68.8	2.3	330	320	79.2	68.8	2.3	67.9	2.5	67.9	2.5	68.8	2.3
Z041	0.077	0.011	0.0097	0.00046	0.0589	0.0083	75	10	62.2	2.9	420	260	85.2	62.2	2.9	60.5	3.2	60.4	3.2	62.2	2.9
Z042	0.128	0.018	0.01584	0.00045	0.0591	0.0086	120	16	101.3	2.8	380	260	73.3	101.3	2.8	101.6	4.9	99.9	3.3	100.2	6.1
Z043	0.1028	0.0051	0.01462	0.00039	0.0522	0.003	99.3	4.7	93.6	2.5	260	120	64.0	93.6	2.5	92.9	2.6	93.1	2.6	91.3	3.7
Z044	0.0548	0.0032	0.00788	0.00018	0.051	0.003	54.1	3.1	50.6	1.2	220	120	77.0	50.6	1.2	50.2	1.2	50.2	1.2	50.2	1.3
Z045	0.152	0.014	0.02118	0.00078	0.0527	0.0049	143	12	135.1	4.9	250	150	46.0	135.1	4.9	133.1	4.5	133.5	4.5	129.2	8.4
Z046	0.0898	0.0079	0.00418	0.00019	0.162	0.015	86.9	7.3	26.9	1.2	2390	170	98.9	26.9	1.2	22.9	1.3	22.9	1.3	26.9	1.2
Z048	0.109	0.0097	0.01557	0.0005	0.0523	0.0054	104.6	8.8	99.6	3.2	260	200	61.7	99.6	3.2	98.7	3.4	98.8	3.4	98.2	3.7
Z049	0.0271	0.0031	0.00422	0.00014	0.0466	0.0055	27.1	3	27.15	0.88	20	200	-35.8	27.2	0.9	27.15	0.92	27.15	0.92	27.15	0.88
Z050	0.0426	0.0027	0.00641	0.00019	0.0481	0.003	42.3	2.6	41.2	1.2	100	120	58.8	41.2	1.2	41.1	1.2	41.1	1.2	40.7	1.3
Z052	0.0304	0.0054	0.00405	0.00016	0.055	0.009	30.2	5.2	26.1	1	330	300	92.1	26.1	1.0	25.31	0.96	25.31	0.96	26.1	1
Z053	0.0518	0.0082	0.00469	0.00016	0.08	0.011	50.9	7.8	30.1	1	930	250	96.8	30.1	1.0	28.55	0.88	28.43	0.87	29.58	0.99
Z054	0.15	0.033	0.01649	0.00049	0.064	0.012	137	26	105.4	3.1	430	270	75.5	105.4	3.1	105.1	4.1	105.2	4.1	104.6	5.1
Z055	0.106	0.015	0.01532	0.00042	0.0512	0.0067	102	13	98	2.7	180	240	45.6	98.0	2.7	97.7	2.9	97.7	2.9	97.9	2.7
Z056	0.0975	0.0099	0.01391	0.00042	0.0521	0.0052	96	9.9	89	2.7	230	190	61.3	89.0	2.7	88.5	2.7	88	2.5	88.3	3
Z057	0.215	0.021	0.02458	0.00095	0.0656	0.0078	201	20	156.5	6	630	210	75.2	156.5	6.0	152.6	6.6	152.5	6.7	154.4	6.9
Z058	1.279	0.048	0.1416	0.0043	0.0669	0.0021	839	19	853	24	818	65	-4.3	853.0	24.0	812	18	850	25	716	42
Z059	1.354	0.046	0.1383	0.0032	0.0715	0.0023	867	20	835	18	969	59	13.8	835.0	18.0	814	16	829	19	798	26
Z060	0.139	0.023	0.01754	0.00084	0.0544	0.0082	129	20	112	5.3	290	280	61.4	112.0	5.3	110.6	5.4	110.8	5.5	108.7	6.9
Z061	0.11	0.0075	0.01683	0.00037	0.0481	0.0033	105.7	6.8	107.6	2.4	100	130	-7.6	107.6	2.4	107.5	2.4	107.7	2.4	105	3.6
Z062	0.722	0.043	0.0862	0.0029	0.0615	0.0037	548	25	533	17	600	120	11.2	533.0	17.0	511	16	529	18	455	40
Z063	0.0502	0.0021	0.00802	0.00028	0.0453	0.0015	49.7	2	51.5	1.8	-13	63	496.2	51.5	1.8	51.6	1.8	51.6	1.8	51	2
Z064	0.072	0.012	0.00752	0.00075	0.08	0.018	70	11	48.2	4.8	730	330	93.4	48.2	4.8	46.3	5.3	46.1	5.4	48.3	4.9
Z065	0.0957	0.0067	0.012	0.00029	0.0581	0.0035	92.6	6.1	76.9	1.9	480	120	84.0	76.9	1.9	75.8	1.8	75.7	1.8	76.8	1.9
Z066	0.1076	0.0088	0.01449	0.0004	0.0541	0.0044	103.3	8.1	92.7	2.5	320	160	71.0	92.7	2.5	92	2.6	92	2.6	91.8	2.7
Z067	0.0749	0.0096	0.00999	0.00057	0.0554	0.007	73.1	9	64.1	3.7	430	290	85.1	64.1	3.7	63.1	3.8	63.1	3.8	63.2	3.5
Z068	0.053	0.0039	0.00775	0.00028	0.0492	0.0031	52.3	3.8	49.7	1.8	170	130	70.8	49.7	1.8	49.6	1.8	49.6	1.8	49.4	1.9

Z069	0.047	0.0024	0.00706	0.00018	0.0485	0.0021	46.6	2.3	45.3	1.2	118	86	61.6	45.3	1.2	45.2	1.2	45.2	1.2	45.2	1.2
Z070	0.067	0.0051	0.01002	0.00036	0.049	0.0037	65.7	4.9	64.3	2.3	140	150	54.1	64.3	2.3	64.1	2.4	64.2	2.4	63.3	2.8
Z071	0.1716	0.0097	0.02354	0.00076	0.0519	0.003	162.6	9.4	150	4.8	320	140	53.1	150.0	4.8	148.5	5	148.9	5	146.3	8.6
Z072	0.1009	0.0081	0.01362	0.00036	0.0541	0.0043	97.2	7.5	87.2	2.3	320	160	72.8	87.2	2.3	86.5	2.4	86.5	2.4	87	2.3
Z073	0.62	0.026	0.0764	0.0013	0.0591	0.0026	489	16	474.8	7.7	543	96	12.6	474.8	7.7	464.5	9.1	472.8	8.2	441	28
Z074	4.23	0.14	0.2873	0.0087	0.1083	0.0023	1682	29	1626	44	1764	40	7.8	1764.0	40.0	1605	42	1612	47	1599	41
Z075	0.068	0.015	0.00677	0.00081	0.068	0.019	65	14	43.5	5.2	430	540	89.9	43.5	5.2	42.1	5.3	42.1	5.3	43.5	5.2
Z076	10.86	0.73	0.365	0.022	0.2148	0.0049	2473	92	1990	110	2936	39	32.2	discordant	discordant	1900	110	1820	110	1990	110
Z077	0.134	0.028	0.01582	0.0008	0.059	0.011	125	25	101.1	5.1	440	380	77.0	101.1	5.1	99.5	5.6	99.4	5.6	101.1	5.1
Z078	1.036	0.082	0.1016	0.0039	0.0733	0.0038	711	40	623	23	970	110	35.8	discordant	discordant	607	24	613	22	603	32
Z079	0.163	0.01	0.0236	0.0009	0.0502	0.0025	152.6	8.8	150.3	5.7	190	100	20.9	150.3	5.7	149.7	5.7	150.1	5.7	145.5	7.9
Z080	2.023	0.085	0.1888	0.0042	0.0784	0.0025	1118	29	1114	23	1142	62	2.5	1114.0	23.0	1085	22	1109	23	1046	34
Z081	0.065	0.007	0.00955	0.00032	0.0499	0.005	63.7	6.6	61.2	2.1	150	190	59.2	61.2	2.1	61	2.1	61	2.1	61	2.1
Z082	0.119	0.016	0.01418	0.00062	0.0605	0.0074	113	14	90.8	4	500	250	81.8	90.8	4.0	89.4	4.2	89.4	4.2	88.4	5.2
Z083	4.58	0.15	0.3084	0.0098	0.1084	0.0023	1741	28	1731	48	1776	36	2.5	1776.0	36.0	1690	38	1721	51	1661	36
Z084	1.41	0.15	0.1307	0.0049	0.0772	0.0063	875	53	791	28	1100	160	28.1	discordant	discordant	755	23	774	27	726	33
Z085	0.1	0.013	0.01067	0.00039	0.0684	0.0085	95	12	68.4	2.5	690	250	90.1	68.4	2.5	66.6	2.6	66.6	2.6	68.2	2.5
Z086	1.776	0.039	0.1655	0.0031	0.0782	0.0013	1035	14	987	17	1148	32	14.0	987.0	17.0	982	18	980	18	986	18
Z087	0.0444	0.0028	0.00714	0.00032	0.0465	0.003	44.1	2.7	45.9	2	40	120	-14.8	45.9	2.0	45.9	2.1	46	2.1	45.8	2.1
Z088	3.32	0.11	0.2488	0.0077	0.0985	0.0029	1483	25	1431	40	1582	55	9.5	1582.0	55.0	1395	32	1415	42	1371	30
Z089	0.096	0.011	0.01432	0.00061	0.0498	0.0059	93	10	91.6	3.9	170	220	46.1	91.6	3.9	91.3	4.1	91.4	4.2	91.9	3.9
Z090	0.1805	0.0062	0.02568	0.0005	0.0512	0.0014	168.4	5.3	163.4	3.2	238	61	31.3	163.4	3.2	162	3.3	163	3.2	151.8	9
Z091	0.0369	0.0076	0.00555	0.0003	0.05	0.011	36.5	7.3	35.7	1.9	100	360	64.3	35.7	1.9	35.4	2.2	35.4	2.2	35.7	1.9
Z093	0.1157	0.0059	0.01681	0.0005	0.0499	0.0024	111	5.3	107.4	3.2	175	96	38.6	107.4	3.2	106.6	3.2	107.1	3.3	103.7	5.2
Z094	0.108	0.012	0.01498	0.00058	0.055	0.0066	104	11	95.9	3.7	320	230	70.0	95.9	3.7	95	3.8	95.1	3.8	95.8	3.8
Z095	0.13	0.018	0.0166	0.0011	0.0581	0.0074	123	16	106.3	7.2	430	260	75.3	106.3	7.2	104.2	7.7	104.2	7.7	106.3	7.2
Z096	0.084	0.012	0.0133	0.00048	0.0467	0.0066	81	11	85.2	3.1	10	240	-752.0	85.2	3.1	85.2	3.4	85.3	3.4	84.5	3.4
Z097	1.58	0.071	0.1623	0.005	0.071	0.0025	958	27	969	28	937	71	-3.4	969.0	28.0	925	23	965	28	837	46
Z099	0.407	0.021	0.0566	0.0024	0.0522	0.0025	346	15	355	15	280	100	-26.8	355.0	15.0	346	14	355	15	301	40
Z100	0.169	0.057	0.0109	0.00072	0.112	0.036	152	47	69.9	4.6	1480	720	95.3	69.9	4.6	64.7	5.3	64.6	5.4	70	4.8
Z101	0.0429	0.0027	0.00671	0.0002	0.0468	0.0028	42.7	2.6	43.1	1.3	50	110	13.8	43.1	1.3	43.1	1.3	43.1	1.3	43.1	1.3
Z102	1.225	0.051	0.1235	0.0041	0.0721	0.0029	809	23	750	23	962	84	22.0	discordant	discordant	733	21	742	24	703	34
Z103	0.0664	0.0045	0.01022	0.00045	0.0477	0.003	65.2	4.2	65.5	2.9	120	130	45.4	65.5	2.9	65.4	3	65.5	3	64	3.6
Z104	0.854	0.028	0.1042	0.0023	0.0598	0.0018	625	16	639	14	580	67	-10.2	discordant	discordant	613	13	637	14	530	32

Z105	0.057	0.0071	0.00837	0.00028	0.0494	0.0059	56	6.8	53.7	1.8	160	230	66.4	53.7	1.8	53.5	1.8	53.5	1.8	53.7	1.8
Z106	0.104	0.013	0.01675	0.00085	0.0463	0.0062	102	13	107	5.4	50	240	-114.0	107.0	5.4	107.2	5.8	107.3	5.8	106.4	5.2
Z107	0.2	0.023	0.0089	0.0005	0.171	0.022	184	19	57.1	3.2	2530	240	97.7	57.1	3.2	49	3.6	47.7	3.7	60.4	7.7
Z108	0.114	0.01	0.01763	0.0007	0.0481	0.0047	109	9.1	112.6	4.4	120	180	6.2	112.6	4.4	112.5	4.8	112.7	4.8	112.6	4.5
Z109	0.087	0.018	0.00817	0.00026	0.071	0.012	83	16	52.5	1.6	690	310	92.4	52.5	1.6	50.1	1.7	50	1.7	52.5	1.6
Z110	2.082	0.095	0.1887	0.0061	0.0807	0.0033	1137	31	1113	33	1186	81	6.2	1113.0	33.0	1070	29	1104	35	1006	40
Z111	0.963	0.057	0.0784	0.0024	0.0905	0.0059	680	29	486	14	1370	130	64.5	486.0	14.0	469	15	467	16	481	15
Z112	0.199	0.048	0.01396	0.00094	0.091	0.016	175	36	89.3	5.9	1130	330	92.1	89.3	5.9	83.6	5.5	83.4	5.5	88.7	6.3
Z113	0.101	0.016	0.01401	0.00059	0.0535	0.0088	97	15	89.7	3.8	260	320	65.5	89.7	3.8	89.1	4.2	89.2	4.2	88	4.6
Z114	0.0303	0.0024	0.0046	0.00011	0.0481	0.0037	30.3	2.3	29.62	0.69	100	150	70.4	29.6	0.7	29.4	0.66	29.41	0.66	29.64	0.71
Z116	0.185	0.015	0.00496	0.00026	0.276	0.021	171	13	31.9	1.7	3270	130	99.0	31.9	1.7	22.4	1.5	22.3	1.5	31.9	1.7
Z117	0.649	0.056	0.0839	0.0037	0.058	0.0056	503	34	519	22	510	220	-1.8	519.0	22.0	501	22	516	23	439	47
Z118	0.0534	0.0047	0.00804	0.00029	0.0483	0.004	52.7	4.5	51.6	1.9	140	160	63.1	51.6	1.9	51.4	1.9	51.5	1.9	51.2	2.5
Z119	0.065	0.013	0.00807	0.00028	0.0514	0.005	63	12	51.8	1.8	300	220	82.7	51.8	1.8	51.3	1.8	51.3	1.8	51.7	1.7
Z120	0.18	0.019	0.0073	0.00062	0.192	0.026	166	16	46.9	4	2550	250	98.2	46.9	4.0	39	4.3	38.9	4.3	46.9	4
Z121	0.0633	0.0058	0.00919	0.0003	0.0504	0.0043	62.1	5.6	59	1.9	230	180	74.3	59.0	1.9	58.6	1.9	58.6	1.9	59	1.9
Z122	3.33	0.2	0.252	0.01	0.0955	0.0032	1474	48	1448	53	1521	63	4.8	1521.0	63.0	1417	49	1438	55	1392	52
Z123	0.086	0.022	0.01416	0.00065	0.044	0.011	81	20	90.6	4.1	-170	360	153.3	90.6	4.1	90.5	4.5	91.3	4.4	88.2	5
Z125	0.1725	0.0074	0.02254	0.0009	0.0552	0.002	161.3	6.5	143.7	5.7	412	83	65.1	143.7	5.7	142.1	5.7	142.5	5.8	141	6.9
Z126	1.447	0.052	0.1491	0.0041	0.0719	0.0025	911	20	895	23	964	70	7.2	895.0	23.0	862	18	886	23	813	35
Z127	0.0759	0.0059	0.00702	0.00031	0.0797	0.0061	74.1	5.6	45.1	2	1080	170	95.8	45.1	2.0	43.3	2	43.3	2	45.1	2
Z128	0.0731	0.0067	0.01036	0.00043	0.0518	0.0046	71.4	6.3	66.4	2.7	220	160	69.8	66.4	2.7	66	2.8	66.1	2.8	65.9	3.1

Sample PAUN

	Ratios						U-Pb ages uncorrected for common lead									Corrected for common lead using Andersen's routine					
Grains	Final207_235	Final207_235_2s	Final206_238	Final206_238_2s	Final207_206	Final207_206_2s	FinalAge 207_235	FinalAge 207_235_2s	FinalAge 206_238	FinalAge 206_238_2s	FinalAge 207_206	FinalAge 207_206_2s	Concordance (%)	Best age	Best age 2s	FinalAgeAnd207_235	FinalAgeAnd207_235_2s	FinalAgeAnd206_238	FinalAgeAnd206_238_2s	FinalAgeAnd207_206	FinalAgeAnd207_206_2s
Z001	0.0992	0.0086	0.01491	0.00066	0.0482	0.0039	95.7	7.9	95.4	4.2	100	150	4.6	95.4	4.2	95.3	4.3	95.4	4.3	94.8	4.7
Z002	0.237	0.05	0.01401	0.00052	0.119	0.02	216	40	89.6	3.3	1620	270	94.5	89.6	3.3	83.2	3.4	82.9	3.4	89.6	3.4
Z003	0.1092	0.0061	0.01604	0.00039	0.049	0.0026	105.1	5.5	102.6	2.5	140	100	26.7	102.6	2.5	102.3	2.6	102.4	2.6	102.7	2.5
Z005	0.0699	0.0057	0.01049	0.00022	0.048	0.0039	68.5	5.4	67.3	1.4	90	150	25.2	67.3	1.4	67.2	1.5	67.2	1.5	66.4	1.6
Z006	0.102	0.0097	0.01395	0.00038	0.0528	0.0048	98.4	8.9	89.3	2.4	300	180	70.2	89.3	2.4	88.7	2.5	88.7	2.5	89.3	2.4
Z007	0.0645	0.0029	0.00947	0.00016	0.049	0.002	63.4	2.7	60.8	1	142	83	57.2	60.8	1.0	60.58	0.98	60.56	0.98	60.5	1.1
Z009	0.102	0.0063	0.0158	0.0004	0.0466	0.0027	98.4	5.8	101	2.6	40	110	-152.5	101.0	2.6	101	2.6	101.2	2.6	98.9	3.9
Z010	1.057	0.042	0.1117	0.0016	0.0687	0.0027	731	21	682.4	9.1	872	83	21.7	discordant	discordant	670	10	676.5	9.9	661	17
Z011	0.0831	0.0082	0.01374	0.00032	0.0439	0.0043	80.7	7.7	88	2	-70	170	225.7	88.0	2.0	88.2	2.2	88.4	2.2	87	3.2
Z012	0.0869	0.0065	0.01323	0.00027	0.0479	0.0039	84.4	6	84.7	1.7	90	150	5.9	84.7	1.7	84.7	1.9	84.7	2	84.8	1.8
Z013	0.0937	0.0085	0.01382	0.00037	0.0482	0.0042	90.6	7.9	88.5	2.3	130	170	31.9	88.5	2.3	88.2	2.4	88.3	2.4	86.1	3.6
Z014	0.0985	0.0078	0.01475	0.00028	0.0484	0.0041	95.1	7.2	94.4	1.8	110	160	14.2	94.4	1.8	94.1	1.9	94.3	1.9	92.8	3.3
Z015	0.121	0.0095	0.01934	0.00036	0.0465	0.004	115.5	8.6	123.5	2.3	40	150	-208.8	123.5	2.3	123.6	2.6	123.8	2.6	123.6	2.4
Z016	0.079	0.013	0.01309	0.00042	0.0454	0.0083	79	14	83.8	2.7	-70	280	219.7	83.8	2.7	84	2.8	84.1	2.8	83.8	2.6
Z017	0.0928	0.0063	0.01459	0.00032	0.0465	0.0034	89.9	5.8	93.4	2	40	140	-133.5	93.4	2.0	93.4	2.2	93.6	2.2	92.4	2.6
Z018	0.084	0.01	0.01382	0.00028	0.044	0.0055	81.7	9.7	88.5	1.8	-70	210	226.4	88.5	1.8	88.8	1.8	88.8	1.8	88.8	2
Z019	0.0827	0.0074	0.01329	0.0003	0.0459	0.0042	80.4	6.9	85.1	1.9	10	160	-751.0	85.1	1.9	85.3	1.9	85.3	1.9	85.1	1.9
Z021	0.117	0.029	0.01477	0.00058	0.058	0.015	108	26	94.5	3.7	200	440	52.8	94.5	3.7	93.4	4.2	93.4	4.2	94.3	3.7
Z022	0.1029	0.0095	0.01512	0.00036	0.0494	0.0045	99	8.8	96.8	2.3	150	170	35.5	96.8	2.3	96.6	2.4	96.6	2.4	96.5	2.3
Z023	0.1037	0.0072	0.0153	0.00035	0.0495	0.0036	99.9	6.7	97.9	2.2	160	140	38.8	97.9	2.2	97.5	2.4	97.7	2.4	93.4	5.2
Z024	0.0971	0.0099	0.01458	0.0005	0.0479	0.0047	93.6	9.2	93.3	3.2	90	180	-3.7	93.3	3.2	93.3	3.3	93.3	3.3	93	3.3
Z025	0.1129	0.0067	0.01616	0.00032	0.0518	0.0037	108.4	6.1	103.3	2	240	140	57.0	103.3	2.0	102.8	2.3	102.9	2.3	102.6	2.4
Z026	0.0723	0.009	0.0106	0.00027	0.05	0.0065	70.5	8.4	68	1.8	130	230	47.7	68.0	1.8	67.7	2	67.7	2	68.1	2.2
Z027	0.098	0.0063	0.01515	0.00025	0.0469	0.003	94.7	5.8	96.9	1.6	50	120	-93.8	96.9	1.6	96.9	1.6	97	1.6	95.5	2.5
Z028	0.116	0.02	0.01452	0.00045	0.058	0.0095	109	17	92.9	2.9	380	280	75.6	92.9	2.9	91.1	2.9	91.2	2.9	93.1	3
Z029	0.088	0.018	0.01479	0.00056	0.0453	0.0096	84	16	94.6	3.6	-30	350	415.3	94.6	3.6	94.6	4.3	94.7	4.4	94.2	3.5
Z030	0.1128	0.0075	0.01631	0.00052	0.0507	0.0031	108.3	6.9	104.3	3.3	220	130	52.6	104.3	3.3	103.4	3.2	103.7	3.2	103.3	3.8
Z031	0.082	0.012	0.01412	0.00041	0.0425	0.0066	79	11	90.4	2.6	-90	260	200.4	90.4	2.6	90.8	3	90.8	3	90.3	2.7
Z032	0.301	0.08	0.01731	0.00063	0.115	0.027	247	58	110.6	4	1190	410	90.7	110.6	4.0	99.5	2.3	99.7	2.4	99.7	9
Z033	0.1051	0.0059	0.01439	0.00033	0.0526	0.003	101.3	5.4	92.1	2.1	290	120	68.2	92.1	2.1	91.5	2.1	91.6	2.1	92.5	2.4

Z034	0.093	0.015	0.0143	0.00041	0.048	0.0079	89	14	91.5	2.6	40	280	-128.8	91.5	2.6	91.5	3	91.5	3	91.5	2.6
Z035	0.103	0.015	0.01593	0.00034	0.0472	0.0068	98	13	101.9	2.2	30	240	-239.7	101.9	2.2	102	2.5	102	2.6	101.8	2.2
Z036	0.129	0.019	0.01649	0.00039	0.0583	0.0083	126	18	105.4	2.4	360	250	70.7	105.4	2.4	103.9	2.4	104	2.4	105.4	2.5
Z037	0.099	0.011	0.01506	0.0004	0.0483	0.0054	95.5	9.9	96.4	2.5	90	200	-7.1	96.4	2.5	96.4	2.8	96.4	2.8	96.8	2.4
Z038	0.0993	0.0085	0.01518	0.00037	0.0479	0.0044	95.8	7.8	97.1	2.3	80	170	-21.4	97.1	2.3	97	2.6	97.1	2.6	97.2	2.4
Z039	0.1057	0.0085	0.01511	0.00038	0.051	0.0042	101.7	7.9	96.7	2.4	210	160	54.0	96.7	2.4	96.1	2.5	96.3	2.5	95.3	3.5
Z040	0.1096	0.0085	0.01504	0.00034	0.053	0.0041	105.3	7.8	96.2	2.2	290	160	66.8	96.2	2.2	95.5	2.2	95.6	2.3	95	2.5
Z041	0.1006	0.0049	0.01514	0.00028	0.0483	0.0024	97.2	4.5	96.9	1.8	140	110	30.8	96.9	1.8	96.6	1.9	96.8	1.9	95.6	2.6
Z042	0.18	0.037	0.0158	0.00046	0.078	0.015	163	30	101.1	2.9	830	340	87.8	101.1	2.9	96.7	3.3	96.6	3.3	100.9	2.9
Z043	0.363	0.021	0.05122	0.00091	0.0518	0.003	314	15	322	5.6	250	120	-28.8	322.0	5.6	315.7	6.9	322	6	270	31
Z044	0.096	0.011	0.01506	0.00029	0.048	0.0059	95	11	96.4	1.8	60	210	-60.7	96.4	1.8	96.3	2.1	96.4	2.2	96.3	1.9
Z045	0.0956	0.0087	0.0148	0.00034	0.0469	0.0041	92.3	8	94.7	2.1	60	160	-57.8	94.7	2.1	94.8	2.2	94.8	2.2	94.7	2.2
Z046	0.11	0.019	0.01499	0.00061	0.0539	0.009	104	17	95.9	3.9	220	300	56.4	95.9	3.9	95.1	4.1	95.2	4.2	95.5	3.9
Z047	0.174	0.03	0.01649	0.00048	0.079	0.013	160	25	105.4	3	930	320	88.7	105.4	3.0	101.7	3.2	101.6	3.2	105.5	3.1
Z048	0.103	0.019	0.0144	0.00055	0.0514	0.0098	97	17	92.2	3.5	170	330	45.8	92.2	3.5	91.7	4.1	91.7	4.1	92.2	3.5
Z049	0.124	0.02	0.01517	0.00041	0.06	0.01	117	17	97.1	2.6	450	290	78.4	97.1	2.6	95.3	3.4	95.2	3.4	97.1	2.6
Z050	0.111	0.013	0.01607	0.00039	0.0525	0.0068	109	12	102.8	2.5	210	230	51.0	102.8	2.5	102.3	3	102.3	3	102.8	2.5
Z051	0.116	0.014	0.01508	0.00034	0.0558	0.0065	110	12	96.5	2.1	340	230	71.6	96.5	2.1	95.5	2.3	95.5	2.3	96.3	2.2
Z052	0.104	0.011	0.01479	0.00041	0.0514	0.0058	99	10	94.7	2.6	200	210	52.7	94.7	2.6	94.3	2.9	94.3	2.9	94.6	2.6
Z053	0.0966	0.0075	0.01389	0.00026	0.0509	0.0042	93.3	7	88.9	1.6	240	170	63.0	88.9	1.6	88.5	1.9	88.5	1.9	88.5	1.7
Z054	0.095	0.012	0.01578	0.00044	0.0436	0.0055	91	12	100.9	2.8	-90	210	212.1	100.9	2.8	101.3	2.9	101.5	2.9	99.4	4.1
Z055	0.1065	0.0095	0.01471	0.00033	0.0533	0.0053	102.3	8.7	94.1	2.1	280	190	66.4	94.1	2.1	93.5	2.4	93.6	2.4	94.3	2.1
Z056	0.1119	0.0098	0.01542	0.00037	0.0523	0.0039	107.2	8.8	98.7	2.4	260	150	62.0	98.7	2.4	97.9	2.3	98.1	2.3	97.2	3.4
Z057	0.1094	0.007	0.01503	0.00055	0.0534	0.0036	105.2	6.4	96.1	3.5	330	140	70.9	96.1	3.5	95.4	3.7	95.4	3.7	95.2	4.1
Z058	0.097	0.012	0.01687	0.00041	0.0417	0.0051	93	11	107.8	2.6	-160	200	167.4	107.8	2.6	108.7	2.8	108.7	2.8	108.1	2.6
Z059	0.1041	0.0066	0.0153	0.00029	0.0487	0.0029	100.4	6	97.9	1.8	150	120	34.7	97.9	1.8	98.1	1.8	98.1	1.8	97.6	1.9
Z060	0.0988	0.0062	0.01513	0.00026	0.0473	0.0029	95.5	5.8	96.8	1.7	70	120	-38.3	96.8	1.7	96.7	1.7	96.9	1.7	95.7	2
Z061	0.204	0.032	0.01583	0.00037	0.093	0.014	185	26	101.2	2.3	1180	300	91.4	101.2	2.3	95.5	2.9	95.4	2.9	101.2	2.4
Z062	0.1115	0.0048	0.01547	0.00042	0.0512	0.0014	107.2	4.3	99	2.7	242	59	59.1	99.0	2.7	97.6	2	98.5	2.7	95.6	5
Z063	0.107	0.01	0.015	0.0003	0.0514	0.0048	102.3	9.5	95.9	1.9	220	180	56.4	95.9	1.9	95.5	2	95.5	2	95.9	1.9
Z064	0.096	0.0097	0.01521	0.00037	0.0469	0.0052	92.6	9	97.3	2.3	40	190	-143.3	97.3	2.3	97.4	2.5	97.4	2.5	97.7	2.8
Z065	0.092	0.01	0.01524	0.00034	0.0439	0.0046	89.2	9.3	97.5	2.1	-70	180	239.3	97.5	2.1	97.4	2	97.5	2	97.3	2.2
Z066	0.1002	0.0059	0.0148	0.00021	0.0492	0.003	96.8	5.5	94.7	1.4	150	120	36.9	94.7	1.4	94.4	1.5	94.5	1.5	92.2	3.5
Z067	0.119	0.013	0.01529	0.00035	0.0568	0.0063	114	12	97.8	2.2	380	220	74.3	97.8	2.2	96.6	2.4	96.7	2.4	97.6	2.3

Z068	0.099	0.0093	0.01514	0.00027	0.0478	0.0047	95.5	8.6	96.9	1.7	80	180	-21.1	96.9	1.7	96.8	1.9	96.9	2	96.5	1.8
Z069	0.0959	0.0051	0.01509	0.00032	0.0464	0.0025	92.9	4.7	96.5	2	40	100	-141.3	96.5	2.0	96.6	2.2	96.8	2.2	95.1	3
Z070	0.0971	0.0068	0.01358	0.0003	0.0518	0.0033	93.9	6.2	87	1.9	250	130	65.2	87.0	1.9	86.5	1.9	86.5	1.9	85.9	2.5
Z071	0.1027	0.0063	0.01548	0.00027	0.0481	0.0031	99	5.8	99	1.7	110	120	10.0	99.0	1.7	98.7	1.8	99	1.8	93.9	5.1
Z072	0.0954	0.007	0.01436	0.00032	0.0485	0.004	92.2	6.5	91.9	2.1	110	150	16.5	91.9	2.1	91.8	2.4	91.9	2.4	92	2.1
Z073	0.099	0.018	0.01443	0.00066	0.0494	0.0084	95	17	92.3	4.2	130	310	29.0	92.3	4.2	91.8	4	92.1	4	89.3	7.5
Z074	0.102	0.027	0.01018	0.00042	0.074	0.019	95	23	65.3	2.7	620	400	89.5	65.3	2.7	63.2	3.1	64.5	2.8	64.2	3.5
Z075	0.0967	0.0037	0.01438	0.00029	0.0487	0.0017	93.6	3.5	92.1	1.9	132	71	30.2	92.1	1.9	91.7	1.9	91.9	1.9	86.8	4.5
Z076	0.065	0.0046	0.01003	0.00027	0.0483	0.0039	64.9	4.7	64.3	1.7	100	150	35.7	64.3	1.7	64.2	1.9	64.3	1.9	64.3	1.7
Z077	0.1019	0.005	0.01524	0.00032	0.0486	0.0023	98.4	4.6	97.5	2.1	129	96	24.4	97.5	2.1	97.1	2.1	97.4	2.1	95.2	3.6
Z078	0.086	0.012	0.01455	0.00036	0.0421	0.0062	83	11	93.1	2.3	-120	240	177.6	93.1	2.3	94.2	2.4	94.3	2.4	92.9	2.3
Z079	0.168	0.038	0.01117	0.00037	0.109	0.022	159	34	71.6	2.3	1300	350	94.5	71.6	2.3	65.5	1.5	65.4	1.5	71.5	2.3
Z080	0.1011	0.0038	0.01345	0.00038	0.0549	0.0018	97.7	3.4	86.1	2.4	393	72	78.1	86.1	2.4	85.3	2.5	85.4	2.5	85.6	3.5
Z081	0.114	0.0069	0.01613	0.00034	0.0529	0.0039	109.5	6.3	103.2	2.2	300	150	65.6	103.2	2.2	102.5	2.3	102.6	2.3	103.1	2.2
Z082	0.0986	0.0093	0.01515	0.00041	0.0477	0.0046	95.2	8.5	96.9	2.6	90	180	-7.7	96.9	2.6	96.9	2.9	97	2.9	97.2	2.7
Z083	0.1144	0.008	0.01559	0.00031	0.0535	0.0041	109.7	7.3	99.7	2	300	150	66.8	99.7	2.0	99	2.1	99	2.2	99.4	1.9
Z084	5.366	0.072	0.3329	0.0032	0.1167	0.0013	1879	11	1852	16	1905	21	2.8	1905.0	21.0	1848	17	1846	18	1850	19
Z085	0.108	0.01	0.01535	0.00035	0.0498	0.0043	103.5	9.2	98.2	2.2	200	170	50.9	98.2	2.2	97.8	2.3	97.8	2.3	97.6	2.4
Z086	1.546	0.042	0.1469	0.0022	0.0758	0.0016	947	16	883	13	1084	43	18.5	883.0	13.0	878	13	875	13	881	14
Z087	0.0744	0.0093	0.01088	0.0004	0.0495	0.0057	72.4	8.6	69.8	2.5	120	200	41.8	69.8	2.5	69.3	2.6	69.3	2.6	68.2	3.3
Z088	0.097	0.012	0.01506	0.00029	0.0464	0.0054	93	11	96.4	1.9	20	200	-382.0	96.4	1.9	96.3	1.9	96.5	2	93.2	3.2
Z089	0.247	0.011	0.03648	0.00059	0.0492	0.0021	223.9	9.2	231	3.6	155	89	-49.0	231.0	3.6	228.7	4.2	231.3	3.7	207	17
Z090	0.103	0.011	0.01483	0.00047	0.051	0.0054	99	10	94.9	3	200	200	52.6	94.9	3.0	94.4	3.1	94.6	3.1	93.6	3.6
Z091	0.0947	0.007	0.01487	0.0005	0.047	0.0039	91.6	6.5	95.1	3.2	60	150	-58.5	95.1	3.2	95.2	3.4	95.3	3.4	93.6	3.3
Z092	0.099	0.017	0.01403	0.00078	0.0511	0.008	94	16	89.8	5	150	280	40.1	89.8	5.0	91.9	7	91.9	7	89.9	5
Z093	0.1	0.01	0.01567	0.00032	0.0465	0.0048	96.3	9.5	100.2	2	30	180	-234.0	100.2	2.0	100.2	2.2	100.4	2.2	99.6	2.4
Z094	0.088	0.013	0.01421	0.00037	0.0454	0.0067	85	12	91	2.3	-40	240	327.5	91.0	2.3	91.1	2.6	91.3	2.6	89.9	3
Z095	0.118	0.024	0.01417	0.00042	0.06	0.012	110	21	90.7	2.7	400	370	77.3	90.7	2.7	88.9	3.2	88.8	3.2	90.4	2.6
Z096	0.0988	0.0058	0.01506	0.00019	0.047	0.0026	95.5	5.4	96.4	1.2	80	110	-20.5	96.4	1.2	96.3	1.3	96.4	1.3	95.5	2
Z097	0.1005	0.0052	0.01471	0.00056	0.0501	0.0026	97.1	4.7	94.1	3.5	190	110	50.5	94.1	3.5	93.8	3.7	93.9	3.7	92.9	3.9
Z098	0.113	0.013	0.01455	0.00032	0.0559	0.0063	107	12	93.1	2.1	350	220	73.4	93.1	2.1	92.1	2.1	92.1	2.1	92.5	2.4
Z099	0.0928	0.0082	0.01011	0.00027	0.0663	0.0052	89.8	7.5	64.8	1.7	730	170	91.1	64.8	1.7	63.3	1.7	63.2	1.7	64.7	1.8
Z100	0.0965	0.008	0.01426	0.00027	0.0495	0.0042	93.4	7.3	91.3	1.7	150	160	39.1	91.3	1.7	90.9	2	91.1	1.9	90.3	2.5
Z101	0.0958	0.0072	0.01485	0.0004	0.0467	0.0034	92.6	6.6	95	2.5	40	130	-137.5	95.0	2.5	94.3	2.3	94.5	2.3	91.6	4.2

Z102	0.0942	0.0096	0.01378	0.00024	0.0498	0.0052	91	8.8	88.2	1.5	150	190	41.2	88.2	1.5	88	1.7	88	1.7	88.2	1.5
Z103	0.1111	0.0046	0.01636	0.00028	0.0494	0.0024	106.9	4.2	104.6	1.8	156	96	32.9	104.6	1.8	104.4	2.2	104.7	2.2	100.8	4.8
Z104	0.099	0.016	0.01438	0.00044	0.0493	0.0074	94	15	92	2.8	150	280	38.7	92.0	2.8	91.5	2.6	91.5	2.6	91.9	2.8
Z105	0.1018	0.0072	0.01484	0.00035	0.05	0.004	98.2	6.7	95	2.2	170	150	44.1	95.0	2.2	94.6	2.4	94.7	2.4	92.7	3.7
Z106	0.1037	0.0071	0.01559	0.0004	0.0503	0.0041	100	6.5	99.7	2.6	180	150	44.6	99.7	2.6	99.3	2.6	99.4	2.6	100.1	3.2
Z107	0.1003	0.0031	0.01496	0.00016	0.0489	0.0016	97	2.9	95.7	1	142	70	32.6	95.7	1.0	95.5	1.1	95.5	1	93.8	2.4
Z108	0.1174	0.0077	0.0158	0.00017	0.0538	0.0035	112.4	7	101.1	1.1	320	130	68.4	101.1	1.1	100.1	1.2	100.1	1.3	100.8	1.2
Z109	0.102	0.013	0.01503	0.00032	0.0481	0.0059	98	12	96.2	2	110	230	12.5	96.2	2.0	96.5	2	96.5	2	96	2
Z110	0.1007	0.0083	0.01509	0.00028	0.0484	0.004	97	7.6	96.6	1.8	110	160	12.2	96.6	1.8	96.5	1.9	96.5	2	96.3	1.7
Z111	0.1097	0.0055	0.0164	0.00031	0.0486	0.0026	105.6	5	104.9	1.9	130	110	19.3	104.9	1.9	104.4	2.1	104.8	2.1	102.9	3.3
Z112	0.105	0.014	0.01569	0.00041	0.0485	0.0064	101	13	100.4	2.6	90	230	-11.6	100.4	2.6	100.1	2.7	100.3	2.7	100.2	2.7
Z113	0.1094	0.0072	0.01565	0.00032	0.0505	0.0031	105.2	6.5	100.1	2	230	130	56.5	100.1	2.0	98.9	1.8	99.1	1.8	98.6	3.7
Z114	0.1052	0.008	0.01577	0.00032	0.0485	0.0032	101.3	7.3	100.9	2	120	130	15.9	100.9	2.0	100.6	2	100.8	1.9	98.6	4.6
Z115	0.094	0.011	0.01499	0.00046	0.0457	0.0056	91	11	95.9	2.9	-10	210	1059.0	95.9	2.9	97	3.4	97	3.4	95.9	2.9
Z116	0.123	0.013	0.01414	0.00045	0.0651	0.0073	117	12	90.5	2.8	660	210	86.3	90.5	2.8	88.4	3	88.5	3	88.3	4
Z117	0.119	0.01	0.01607	0.00027	0.0534	0.0045	113.6	9.3	102.8	1.7	300	170	65.7	102.8	1.7	101.8	1.8	102	1.8	101.6	2.9
Z118	0.0924	0.0049	0.01535	0.00027	0.0443	0.0025	89.6	4.5	98.2	1.7	-50	100	296.4	98.2	1.7	98.5	1.9	98.7	1.8	95.7	2.9
Z119	0.099	0.011	0.01457	0.00028	0.0495	0.0052	95.3	9.7	93.2	1.8	130	190	28.3	93.2	1.8	92.5	2.1	92.5	2.1	93	1.8
Z120	0.0944	0.0093	0.0147	0.00034	0.048	0.0051	91.2	8.6	94.1	2.1	80	190	-17.6	94.1	2.1	94	2.3	94.1	2.3	94.2	2.2
Z121	0.094	0.012	0.014	0.00034	0.049	0.0064	90	11	89.6	2.1	90	220	0.4	89.6	2.1	89.4	2.4	89.5	2.5	89.1	2.3
Z122	0.0989	0.0055	0.01473	0.00022	0.0489	0.0029	95.6	5.1	94.3	1.4	130	120	27.5	94.3	1.4	94.1	1.5	94.2	1.5	94.2	1.4
Z123	0.086	0.01	0.0124	0.00057	0.0514	0.0065	83.2	9.8	79.4	3.7	240	240	66.9	79.4	3.7	78.8	3.8	78.9	3.8	78.6	3.7
Z124	0.0861	0.0095	0.01479	0.00035	0.0424	0.0046	83.4	8.9	94.6	2.2	-120	180	178.8	94.6	2.2	95.3	2.3	95.3	2.3	94.6	2.2
Z125	0.097	0.019	0.01435	0.00036	0.0502	0.0096	93	17	91.8	2.3	60	300	-53.0	91.8	2.3	91	2.9	91.1	2.9	90.7	2.8
Z126	0.1033	0.0093	0.01529	0.00034	0.0492	0.0043	99.4	8.5	97.8	2.1	130	160	24.8	97.8	2.1	97.7	2.3	97.7	2.3	97.8	2.1
Z127	0.106	0.011	0.01469	0.00033	0.0524	0.0053	102	10	94	2.1	240	190	60.8	94.0	2.1	93.3	2.1	93.4	2.1	92.9	2.7
Z128	0.093	0.0075	0.01464	0.00028	0.0461	0.0039	90	7	93.7	1.8	20	150	-368.5	93.7	1.8	93.8	2.1	93.9	2.1	93.3	2
Z129	0.104	0.009	0.01517	0.00029	0.0497	0.0044	100.1	8.2	97.1	1.8	150	160	35.3	97.1	1.8	97.2	2.1	96.9	2	95.9	2.4
Z130	0.095	0.017	0.01462	0.00052	0.0495	0.0094	91	16	93.5	3.3	50	320	-87.0	93.5	3.3	93.3	3.4	93.3	3.4	93.5	3.3
Z131	0.084	0.012	0.01475	0.00037	0.0419	0.0061	85	13	94.4	2.3	-130	230	172.6	94.4	2.3	94.9	2.6	95	2.6	92.8	4
Z132	0.1013	0.0093	0.01524	0.00042	0.0472	0.0037	97.6	8.5	97.5	2.6	90	150	-8.3	97.5	2.6	97.3	2.7	97.5	2.7	96	3.8
Z133	0.0916	0.0068	0.01479	0.00032	0.0459	0.0036	88.7	6.3	94.7	2.1	10	140	-847.0	94.7	2.1	94.3	2	94.4	2	94.6	2.1
Z134	0.085	0.012	0.01518	0.00037	0.0427	0.0064	82	11	97.1	2.3	-140	230	169.4	97.1	2.3	97.8	2.7	97.8	2.7	97.4	2.4
Z135	0.092	0.012	0.01481	0.00036	0.0448	0.0057	88	11	94.7	2.3	-10	220	1047.0	94.7	2.3	94.8	2.5	94.9	2.5	93.2	3.1

Z136	0.0967	0.0038	0.01484	0.00017	0.0476	0.0018	93.7	3.5	95	1.1	84	76	-13.1	95.0	1.1	94.8	1	95	1	93.2	2.6
Z137	0.09	0.022	0.01417	0.00051	0.048	0.012	85	20	90.7	3.3	30	420	-202.3	90.7	3.3	90.4	4.1	90.4	4.1	90.7	3.3
Z138	0.111	0.013	0.01578	0.00031	0.0512	0.006	106	12	100.9	1.9	190	210	46.9	100.9	1.9	100.5	2.2	100.5	2.3	100.9	2
Z139	0.098	0.017	0.01418	0.00048	0.0505	0.0091	94	16	90.8	3.1	90	310	-0.9	90.8	3.1	90.5	3.3	90.5	3.4	90.8	3.1
Z140	0.1136	0.0086	0.01567	0.00023	0.0524	0.0041	108.9	7.8	100.2	1.5	260	150	61.5	100.2	1.5	99.5	1.6	99.6	1.6	99.3	1.8

Sample 17MBV01

	Ratios						U-Pb ages uncorrected for common lead									Corrected for common lead using Andersen's routine					
Grains	Final207_235	Final207_235_2s	Final206_238	Final206_238_2s	Final207_206	Final207_206_2s	FinalAge 207_235	FinalAge 207_235_2s	FinalAge 206_238	FinalAge 206_238_2s	FinalAge 207_206	FinalAge 207_206_2s	Concordance (%)	Best age	Best age 2s	FinalAgeAnd207_235	FinalAgeAnd207_235_2s	FinalAgeAnd206_238	FinalAgeAnd206_238_2s	FinalAgeAnd207_206	FinalAgeAnd207_206_2s
ZB01	0.0387	0.0055	0.00549	0.00017	0.0506	0.0073	38.3	5.3	35.3	1.1	150	260	76.5	35.3	1.1	35.1	1.2	35.1	1.2	35.3	1.1
ZB02	0.0432	0.0051	0.00585	0.00017	0.0555	0.0075	42.8	5	37.6	1.1	290	240	87.0	37.6	1.1	37.2	1.2	37.2	1.2	37.6	1.1
ZB04	0.075	0.012	0.00611	0.00019	0.086	0.012	73	11	39.2	1.2	1050	300	96.3	39.2	1.2	37.1	1.2	37.1	1.2	39.2	1.2
ZB09	0.0477	0.006	0.00604	0.0002	0.0572	0.0065	47.2	5.8	38.8	1.3	440	240	91.2	38.8	1.3	38.3	1.3	38.3	1.3	38.8	1.3
ZB10	0.0395	0.0057	0.00584	0.00016	0.0489	0.0073	39.2	5.5	37.6	1	70	250	46.3	37.6	1.0	37.7	1.3	37.7	1.3	37.4	1.3
ZB11	0.0414	0.005	0.00566	0.00017	0.0533	0.0067	41.1	4.8	36.4	1.1	240	220	84.8	36.4	1.1	36.1	1.2	36.1	1.2	36.4	1.1
ZB12	0.0369	0.0074	0.00604	0.00022	0.0444	0.0091	36.4	7.2	38.8	1.4	-110	330	135.3	38.8	1.4	39	1.6	39	1.6	38.8	1.4
ZB14	0.0372	0.0052	0.00596	0.00019	0.0457	0.0069	37	5.1	38.3	1.2	-30	250	227.7	38.3	1.2	38.4	1.3	38.4	1.3	38.3	1.2
ZB15	0.0394	0.0027	0.005969	0.000092	0.0475	0.0035	39.2	2.6	38.37	0.59	100	140	61.6	38.4	0.6	38.3	0.62	38.27	0.63	38.45	0.58
ZB17	0.035	0.0022	0.005873	0.000079	0.0424	0.0025	34.9	2.1	37.75	0.5	-120	100	131.5	37.8	0.5	37.87	0.53	37.93	0.53	37.99	0.68
ZB19	0.0411	0.0051	0.00573	0.00018	0.0521	0.0065	40.8	4.9	36.8	1.1	220	230	83.3	36.8	1.1	36.6	1.3	36.6	1.3	36.8	1.1
ZB22	0.0443	0.0099	0.00602	0.00021	0.054	0.012	43.7	9.6	38.7	1.4	220	390	82.4	38.7	1.4	38.4	1.5	38.4	1.5	38.7	1.4
ZB25	0.0429	0.004	0.00578	0.00014	0.0544	0.0051	42.6	3.9	37.14	0.89	320	180	88.4	37.1	0.9	36.73	0.9	36.73	0.9	37.14	0.89
ZB27	0.0376	0.005	0.00583	0.0002	0.0462	0.0062	37.3	4.9	37.5	1.3	0	230	#DIV/0!	37.5	1.3	37.5	1.3	37.5	1.3	37.3	1.2
ZB28	0.055	0.01	0.0059	0.00019	0.067	0.011	53.8	9.5	37.9	1.2	700	280	94.6	37.9	1.2	36.7	1	36.7	1	37.9	1.2
ZB29	0.0409	0.0024	0.00624	0.00014	0.0467	0.0024	40.7	2.4	40.08	0.89	51	99	21.4	40.1	0.9	39.98	0.88	40	0.88	39.9	1
ZB30	0.0573	0.0084	0.00607	0.00012	0.0647	0.0082	56.2	7.9	39.01	0.74	690	260	94.3	39.0	0.7	38.05	0.82	38.03	0.82	39.27	0.99
ZB32	0.0405	0.0037	0.0063	0.00016	0.0474	0.0044	40.3	3.6	40.5	1	100	180	59.5	40.5	1.0	40.3	1	40.3	1	40.3	1.1